The Zebrafish Homologues of JAM-B and JAM-C are Essential for Myoblast Fusion

Gareth T. Powell

September 2010

Magdalene College, University of Cambridge

This thesis is submitted for the degree of Doctor of Philosophy

Dedicated to

my mother and father, Lizbeth and David;

my siblings, Alexis, James, Robert, William and Rosie;

and

my love, Nirvana.

Declaration

This dissertation is the result of my own work and includes nothing which is the outcome of work done in collaboration except where specifically indicated in the text. This dissertation does not exceed the word limit set by the Biology Degree Committee.

Abstract

The cell surface proteins JAM-B and JAM-C are a receptor:ligand pair that is important for leukocyte extravasation, tight junction formation and cell polarity. Both proteins are expressed during embryogenesis, but their developmental function has not yet been described. Through studying the biochemistry and embryonic expression patterns of the zebrafish homologues, named *jamb* and *jamc* respectively, I have hypothesised that the interaction between them has a role in vertebrate myoblast fusion. Consistent with this, zebrafish embryos mutant for *jamb* or *jamc* develop mononuclear fast muscle fibres. This suggests that these proteins are a novel receptor:ligand pair that function in myoblast fusion in vertebrates. The severity of the phenotype suggests that *jamb* and *jamc* are critical for the initiation of fusion.

In contrast to the *Drosophila* paradigm, loss of myoblast fusion in the *jamb* or *jamc* mutant results in an increase in fast muscle fibres with no apparent accumulation of unfused myoblasts. This suggests that every myoblast is able to form a mature muscle fibre. Also, *jamc* is misexpressed in *prdm1* mutant embryos, which lack the transcriptional repressor that is known to control the differentiation of slow and fast muscle. Expression of *jamc* is dynamic throughout primary differentiation. Taken together, these results suggest that myoblast fusion is regulated by relative expression of both Jamb and its binding partner Jamc, and that zebrafish myoblasts are not specified into sub-populations of founder cells and fusion-competent myoblasts.

Acknowledgements

Many thanks to Gavin Wright for being a great teacher, mentor, sounding board and proof-reader.

Thanks to Mark Bushell, Christian Söllner and Stephen Martin who were there to help me find my feet in the laboratory; Céçile Wright-Crosnier for trying to set the muscles free, amongst other wayward experiments; Mariella Ferrante for providing the *mrfp* plasmid and other crucial reagents; Elisabeth Busch-Nentwich for expert advice and *jamb* mutant fish; Richard White for technical wizardry, transplant reagents and manuscript advice; Stone Elworthy for *prdm1*^{tp39} embryos; Ross Kettleborough and Ewart de Bruijn for *jamb* and *jamc* mutants; Huw Williams, Annabel Scott and Yung-yao Lin for support and advice; Fruzsina Fenyes for protocols and reagents.

Many thanks to Alex Bateman, Annabel Smith, Christina Hedberg-Deloukas and the WTSI Committee of Graduate Studies for their continued support of my studies.

Thanks to Derek Stemple, David Tannahill, & Bertie Göttgens for their contributions as part of my Thesis Committee.

Finally, thanks to all members, past and present, of the Stemple and Wright groups for their kindness, support and collegiality.

Table of Contents

List of Figures

List of Tables

Chapter 1

Introduction

Project Aims and Summary

Prior to the commencement of this project, zebrafish homologues of JAM-B and JAM-C were included in a screen designed to identify novel cell surface receptor:ligand pairs using AVEXIS, a methodology developed in the lab. The purpose of this PhD project was to determine the biological function of the interaction between Jamb and Jamc during early development of the zebrafish embryo, if any. In pursuit of this aim, I studied the evolution and homology, developmental expression and biochemistry of the zebrafish *jam* family members to better understand the developmental role of *jamb* and *jamc*. I then characterized loss-of-function mutants and identified a novel role for these proteins in myoblast fusion. Finally, I demonstrated the necessity of interaction between Jamb and Jamc *in trans* between myoblasts for fusion.

In this chapter I describe what is known about JAM family proteins in other contexts, the role of cell surface proteins in myogenesis, the process of myoblast fusion and the use of the zebrafish as a model for vertebrate muscle development.

1.1 The *JAM* family

The mammalian junctional adhesion molecule (JAM) family consists of three immunoglobulin superfamily domain-containing cell surface proteins that have been implicated in a wide array of functions such as, but not limited to, angiogenesis (Lamanga *et al*, 2005a; Cooke *et al*, 2006; Rabquer *et al*, 2010), cancer (Santoso *et al*, 2005; Murakami et al, 2010; Tenan *et al*, 2010), tight junction formation (Ebnet *et al*, 2003; Mandell *et al*, 2004; Rehder *et al*, 2006; Mandicourt *et al*, 2007), leukocyte extravastion and inflammation (Johnson-Léger *et al*, 2002; Cera *et al*, 2004; Chavakis *et al*, 2004; Aurrand-Lions *et al*, 2005; Ludwig *et al*, 2005; Vonlaufen *et al*, 2007) and spermatogenesis (Gliki *et al*, 2004; Shao *et al*, 2008; Wang and Lui, 2009). These studies have largely been restricted to post-natal or adult mice and cultured cells. A common thread to most of these ascribed functions is the regulation of stability, permeability, and polarity of epithelia and endothelia and subsequent interactions with leukocytes (reviewed in Weber *et al*, 2007).

The purpose of this PhD project was to assess the biological function of the interaction between zebrafish homologues of *jamb* and *jamc* during development. This interaction was identified in a screen for physical interactions between cell surface proteins *in vitro*, using a specialised methodology developed in the laboratory: avidity-based extracellular interaction screen (AVEXIS; Bushell *et al*, 2008). For this reason I will restrict the scope of discussion to the functions of Jam-B and Jam-C that have been elucidated from studies of mutant animals.

Jam-B and Jam-C were discovered by different groups in different organisms at different times and given different names (Palmeri *et al*, 2000; Cunningham *et al*, 2000; Aurrand-Lions *et al*, 2001; Arrate *et al*, *2001*; Liang *et al*, 2002), based upon their homology to Jam-A, a cell surface protein characterised as a receptor for a stimulatory platelet antibody (Naik *et al*, 1995). The nomenclature of the homologues was rationalised much later by discussion within the field (Muller, 2003), but the widely accepted new system remains unofficial (see Chapter 3).

Jam-B and Jam-C were identified as binding partners that facilitate the binding of peripheral blood leukocytes to vascular endothelia and transmigration (Arrate *et al*, 2001; Liang *et al*, 2002). *Jam-C* has subsequently been extensively studied in the context of inflammatory diseases, for example, acute pancreatitis (Vonlaufen *et al*, 2006), and the immune system (Imhof *et al*, 2007) throughout the last decade. Most recently, studies of *Jam-C* knockout mice have revealed considerable deficiencies in the development and function of the immune system (Praetor *et al*, 2009; Zimmerli *et*

al, 2009). *Jam-C* is highly expressed on hematopoietic stem cells (HSCs), and loss-of-function of *Jam-C* results in a large increase in myeloid progenitors, suggesting Jam-C functions in the differentiation of HSCs (Praetor *et al*, 2009). However, this phenotype might be a secondary consequence of the susceptibility of *Jam-C* knockout mice to infection (Imhof *et al*, 2007; Zimmerli *et al*, 2009), that is, upregulated differentiation of hematopoietic stem cells may be a result of unchecked bacterial challenge (Scumpia *et al*, 2010).

In further studying the function of Jam-C in the immune system, Scheiermann *et al* (2007) observed defects in the peripheral nervous system. Jam-C is expressed by Schwann cells and is localised to paranodes surrounding Nodes of Ranvier, Schmidt-Lanterman incisures and mesaxonal bands (Scheiermann *et al*, 2007). Jam-C knockout mice show decreased nerve conductivity in electrophysiological experiments using sciatic nerves, likely resulting from a loss of integrity of the myelin sheath which surrounds axons. In addition, the authors noted a general muscle weakness quantified by reduced grip strength and stride length. This peripheral nerve phenotype might also explain the dilated oesophagus present in *Jam-C* knockout mice (Imhof *et al*, 2007). Megaoesophagus results from a lack of peristalsis in the oesophagus, suggesting a neural deficit (Shiina *et al*, 2010). The authors of this study suggested a function for *Jam-C* in the contractions of the smooth muscle cells lining the oesophagus and bronchial airways (Imhof *et al*, 2007), but did not speculate on the precise role of Jam-C. It is possible that the protein maintains coherent tight junctions between smooth muscle cells, in order to allow progression of the peristaltic movement.

The first *Jam-C* knockout mice phenotype described was that of complete male sterility (Gliki *et al*, 2004) resulting from defective polarisation of spermatids and subsequent arrest in maturation. The authors proposed that this defect resulted from a loss of interaction between Jam-C, expressed on the surface of spermatids, and Jam-B, expressed on the apical surface of Sertoli cells, to which spermatids are bound. The authors demonstrated that loss of Jam-C resulted in unpolarised localisation of the Par3-Par6-aPKCγ-Cdc42 cell polarity complex. Addition of soluble Jam-B could restore this localisation *in vitro*. Both Jam-B and Jam-C had previously been demonstrated to directly interact with Par3 through the cytoplasmic PDZ domain-binding motif (Ebnet *et al*, 2003).

In contrast, relatively few reports of *Jam-B* function have been published since its identification, including very little immunological research (Ludwig *et al*, 2005). It has been used as a marker to detect an unusual retinal ganglion cell type that is

polarised and only responds to upward movements, but no functional role for Jam-B was reported (Kim *et al*, 2008). Indeed, the paucity of functional data is likely because loss-of-function of *Jam-B* has no detectable impact on the phenotype of mice (Sakaguchi *et al*, 2006). None of the phenotypic characteristics of the *Jam-C* knockout mice have been replicated in *Jam-B* knockout mice, despite extensive characterisation. It is therefore difficult to establish which functions of Jam-C *in vivo*, if any, are a direct result of interaction with Jam-B. Most functions might be mediated by homophilic Jam-C interactions (Scheiermann *et al*, 2007; Mandicourt *et al*, 2007; Santoso *et al*, 2005), by interaction or regulation of various integrins (Cunningham *et al*, 2002; Santoso *et al*, 2002; Lamanga *et al*, 2005b; Mandicourt *et al*, 2007;) or other cell surface proteins, such as CAR (Mirza *et al*, 2006). There also remains the possibility of some functional redundancy amongst family members. For example, Jam-A is also expressed in Sertoli cells, though it is restricted to basal tight junctions (Gliki *et al*, 2004). In the absence of Jam-B, Jam-A might redistribute to the surface of Sertoli cells and act as a substitute. However, no interaction between Jam-A and Jam-C has been previously described.

No developmental function for JAM-B and JAM-C has been reported previously, and neither gene has been studied with respect to muscle development, despite being known to be expressed in skeletal muscle (see Chapter 4). What potential functions might these cell surface proteins have in myogenesis?

1.2 The role of cell surface proteins during myogenesis

Skeletal muscle development is a complex process involving multiple, co-ordinated behaviours and interactions between myocytes in order to form an ordely array of elongated, differentiated syncytia capable of the remarkable feat of translating chemical energy into mechanical force. This property has fascinated scientists and medics for centuries, resulting in a wealth of knowledge delineating the development and function of muscles. Here I highlight some of the important phases of muscle development that must require interactions between cell surface molecules, but have not necessarily been fully characterised.

Migration of muscle cells plays a key role in the development of all muscles in every model system examined. These movements can be local, for example, fusion competent myoblasts migrating to fuse with founder cells (Ruiz-Gomez *et al*, 2000; Strünkelnberg *et al*, 2001), the positional rotation of myoblasts within the somite of the zebrafish embryo (Hollway *et al*, 2007; Stellabotte *et al*, 2007), or myocytes delaminating from the dermomyotome to form the primary myotome in chick (Kahane

et al, 2002). They can also be long range, for example, the migration of myoblasts from the somites into the limbs of mouse embryos (Dietrich *et al*, 1999). In some cases, migration need not depend on the differentiation state of the muscle cell; for example, elongated and differentiated slow muscle fibres migrate through the myotome in zebrafish (Devoto *et al*, 1996). These migrations must clearly depend upon interactions between cell surface molecules and the extracellular matrix and other cells to gain traction, but also short or long range signalling for pathfinding, as exemplified by the tyrosine receptor kinase c-met and secreted hepatocyte growth factor (Dietrich *et al*, 1999).

Muscles are characteristically long fibres that link distant anatomical regions. It is necessary for the muscle cells to elongate and form myotendinous junctions after contact with extracellular matrix in vertebrates (Bassett *et al*, 2003; Kudo *et al*, 2004; Henry *et al*, 2005; Snow *et al*, 2008a) or tendon cells in *Drosophila* (Steigemann *et al*, 2004; Schnorrer *et al*, 2007; reviewed in Schnorrer and Dixon, 2004). This also requires some form of polarity and directional signalling through cell surface and secreted proteins, as demonstrated by *slit* mutants in *Drosophila* (Kramer *et al*, 2001), or loss-of-function of Wnt11 in chick (Gros *et al*, 2008). The formation of a specialised junction at the attachment site of muscles is crucial for force transduction, and therefore maintenance of the fibre, as is clearly evident in the wide-spectrum of dystrophies (Conti *et al*, 2009).

Muscle fibres are syncytia formed by the fusion of muscle cells, not mitosis of a muscle cell without division (Capers, 1960). This has been clearly demonstrated recently in time-lapse studies of zebrafish embryos expressing transgenic fluorescent reporter genes (Collins *et al*, 2010). Myoblast fusion involves multiple processes that occur between two muscle cells: recognition, adhesion and controlled breakdown and union of the membranes of both cells. Each of these steps require interactions between cell surface proteins, and these may have overlapping functions. The cell surface molecules involved in this process in *Drosophila* are well characterised, but less well understood in vertebrates (see below for more detailed discussion).

For skeletal muscle fibres to be functional, each fibre needs to be directly innervated. Innervation is not required for muscles to form (Bate, 1990; Hughes *et al*, 1992; Broadie and Bate 1993), but is important for secondary myogenesis (Ross *et al*, 1987; Condon *et al*, 1990). How motor axons project from the spinal cord into muscle and innervate specific muscle groups is an active area of research (reviewed in Bonanomi and Pfaff, 2010). Initial pathfinding of axon bundles to the axial muscles in chick is thought to require chemoattractants secreted by the dermomyotome, for

example FGF (Shirasaki *et al*, 2006), with further patterning of individual axons to different muscles based upon specific target identity, likely resulting from the expression of different cell surface molecules. One interesting example is *unplugged*, a zebrafish homologue of MuSK (Zhang *et al*, 2004). Loss-of-function of a splice variant of *unplugged* (SV1) expressed by adaxial cells results in severe axon pathfinding defects. The formation of neuromuscular junctions requires interactions between the muscle cell surface proteins MuSK (Kim and Burden, 2008) and Rapsyn (Gautam *et al*, 1995) which pre-pattern acetylcholine receptors (AChR) on the surface of muscle fibres into a centralised domain, independent of nerve contact (Yang *et al*, 2001). In zebrafish, it has been proposed that Wnt signalling activates MuSK to create a centralised muscle domain that defines axon pathfinding and clustering of AChRs (Jing *et al*, 2009).

These different aspects of muscle development require careful co-ordination and tight control. Unsurprisingly, many different signalling pathways have been implicated in the regulation of muscle development, with many of them seemingly multipurpose. For example, Hedgehog signalling is known to play a role in differentiation (Feng *et al*, 2006) general specification of muscle cells and fibre-type switching (reviewed in Ingham and Kim, 2005) and, indirectly, elongation of fast muscle cells (Peterson and Henry, 2010). These signalling pathways may also be partially redundant or overlapping, for example Hedgehog and FGF signalling regulating differentiation (Coutelle *et al*, 2001; Groves *et al*, 2005). Some may also be interpreted in different contexts, for instance, WNT signalling is a directional cue for the elongation of chick myocytes (Gros *et al*, 2008), is also necessary for myogenesis in the limb (Geetha-Loganathan *et al*, 2005), and is proposed to regulate motor axon pathfinding (Jing *et al*, 2009).

The nature of the loss-of-function of both Jamb and Jamc immediately suggested that both proteins play a critical role in myoblast fusion *in vivo* (Chapter 6). For this reason, I will discuss myoblast fusion in greater detail below.

1.3 Current opinions in myoblast fusion

Myoblast fusion has been best characterised in *Drosophila*, through extensive genetic screens and careful morphological description. There are several recent reviews describing the state of the art (Rochlin *et al*, 2009; Haralalka and Abmayr, 2010). Vertebrate myoblast fusion is somewhat less well described and implicitly assumed to be conserved with respect to regulation, mechanism and the molecules involved. There are similarities between the vertebrate and invertebrate models, but

not much has been made of apparent differences. Here I will describe the process of myoblast fusion in *Drosophila* and compare that to vertebrate models.

The musculature of the *Drosophila* larva abdomen segments, A2-A7, is composed of a repeating pattern of 30 morphologically distinct muscles, each a single syncytial fibre (Bate, 1990). Each of these muscles is pre-figured by a founder cell, specified within *twist, sloppy paired*-expressing somatic muscle mesoderm cells by *Notch*-mediated lateral inhibition (Carmena *et al*, 1995). This rare sub-population of myoblasts migrate to different positions within the external layers of each hemisegment (Bate, 1990), express a different set of transcription factors (reviewed in Baylies *et al*, 1998) and fuse to fusion competent myoblasts (FCMs; Ruiz-Gomez *et al*, 2000; Bour *et al*, 2000; Strünkelnberg *et al*, 2001;) to form elongated muscle fibres that make contact with tendon cells of the epidermis (Steigemann *et al*, 2004; Schnorrer *et al*, 2007) and are subsequently innervated (Bate, 1990). FCMs are the more numerous sub-population of myoblasts that are identified by expression of *lameduck* (Ruiz-Gomez *et al*, 2002). Those FCMs nearest to founder cells are the first to fuse to the muscle precursors, with more internal FCMs migrating through the somatic mesoderm later (Beckett and Baylies, 2007). The process of myoblast fusion is iterative, with each muscle containing between 2 to 24 nuclei after the end of fusion at stage 15 (Bate, 1990).

The founder cells and FCMs recognise and adhere to each other through the cell surface proteins *roughest* (*rst*), *dumbfounded/kirre* (*duf*), *hibris* (*hbs*) and *sticks-and-stones (sns*; Galleta *et al*, 2004, Artero *et al*, 2001). The current paradigm posits that the founder cell-specific receptor Duf interacts with the FCM-specific receptor SNS to localise the intracellular molecular machinery necessary for fusion, to a specific site within the membrane. This results in actin-rich foci (Richardson *et al*, 2007) surrounded by a protein-dense structure, termed the fusion-restricted myogenic adhesion structure (FuRMAS; Kesper *et al*, 2007). Following this, small fusion pores occur at the site of fusion and expand over time (Doberstein *et al*, 1997). These processes require Rac signalling and actin cytoskeletal rearrangement via the Arp2/3 complex (Richardson *et al*, 2007), to regulate vesicle trafficking to and from the site of fusion (Kim *et al*, 2007; Estrada *et al*, 2007). The exact role of *roughest* and *hibris* is uncertain, as both are partially redundant with *dumbfounded* and *sticks-and-stones* (Strünkelnberg *et al*, 2001; Artero *et al*, 2001). *roughest* is expressed in both founders and FCMs (Strünkelnberg *et al*, 2001), whilst *hibris* is only expressed in a few FCMs (Artero *et al*, 2001). The functional differences between the paralogues *roughest* and *dumbfounded*, *hibris* and *sticks-and-stones*, likely result from

differences in the cytoplasmic domains of the proteins (Strünkelnberg *et al*, 2001; Shelton *et al*, 2009).

The critical receptor:ligand pair for recognition and adhesion has been identified in *Drosophila* – deletion of the partially redundant *rst*/*duf* or *sns* results in a complete block of myoblast fusion (Strünkelnberg *et al*, 2001; Bour *et al*, 2000). The FCMs persist as unfused, rounded cells that express myosin heavy chain (MyHC) and are eventually cleared by macrophages. In contrast, the founder cells elongate to form mononucleate muscle fibres. The mutant embryos subsequently die as they are unable to break free from the vitelline membrane.

No such receptor:ligand pair has been identified in any other model system. The role of vertebrate orthologues of *rst*/*duf* and *sns* have often been hinted at as drawing clear parallels between invertebrate and vertebrate myoblast fusion, but yet the applicability of this paradigm remains to be definitively proven. Loss-of-function of *kirrel,* a homologue of *rst*/*duf* in zebrafish, results in a severe myoblast fusion phenotype (Srinivas *et al*, 2007). It is unclear if the phenotypic consequences of morpholinos targeted against *kirrel* are similar to those seen in *Drosophila* mutants. It is also unclear if Kirrel acts homophilically or interacts with other receptors (see Chapter 8). The evolutionary relationship between *kirrel*, *duf* and *rst* has also yet to be fully explored. No muscle phenotype has been reported for any of the mammalian *duf* homologues (Donoviel *et al*, 2001; Tang *et al*, 2010). The *sns* homologue *nephrin* has been implicated in myoblast fusion in mouse and zebrafish, largely because of its orthology. Its role in myoblast fusion, if any, has been very poorly characterised with respect to expression or function (Sohn *et al*, 2009). Other cell surface molecules such as CDO (Cole *et al*, 2004), cadherins (Charlton *et al*, 1997; Hollnagel *et al*, 2002), neogenin and netrin (Bae *et al*, 2009) and NCAM (Charlton *et al*, 2000) have all been suggested to play a role in myoblast fusion, but none seem to have a detectable effect on myoblast fusion in mouse embryos.

In summary, it is uncertain if vertebrate myoblast fusion requires the specification of a founder cell population that prefigures muscle pattern. Identification of critical cell surface molecules that are relevant to all vertebrate models would be of great assistance to elucidating the mechanism and regulation of fusion within the developing embryo.

1.4 Zebrafish as a model for vertebrate myogenesis

It is not surprising that many cell surface molecules have been implicated in muscle development, given the many possible important roles they may play. The

predominant functional annotation in vertebrate studies, however, is mild reduction in myoblast fusion, often only determined in cell culture after little or no noticeable effect in animal models. There is little ability to discern between the subtly different physiological functions of cell surface proteins in cell culture, many of which may play partially redundant roles, for example, cadherins (Krauss, 2010). In mouse knockout models, no muscle phenotype has been described for cadherins (Charlton *et al*, 1997; Hollnagel *et al*, 2002), even M-cadherin which is almost exclusively expressed in developing muscle (Hollnagel *et al*, 2002). In contrast, knockdown of M- and N-cadherin in zebrafish has been shown to be essential for the migration of slow muscle fibres through the myotome (Cortés *et al*, 2003). These genes are unlikely to play exactly the same role in mammals, where slow and fast fibre types are not spatially separated (Hämäläinen and Pette, 1995), but this example does highlight the power of the zebrafish as a model system for functional analysis of genes involved in muscle development.

Use of the zebrafish model has great potential to pick apart the subtle functions of cell surface proteins during muscle development, because of a unique combination of factors. Zebrafish embryos develop externally, are translucent and available in large numbers from a single mating event. Very rapid, easy to perform, loss-of-function experiments are possible through the use of targeted morpholinos, though these reagents need to be used with extreme care to avoid spurious results. In addition, the bulk of individual zebrafish is made up of axial muscle tissue, repeated in a stereotypical pattern along the length of the animal. These elements make it very easy to visualise and quantify even subtle muscle defects caused by loss-of-function of cell surface proteins *in vivo*, and in time-lapse with transgenic reporter lines.

There are technological drawbacks currently, particularly with respect to obtaining targeted, heritable mutants in genes of interest, but improvements to loss-of-function methods are in progress (see Chapter 6). Researchers using the zebrafish as a model system should also be aware of the genetic complications resulting from an ancient genome duplication event in teleosts (see Chapter 3). The effects of gene duplication on gene orthology and function, such as sub-functionalisation, have to be assessed in each case. Nevertheless, the ease of use and powerful imaging capabilities make the zebrafish an attractive model for further in-depth study of muscle development.

In summary, there is no known developmental function for JAM-B and JAM-C, though they are known to interact and are co-expressed during development. The zebrafish is an attractive and powerful model to explore the possible functions of the

interaction between these proteins, particularly in the context of myogenesis. I determined that physical interaction between Jamb and Jamc is necessary and critical for normal muscle development. This work represents the first discovery of a vertebrate-specific receptor:ligand pair vital for myoblast fusion, opening up the possibility of a full understanding of the mechanism and regulation of the process in vertebrates.

Chapter 2

Materials and Methods

Summary

In this chapter I describe the methods used to identify and clone zebrafish *jam* paralogues; analyse homology and evolutionary relationships; characterize gene expression and protein localization; maintain, genotype and characterize *jamb* and *jamc* mutant fish; produce recombinant forms of zebrafish Jam proteins and test interactions between them using surface plasmon resonance.

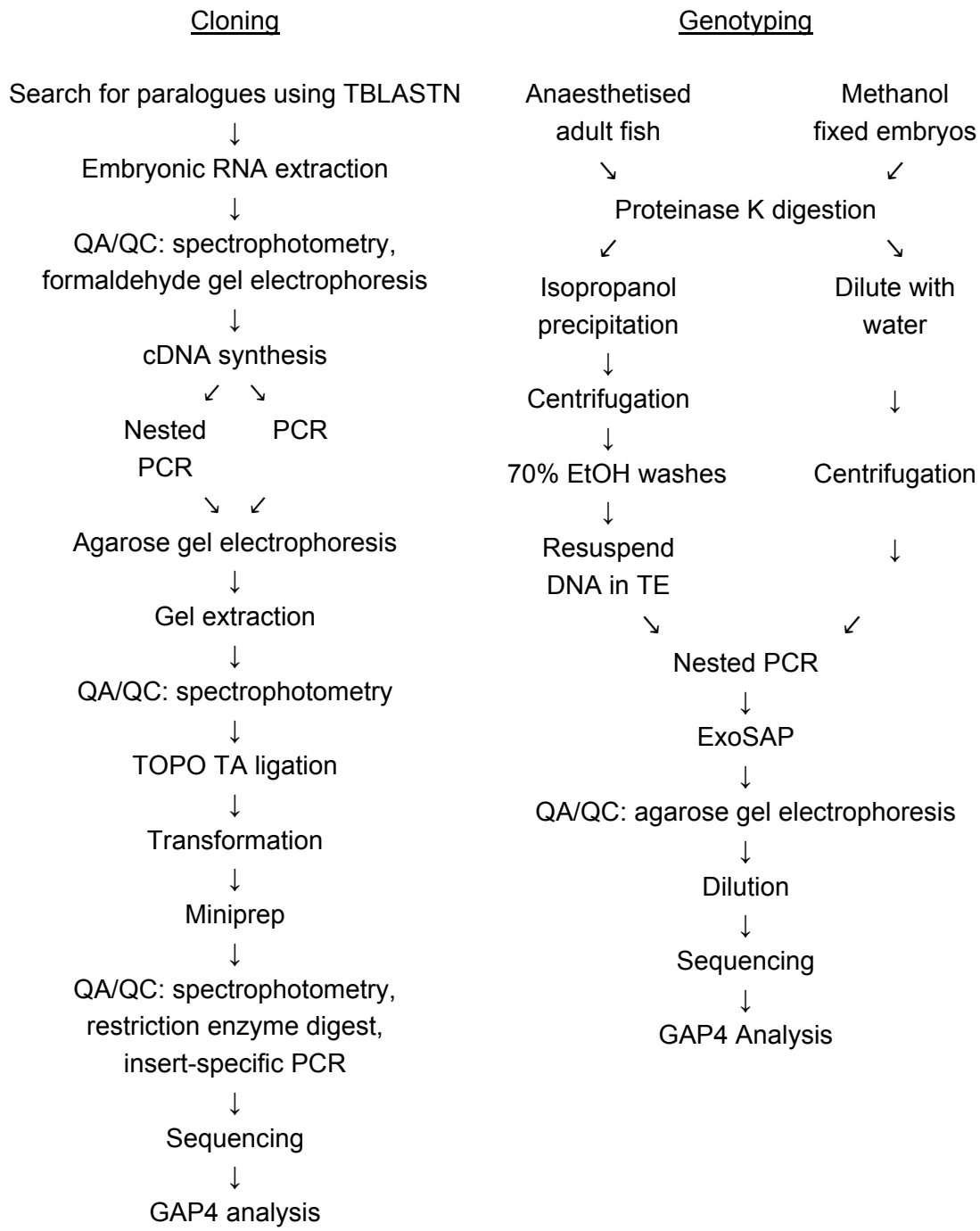

Figure 2.1 Flow diagram of cloning and genotyping methods.

Flow diagram of methods used to clone novel *jam* family paralogues and genotype zebrafish mutant adults and embryos, outlined in sections 2.1 and 2.2.

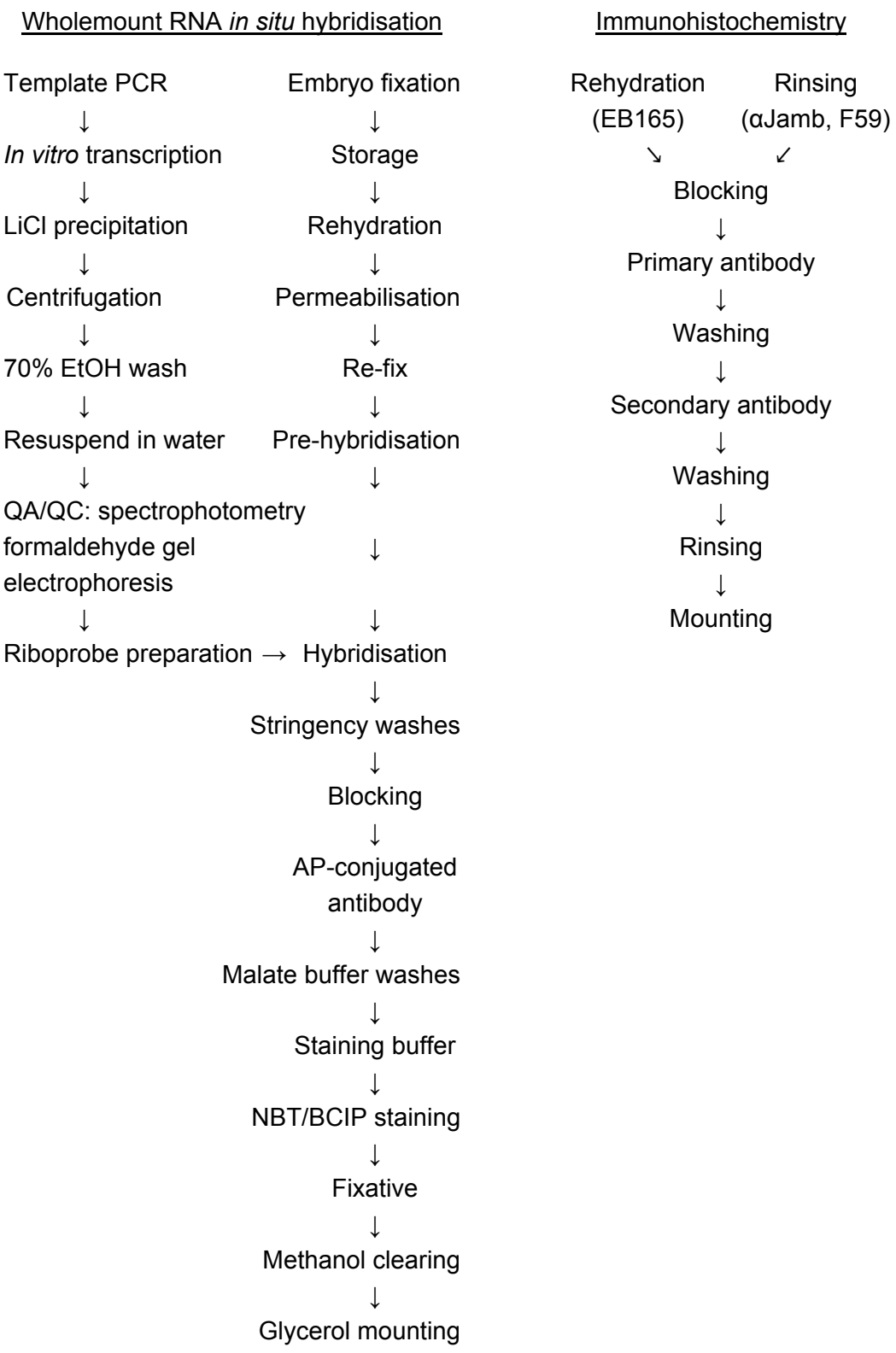

Figure 2.2 Flow diagram of RNA and protein expression detection methods.

Flow diagram of methods used to detect RNA and protein expression in wild-type and mutant embryos, outlined in section 2.3.

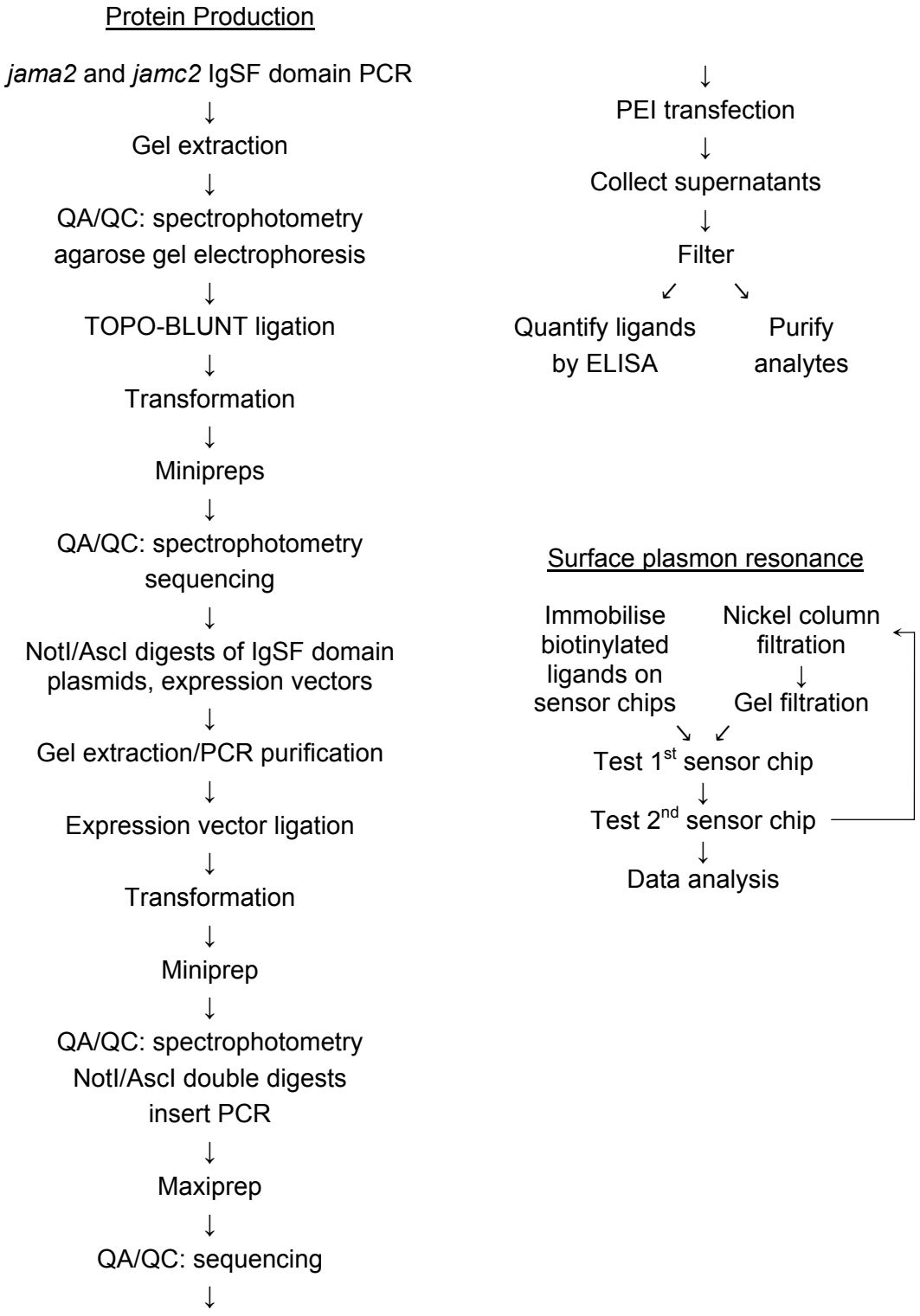

Figure 2.3 Flow diagram of protein production and biochemistry methods.

Flow diagram of methods used to produce recombinant Jam immunoglobulin superfamily domains and test biochemical interactions between the proteins, outlined in section 2.6.

2.1 Cloning and homology

Novel zebrafish *jam* family genes, *jama2* and *jamc2*, were identified by TBLASTN searching in the zebrafish genome sequence (Zv6; Hubbard *et al*, 2007) at Ensembl (www.ensembl.org) using the primary amino acid sequence of the extracellular immunoglobulin domains of Jama and Jamc. Both genes were subsequently cloned through 3′ RACE and RT-PCR (see below and figure 2.1).

2.1.1 Cloning of *jama2* by 3′ RACE

The full-length sequence of *jama2* was subsequently determined by sequencing of cloned 3′ RACE products amplified from cDNA prepared from RNA extracted from 24 hours post fertilisation (h. p. f.) wild-type embryos, as follows:

Zebrafish embryonic RNA was extracted from approximately 30-50 wild-type embryos fixed in methanol, using the Nucleospin RNA II kit (Macherey-Nagal) according to the manufacturer's instructions. The RNA was assessed for purity and quantity by absorbance at 260 and 280 nm using a spectrophotometer and formaldehyde gel electrophoresis, described below (see section 2.1.3).

First strand cDNA was then synthesised from RNA using the SMART RACE kit (Clontech) as per manufacturer's instructions (+RT cDNA). A negative control synthesis without reverse transcriptase (-RT cDNA) was prepared in parallel.

Gene-specific nested 5′ primers (0511, 0512, 3565, 3566; table 2.1) and SMART RACE universal primers (0141 and 0142; table 2.1) were used to amplify *jama2* and a positive control, *igsf11*, by touchdown PCR with Advantage II Polymerase Mix (Clontech). The same reactions were performed in parallel using the negative control -RT cDNA preparation in place of the +RT cDNA template.

The PCR products were analysed by agarose gel electrophoresis, described below (see section 2.1.3). A single 1.5 kbp band, present only in the +RT cDNA nested PCR reaction, was purified from an agarose gel using the QIAquick Gel Extraction kit (QIAGEN) as per manufacturer's instructions. The purified product was assessed for quantity and quality by absorbance at 260 and 280 nm using a spectrophotometer.

The purified *jama2* 3′ RACE product was cloned into the pCR4-TOPO (Invitrogen) by incubation with different concentrations of the vector-topoisomerase complex. TOP10 chemically competent bacteria (Invitrogen) were transformed with each ligation reaction by preincubation on ice, followed by a 30 second heat shock at 42°C. The bacteria were allowed to recover in SOC media (2% tryptone, 0.5% yeast extract, 8.55 mM NaCl, 20 mM $MgSO_4 \cdot 7H_20$, 20 mM dextrose monohydrate;

Invitrogen) by shaking at 37°C, 200 r. p. m. for 1 hour, before plating onto pre-warmed LB agar plates containing kanamycin (50 µg/ml). Inoculated plates were incubated overnight at 37°C.

Colonies that had grown on the selective plates were counted to assess transformation efficiency: approximately 5.0 x 10^5 colony forming units. Six different colonies were transferred to 3 ml 2 x TY (1.6% tryptone, 1% yeast extract, 85.5 mM NaCl) cultures supplemented with kanamycin (50 µg/ml). The cultures were incubated at 37°C, 200 r. p .m. overnight.

Plasmids were purified from the overnight cultures using the QIAprep Miniprep Spin kit (QIAGEN) as per manufacturer's instructions. Each plasmid preparation was assessed for quantity and quality by absorbance at 260 and 280 nm using a spectrophotometer.

The ligated plasmids were tested for the correct insert by digestion of a small sample with the restriction enzyme EcoRI (NEB), used according to the manufacturer's instructions. Also, the vector insert was amplified from each plasmid by touchdown PCR using insert-specific primers (0142 and 3566; table 2.1). The restriction digests and PCR products were analysed by agarose gel electrophoresis. All plasmids contained an insert of expected size.

Each plasmid was sequenced by the Sanger Centre Small Sequencing Facility using the ABI PRISM big dye terminator cycle sequencing ready reaction kit according to the manufacturer's instructions, in an ABI 3730x1 automatic sequencer. Four primers (M13F, M13R, 3566, 0142; table 2.1) were used to direct sequencing of both strands of the plasmids.

The sequences from each successful sequencing reaction were aligned and compiled into a GAP4 database for analysis.

2.1.2 Cloning of *jamc2* by RT-PCR

The near-complete sequence of *jamc2* was determined by sequencing of PCR products from cDNA prepared using RNA extracted from 24 h. p. f. wild-type embryos (described above) as follows:

First strand synthesis of cDNA from extracted zebrafish RNA was performed using a T_{20}VN oligomer and Superscript III reverse transcriptase (Invitrogen). Negative control synthesis reactions without reverse transcriptase (-RT cDNA) were performed in parallel.

Different combination of *jamc2*-specific primers (3503, 3504, 3505, 3506, 3533; table 2.1) were then used in touchdown PCR reactions with Advantage II Polymerase

Mix (Clontech). Additional positive control primers directed against *ef1α* and *jamb* (3408, 3409, 3489, 3490; table 2.1) and an -RT cDNA template negative control were used in parallel reactions. The products were analysed by agarose gel electrophoresis.

The presumed full-length *jamc2* PCR product (3506 and 3533; table 2.1) was purified from an agarose gel, cloned into pCR-TOPO4 (Invitrogen), verified by EcoRI digestion and insert-specific touchdown PCR (3506 and 3533; table 2.1) and sequenced as previously described.

2.1.3 Gel electrophoresis of DNA or RNA

DNA samples were diluted with sample loading buffer (30% glycerol, 0.25% bromophenol blue, 0.25% xylene cyanol FF) and loaded onto 1.5% agarose, TAE-buffered (40 mM tris, 20 mM acetic acid, 1 mM EDTA) gels containing ethidium bromide (0.1 µg/ml). The samples were run through the gel with a current of 120 V for varying times, and visualised on a UV transilluminator (BIORAD).

RNA samples were diluted in sample loading buffer (30% formamide, 20% glycerol, 80 mM MOPS free acid, 20 mM sodium acetate, 8 mM EDTA, 2.5% formaldehyde, 0.2% bromophenol blue, pH 7) and loaded onto 1.5% agarose, formaldehyde-buffered (20 mM MOPS free acid, 5 mM sodium acetate, 1 mM EDTA, 0.7% formaldehyde) gels containing ethidium bromide (0.1 µg/ml). The samples were run through the gel with a current of 120 V for varying times and visualised on a UV transilluminator (BIORAD).

2.1.4 Homology and molecular genetics analysis

Amino acid sequences for mouse and human JAM-A, JAM-B, JAM-C, ESAM, CAR, A33 and JAM4 were retrieved from the NCBI database (www.ncbi.nlm.nih.gov). Alignments of nucleotide and amino acid sequences were performed using ClustalW (www.ebi.ac.uk/ClustalW). A neighbour-joining tree was drawn from this alignment using the Poisson Distribution model in MEGA (v3.1; Kumar *et al*, 2004) using 500 bootstrap replicates.

Signal peptide cleavage sites and transmembrane domains were predicted from amino acid sequences using SignalP (v3.0; Bendsten *et al*, 2004) and TMHMM (v2.0; Krogh *et al*, 2001).

A detailed comparison of *jamc* and *jamc2* genomic loci was performed using zPicture, an interactive Blastz web tool (zpicture.dcode.org; Ovcharenko *et al*, 2004), and zebrafish genome sequence data (Zv6; Hubbard *et al*, 2007).

2.2 Zebrafish husbandry and genotyping

2.2.1 General husbandry and embryo collection

Embryos heterozygous for the *jamb*^{HU3319} allele were kindly provided by the Dr. Edwin van der Cuppen of the Hubrecht Laboratory, Utrecht, Netherlands. Embyros heterozygous for the *jamc*^{sa0037} allele were kindly provided by the Wellcome Trust Sanger Institute Zebrafish Mutation Resource, Hinxton, Cambridge. The mutants were inbred to generate homozygous lines, and maintained as outcrossed heterozygous lines. All fish were maintained according to Institute and Home Office regulations.

Fixed *prdm1*^{tp39} embryos were kindly provided by Dr Stone Elworthy.

For breeding, male and female pairs were put into breeding tanks with a mesh divider designed to separate adults from eggs released during mating. Mating pairs spawned after light cycle activation at 8.30 AM. Any embryos were collected into egg water (0.18 g/l sea salt, 2 mg/l methylene blue) and raised at 28°C. Embryos were staged accordingly to morphology, as outlined by Kimmel *et al* (1995).

2.2.2 Genotyping zebrafish adults and embryos

To genotype adult and embryonic zebrafish I extracted DNA from amputated fin tissue or whole embryos, respectively, using a proteinase K digestion method, followed by nested PCR and sequencing (figure 2.1).

Zebrafish adults, no younger than three months old, were anaesthetized in 0.02% 3-amino-benzoic acid ethyl ester (tricaine), before amputation of the tip of the tail fin. Adult fish were subsequently placed in individual tanks until genotyping was completed. Fin tissue was digested in 100 µg/ml of proteinase K (Invitrogen) in lysis buffer (100 mM tris-HCl, 200 mM NaCl, 0.2% SDS, 5 mM EDTA, pH 8) at 55°C overnight, followed by vortexing to ensure disruption of the tissue. The proteinase was inactivated by incubation of the sample at 80°C for 30 min. DNA was purified from the lysed tissue by precipitation upon the addition of 300 µl isopropanol. After repeated inversion of the sample to ensure mixing, the precipitant was collected into a pellet by centrifugation for 40 minutes at high speed (96 well plates: 3220 x *g*; eppendorf tubes: 16100 x *g*). Precipated DNA was washed twice with 70% ethanol, allowed to dry and then dissolved in 500 µl TE (10 mM tris-HCl, 1 mM EDTA, pH 8).

Whole zebrafish embryos were fixed at an appropriate stage in methanol overnight at -20°C. Individual embryos were placed in each well of a 96-well plate and any remaining methanol allowed to evaporate. The embryos were then digested

in 25 µl of 1.5 mg/ml proteinase K in TE for at least 4 hours at 55°C. The enzyme was inactivated at 80°C for 10 minutes and samples allowed to cool before diluting with 75 µl sterile water. Before use of the samples in PCR reactions, any undigested debris was collected at the bottom of each well by centrifugation.

Purified adult DNA or digested embryos were subsequently used in nested touchdown PCR reactions using primers specific to exon 3 of *jamb* (B3-1, B3-2, B3-3, B3-4; table 2.1) or exon 5 of *jamc* (C5-1, C5-2, C5-3, C5-4; table 2.1). The PCR products were treated with exonuclease I (0.1 units/µl, NEB), to remove excess primers, and shrimp alkaline phosphatase (0.05 units/µl, NEB) to dephosphorylate PCR products, in buffer (20 mM tris-HCl pH 8, 10 mM $MgCl_2$) at 37°C for 1 hour. The enzymes were inactivated at 80°C for 20 minutes. Each PCR reaction was checked for quality by agarose gel electrophoresis and then diluted 1:2 with sterile water. The nested primers (B3-2, B3-3 and C5-2, C5-3) have M13 forward and reverse sequence tails, allowing all products to be sequenced with generic primers (M13F and M13R; table 2.1) as previously described. The sequence data was compiled into a GAP4 database for analysis.

2.3 Protein and RNA expression detection

2.3.1 Embryo fixation

Embryos collected from mating pairs were allowed to develop to an appropriate stage according to their morphology, as outlined by Kimmel *et al* (1995) and subsequently fixed according to use. For immunohistochemistry with Jamb (Everest Biotech), F59 (Developmental Studies Hybridoma Bank, University of Iowa, U. S. A.) antibodies or Alexa-488 conjugated phalloidin (Molecular Probes), embryos were fixed with 4% paraformaldehyde in phosphate-buffered saline (PBS; 135 mM NaCl, 1.3 mM KCl, 3.2 mM Na_2HPO_4, 0.5 mM KH_2PO_4, pH 7.4) at room temperature for 2 hours or overnight at 4°C. For immunohistochemistry with EB165 antibody (Developmental Studies Hybridoma Bank) or wholemount RNA *in situ* hybridisation, embryos were fixed with 4% paraformaldehyde in PBS at 4°C for 15-30 minutes and then stored in methanol at -20°C overnight or longer for storage.

2.3.2 Wholemount RNA *in situ* hybridisation

The expression patterns of *jam* family genes during development were characterised by wholemount RNA *in situ* hybridisation (figure 2.2) using antisense riboprobes transcribed from the immunoglobulin superfamily domain-encoding regions of each gene. The *kirrel* riboprobe was transcribed from the extracellular domain-encoding region, which had been cloned into protein expression vectors

previously.

Antisense hapten-labelled riboprobes were prepared by *in vitro* transcription of PCR templates amplified from expression plasmids described below (see 2.6.1), using touchdown PCR and flanking vector specific primers (3268 and 3269; table 2.1). The antisense primer (3268) contains a T7 polymerase binding site. PCR products were analysed by agarose gel electrophoresis, then purified using QIAquick PCR Purification kit (QIAGEN) as per manufacturer's instructions. The purified templates were assessed for quality and quantity by absorbance at 260 and 280 nm using a spectrophotometer. The templates (50 ng/µl) were transcribed using T7 polymerase (Roche; 1 units/µl) and a NTP labelling mix spiked with digoxygenin-11-UTP (1 mM ATP, CTP, GTP, 0.65 mM UTP, 0.35 mM digoxygenin-11-UTP) in transcription buffer (Roche; 40 mM tris-HCl, 6 mM $MgCl_2$, 10 mM dithiothreitol, 2 mM spermidine) with RNAseOUT ribonuclease inhibitor (Invitrogen; 2 units/µl) for 1 – 2 hours at 37°C. Transciption was stopped by addition of DNAseI (1 units/ µl) to degrade the template and ethylenediaminetetraacetic acid (EDTA; 16 mM). Transcribed riboprobes were precipitated used lithium chloride (0.1 M) and cold ethanol. The samples were inverted to ensure mixing, incubated at -80°C for 30 minutes then the precipitated RNA was collected by centrifugation at 13000 x *g* at 4°C for 15 minutes. The pellet was washed with 70% ethanol and allowed to partially dry in air before resuspension in diethylpyrocarbonate-treated (DEPC) water. The riboprobes were assessed for quality and quantity by formaldehyde gel electrophoresis and absorbance at 260 and 280 nm using a spectrophotometer. Riboprobes were stored at -80°C until use.

Wholemount RNA *in situ* hybridisation was performed essentially as described in Thisse and Thisse (2007). Briefly, embryos were rehydrated through a methanol series, rinsed in PBST (PBS, 0.1% tween-20), and permeabilised in proteinase K (10 µg/ml in PBST) according to stage: shield – 1 minute, 1-10 somites – 2 minutes, 21 somites – 8 minutes, 24 h. p. f. – 10 minutes, 48 h. p. f. – 25 minutes. Embryos were rinsed in PSBT then fixed in 4% paraformaldehyde in PBS for 20 minutes, rinsed in PBST again and then placed in hybridisation buffer (50% formamide, 5 x SSC, 50 µg/ml heparin, 0.5 mg/ml RNAse free torula yeast tRNA, 10 µM citric acid, 0.1% tween-20, pH 6; 5 x SSC: 75 µM sodium citrate, 750 µM NaCl) for 5 minutes at 68°C. The buffer was replaced with fresh prewarmed hybridisation buffer and left to incubate at 68°C for two hours. Riboprobes were prepared before use by heating 100 ng of each probe in 100 µl of hybridisation buffer to 80°C for 5 minutes, followed by storage on ice. Hybridisation buffer was removed from the embryos, without allowing

them to touch the air, and replaced with the prepared riboprobes and then incubated at 67°C overnight. The riboprobe was then removed and embryos were incubated with pre-warmed 50% formamide, 2 x SSCT (2 x SSC, 0.1% tween-20) for 30 minutes at 68°C, twice, then pre-warmed 2 x SSCT for 15 minutes at 68°C, then pre-warmed 0.2 x SSCT for 30 minutes at 68°C, twice. The embryos were placed at room temperature, rinsed in malate buffer (0.1 M maleic acid, 0.15 M NaCl, pH 7.5) then blocked for two hours in 2% Boeringher blocking reagent in malate buffer on a rotating wheel at room temperature. After blocking, the embryos were incubated with an alkaline phospatase-conjugated anti-digoxygenin antibody (Roche) diluted 1:5000 in 2% blocking solution overnight at 4°C on a rotating wheel. The antibody solution was removed and embryos were washed six times with malate buffer for 20 minutes, rinsed with freshly prepared staining buffer (100 mM tris-HCl, 100 mM NaCl, 50 mM $MgCl_2$, pH 9.5) then incubated with nitro blue tetrazolium chloride (NBT) and 5-bromo-4-chloro-indoyl phosphate (BCIP) in staining buffer (Roche; 0.4 mg/ml NBT, 0.19 mg/ml BCIP). The colour development was stopped, as required, by rinsing in PBST and fixation in 4% paraformaldehyde for 20 minutes at room temperature or overnight at 4°C. The embryos were rinsed with PBST, cleared through a methanol series (25% – 100% – 25%) rinsed with PBST and mounted in glycerol, beginning at 50% glycerol PBST and gradually transferred to 100% glycerol. Embryos were then stored at 4°C.

2.3.3 Immunohistochemistry

Immunohistochemistry was used to characterise the subcellular localisation of Jamb protein and the differentiation of fast and slow muscle in mutant embryos (figure 2.2). Prior to commencement of this project, a polyclonal antibody was raised against the recombinant extracellular domain of Jamb in goats, tested for activity against Jamb and Jamc by enzyme-linked immunosorbent assay (ELISA) and then subsequently affinity purified by Everest Biotech.

Fixed embryos were rinsed in PBSTri (phosphate buffered saline and 1% triton X-100) and then incubated in a blocking solution of 10% normal donkey serum in PBSTri for 2-3 hours at room temperature on a rotating wheel. Embryos were then incubated in anti-Jamb antibody, diluted 1:4 and preincubated in blocking solution, at 4°C on a rotating wheel, followed by six, 20 minute washes with PBSTri. The primary antibody was detected by either Alexa-488 or Alexa-568-conjugated anti-goat secondary antibody raised in donkeys (Molecular Probes), diluted 1:1000 and pre-incubated in blocking solution, overnight at 4°C on a rotating wheel. The embryos were washed six times for 20 minutes in PBSTri, then rinsed in PBS and mounted

in SlowFade Gold with 4',6-diamidino-2-phenylindole (DAPI; Molecular Probes).

Slow muscle-specific myosin heavy chain (sMyHC) was detected with the mouse monoclonal antibody F59 (Developmental Studies Hybridoma Bank) using the same protocol, with the exception of blocking with 10% normal goat serum in PBSTri, dilution of the antibody by 1:200 in blocking solution, an Alexa-488 or Alexa-568-conjugated anti-mouse antibody raised in goats (Molecular Probes) diluted 1:1000 in blocking solution.

Fast muscle-specific myosin heavy chain (fMyHC) was detected with the mouse monoclonal antibody EB165 (Developmental Studies Hybridoma Bank) as with the F59 antibody, with the exception that the methanol-fixed embryos are rehydrated into PBS.

F-actin was detected by Alexa-488-conjugated phalloidin (Molecular Probes), diluted 1:40 – 1:80 in PBSTri and incubated for one hour at room temperature on a rotating wheel, rinsed in PBS and mounted in SlowFade Gold with DAPI (Molecular Probes).

2.3.4 Microscopy and image processing

Images of wholemount RNA *in situ* hybridisation embryos were taken using either a Leica MZ16FA dissecting microscope or a Zeiss AXIO Imager M1 microscope with a Zeiss AxioCam HRc digital camera and Zeiss AxioVision (v4.5) software. Images of wholemount fluorescent immunohistochemistry or mRFP-labelled embryos were captured using either a Zeiss Axioplan 2 microscope with a Hamamatsu ORCA-ER digital camera and Improvision Volocity (v4.2.0) software, or a Leica TCS SP5/DM6000 confocal microscope with Leica Application Suite Advanced Fluorescence (v2.0.0 build 1934) software.

Images were globally adjusted for dynamic range and resampled to a consistent resolution of 300 dots per inch. Colour images of wholemount RNA *in situ* embryos were corrected for colour balance. All figures and image processing were performed using Adobe Photoshop CS2 (v9.0).

2.4 Characterisation of loss-of-function mutants

2.4.1 Morpholino injections

1- and 2- cell stage embryos were injected with approximately 4 nl of translation blocking morpholinos (approximately 200 μM, 5-7.5 ng per embryo) diluted in sterile water with 0.1% phenol red (Sigma). Translation blocking morpholino sequences were as follows: *jamb*: GCA CAC CAG CAT TTT CTC CAC AGT G; *jamc*: TTA ACG

CCA TCT TGG AGT CGG TGA A.

2.4.2 Labelling cell membranes with membrane-targeted RFP

To label all cell membranes, embryos were injected with mRNA encoding red fluorescent protein (RFP) fused to two N-terminal Lyn kinase myristolation sites. Briefly, capped membrane-targeted red fluorescent protein (mRFP) mRNA was transcribed from a NotI linearised plasmid, kindly provided by Dr Mariella Ferrante, using the mMessage mMachine kit (Ambion) and SP6 polymerase. Transcription was stopped by addition of stop solution (0.5 M ammonium acetate, 10 mM EDTA) and the template was degraded by DNaseI for 30 minutes at 37°C. Transcribed mRNA was purified by addition of 1 volume of water saturated phenol/chloroform, mixing by inversion and centrifugation at high speed (13000 x *g*). The aqueous phase was mixed with 1 volume of chloroform followed by centrifugation (13000 x *g*). The mRNA was then precipitated from the aqueous phase with 1 volume of cold isopropanol, mixed by inversion and incubated at -20°C for 30 minutes. The mRNA was collected into a pellet by centrifugation (13000 x *g*) for 30 minutes at 4°C, then washed with 70% ethanol, allowed to partially dry in air, resuspended in DEPC-treated water and stored frozen at -80°C. 1-2 cell stage embryos were microinjected with approximately 4 nl of mRNA (25 ng/µl) diluted in sterile water, 0.1% phenol red (Sigma-Aldrich). The injected embryos were fixed with 4% paraformaldehyde overnight at 4°C, rinsed with PBSTri, mounted in SlowFade Gold with DAPI (Molecular Probes) and observed by confocal microscopy.

2.4.3 Quantification of fast muscle fibres

Wild-type and mutant embryos labelled with mRFP (see 2.4.2) were fixed at 24, 32 or 48 h. p. f. in 4% paraformaldehyde, overnight at 4°C. Fixed embryos were treated with Alexa-488-conjugated phalloidin and mounted in SlowFade Gold with DAPI (see 2.3.3). Z-stacks of confocal microscopy images were taken between myotomes 10-15 of mRFP, Alexa-488-conjugated phalloidin-labelled embryos. Optical cross-sections were computed from the microscopy data using Leica Application Suite Advanced Fluorescence software. Fibres were manually counted in each cross-section; superficial slow muscle fibres were excluded from analysis. Statistical significance between wild-type and mutant fibre counts was determined by one-tailed Student's t-test, modified to take unequal sample size and variance into account:

$$t = \frac{\bar{X}_1 - \bar{X}_2}{s_{\bar{X}_1 - \bar{X}_2}}; \quad s_{\bar{X}_1 - \bar{X}_2} = \sqrt{\frac{s_1^2}{n_1} + \frac{s_2^2}{n_2}}$$

and degrees of freedom are calculated by:

$$d.f. = \frac{(s_1^2/n_1 + s_2^2/n_2)^2}{\frac{(s_1^2/n_1)^2}{(n_1 - 1)} + \frac{(s_2^2/n_2)^2}{(n_2 - 1)}}$$

where $\bar{X}_i$ is the mean, s_i is the standard deviation and n_i is the number of embryos in the i-th population.

2.4.4 Acridine orange assay

Dechorionated wild-type and mutant embryos were incubated in staining solution (17 µg/ml acridine orange, 0.18 g/l sea salt, 50 units/ml penicillin, 50 µg/ml streptomycin) for 30 minutes in the dark at room temperature. The embryos were washed with buffer (0.18 g/l sea salt, 50 units/ml penicillin, 50 µg/ml streptomycin) and analysed with a fluorescent dissecting microscope.

2.5 Transplant experiments

Transplants were performed essentially as described by Xu *et al* (2008). Briefly, 1-2 stage donor embryos were injected with lysine-fixable fluorescein or rhodamine labelled dextran (10000 Da, 1% in sterile water; Molecular Probes). Donor and host embryos were immobilised in 2% methylcellulose (Sigma) on glass slides. Fluorescently-labelled donor cells were then transplanted into the marginal cells of unlabelled host embryos between high/sphere to approximately 30% epiboly stages. Transplanted embryos were maintained in embryo media supplemented with penicillin (50 units/ml) and streptomycin (50 µg/ml), fixed in 4% paraformaldehyde for 2 hours at room temperature, washed several times with PBSTri, mounted in SlowFade Gold with DAPI (Molecular Probes) and analysed by confocal microscopy.

2.6 Protein production and biochemistry

To test the biochemical interactions amongst Jam family proteins systematically, recombinant immunoglobulin superfamily domains of each protein were produced in mammalian cell culture and tested for interaction through surface plasmon resonance (figure 2.3).

2.6.1 Expression vectors

Jam family immunoglobulin superfamily domains, including the native signal peptide, were cloned into expression vectors based upon modified pTT vectors (Durocher *et al*, 2002) containing (figure 2.4): an in-frame CD4-d3&4 tag-encoding region, that improves the efficiency of protein production and is detectable by the monoclonal antibody OX68 (Brown and Barclay, 1994); either a hexa-histidine tag (6-

His) or a peptide substrate for a biotinylation enzyme, BirA; an Epstein-Barr virus origin for episomal replication of the plasmid; and regulatory elements (cytomegalovirus promoter, SV40 polyA signal). This had previously been performed for *jama*, *jamb*, *jamc* and *jamb2*.

Briefly, the immunoglobulin superfamily domains of *jama2* and *jamc2* were amplified from 3′ RACE and RT-PCR clones, described previously (see 2.1.1 and 2.1.2) by touchdown PCR using primers containing NotI and AscI restriction enzyme recognition sites (3595, 3596, 3597, 3598; table 2.1) and a proof-reading polymerase, Advantage II Polymerase Mix (Clontech). The PCR products were analysed by gel electrophoresis. Single bands corresponding to the predicted size were purified using QIAquick Gel Extraction kit (QIAGEN) as per manufacturer's instructions, and assessed for quantity and quality by spectrophotometry. The PCR products were ligated to pCR-BLUNTII-TOPO (Invitrogen) as per maufacturer's instructions. The ligation products were used to transform chemically-competent bacteria. Transformed clones were selected for on LB agar plates containing kanamycin and grown in 3 ml cultures of 2 x TY media with kanamycin. The *jama2/jamc2* insert-containing plasmids were purified from the cultures using the QIAprep Miniprep Spin kit (QIAGEN) as per manufacturer's instructions, assessed for quality and quantity by spectrophotometry and sequenced using vector-specific primers flanking the insert site (M13F and M13R; table 2.1).

Both histidine-tag and biotin-tag expression vectors and sequence-verified *jama2* and *jamc2* subcloning pCR-BLUNTII plasmids were incubated with NotI and AscI restriction enzymes (NEB) according to manufacturer's instructions. The enzymes were heat inactivated and the cleaved DNA products purified using either QIAquick PCR Purification kit (for PCR products) or QIAquick Gel Extraction kit (for vectors; QIAGEN), quantified by spectrophotometry. Digested vector and PCR products were mixed in different ratios and incubated with T4 DNA ligase (NEB) in ligation buffer (50 mM tris-HCl, 10 mM $MgCl_2$, 1 mM ATP, 10 mM dithiothreitol, pH 7.5) overnight. Chemically-competent bacteria were transformed with the ligation products and positive clones selected on LB agar plates containing ampicillin. Several clones were used to inoculate 3 ml cultures of 2 x TY with ampicillin which were incubated overnight. The *jama2*/*jamc2* histidine-tag and biotin-tag plasmids were purified from the cultures using the QIAprep Miniprep Spin kit (QIAGEN) as per manufacturer's instructions, assessed for quality and quantity by spectrophotometry and then tested for the correct insert through NotI and AscI double digest and PCR using primers flanking the insert site (178, 180, 3534, 3538; table 2.1).

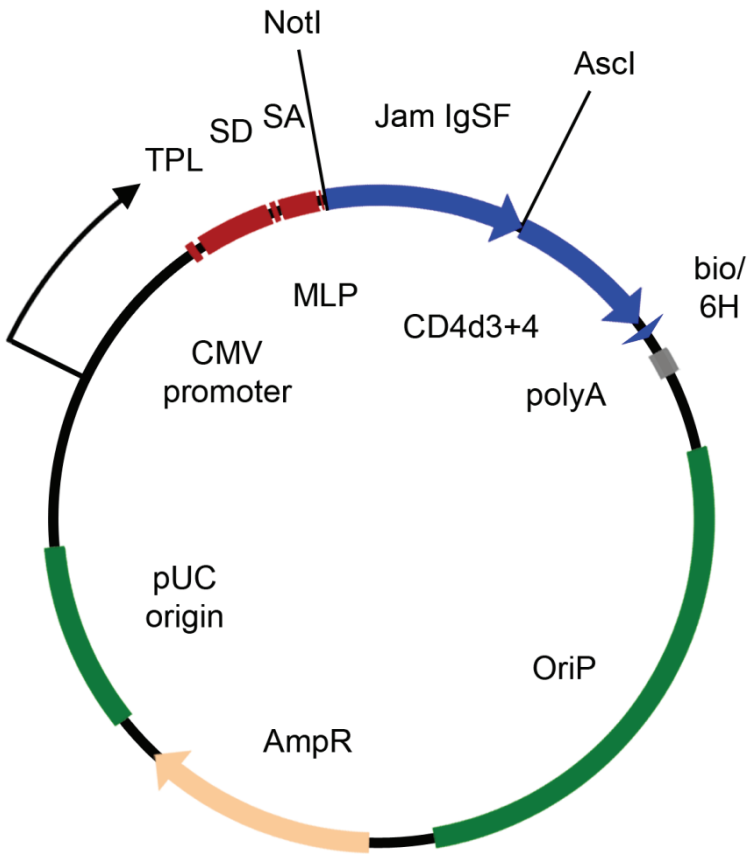

Figure 2.4 Genetic map of Jam protein expression vectors.

Diagram of genetic map of JAM protein expression vectors, drawn to scale. TPL – tripartite leader sequence, SD – splice donor, MLP – adenovirus major late promoter enhancer, SA – splice acceptor, NotI – NotI resctriction enzyme recognition site, Jam IgSF – sequence encoding Jam family immunoglobulin superfamily domains, AscI – AscI restriction enzyme recognition site, CD4d3+4 – CD4 domains 3 and 4 tag sequence, bio/6H – biotinylatable peptide tag or hexa-histidine tag sequence and stop codon, polyA – SV40 polyadenylation sequence, OriP – Epstein-Barr virus origin of replication, *AmpR* – β-lactamase gene, pUC origin – bacterial origin of replication, CMV promoter – cytomegalovirus promoter. Expression plasmid is approximately 6.5 kbp long without insert.

Verified *jama2* and *jamc2* expression vectors were used to transform chemically competent bacteria, which were selected for on ampicillin-containing LB agar plates. Single positive clones were used to inoculate 50 ml cultures of 2 x TY media supplemented with ampicillin. The cultures were incubated at 37°C with shaking at 200 r. p. m. overnight. Plasmids were purified from these cultures using the PureLink Hipure Plasmid Maxiprep kit (Invitrogen), quantified by spectrophotometry and diluted to 1 mg/ml in TE. The *jama2* plasmids were sequenced with vector-specific primers flanking the insert site (178 and 180; table 2.1). The *jamc2* plasmids were sequenced with insert-specific primers (3534 and 3538; table 2.1).

2.6.2 Transfection and purification

Protein production was based on an established system in our laboratory using polyethlyenimine-based (PEI) transfection of the HEK293E mammalian cell line (Durocher *et al*, 2002; Bushell *et al*, 2008). This cell line grows in suspension, allowing large quantities of protein to be produced from single transfections, and is kept under constant selection using G418 (also known as Geneticin) in order to maintain expression of the Epstein-Barr virus nuclear antigen 1 (EBNA1), allowing episomal replication of expression plasmids containing the Epstein-Barr virus origin. PEI forms polycationic complexes with the vector DNA, improving delivery of the plasmid to the cytoplasm of treated cells (Boussif *et al*, 1995).

HEK293E cells were maintained in Freestyle media (Invitrogen) supplemented with 1% fetal calf serum and G418 (50 µg/ml; Sigma), incubated at 37°C, 5% CO_2, 70% humidity with orbital shaking at 120 r. p. m. in baffled polycarbonate flasks (Corning). The cells were passaged to a density of 2.5 x 10^5 cells/ml in fresh media approximately every fourth day.

For transfection of histidine-tag expression vectors, cells were split into 50 ml of fresh media at a density of 2.5 x 10^5 cells/ml and allowed to recover for 24 hours. 50 µl of expression vector (1 mg/ml) was mixed with 110 µl linear 25 kDa PEI (1 mg/ml; Polyscience) in 2 ml of Freestyle media (without calf serum), left to rest for 5 minutes at room temperature, then added to the cell suspension. After six days of incubation, the supernatants are harvested from the cell suspension by centrifugation (3220 x *g*), filtered through a 0.22 µm filter and stored at 4°C. The same protocol was used for the transfection of biotin-tag expression vectors, with the exception of supplementing cell culture media with D-biotin (100 µM), and co-transfecting cells with a plasmid containing a secreted form of the *E. coli* biotin ligase *BirA* (5 µl, 1 mg/ml). The harvested supernatants were decanted into SnakeSkin dialysis tubing (molecular weight cutoff 10,000 Da; Thermo Scientific) and dialysed against PBS over 2-3 days

with approximately six changes of buffer, 25 to 30 L of buffer in total. The dialysed supernatants were filtered through a 0.22 µm filter and stored at 4°C.

Prior to use in surface plasmon resonance experiments, histidine-tag analyte proteins were purified from harvested supernatants using sepharose columns charged with nickel (HisTrap HP 1ml; GE Healthcare) and ÄKTAprime plus purification system (GE Healthcare) with real-time monitoring of flow-through absorbance at 280 nm. Briefly, a fresh nickel column was prepared by pre-elution with elution buffer (10 mM Na_2HPO_4, 10 mM NaH_2PO_4, 0.5 M NaCl, 0.4 M imidazole, pH 7.4, filtered and degassed under vacuum) and allowed to equilibrate in running buffer (10 mM Na_2HPO_4, 10 mM NaH_2PO_4, 0.5 M NaCl, 40 mM imidazole, pH 7.4, filtered and degassed under vacuum) at a flow rate of 1 ml/min. Meanwhile, imidazole (10 mM) and NaCl (100 mM) was added to approximately 150 ml of harvested supernatant, warmed to room temperature. The sample was passed over the equilibrated column at a flow rate of 1 ml/min, washed with 15 column volumes of running buffer and eluted with 10 column volumes of elution buffer. The eluant was collected into 0.5 ml fractions. The peak fractions were combined for gel filtration (between 1.5 and 2.0 ml of eluant).

Immediately before use in surface plasmon resonance experiments, the combined fractions from nickel column purification were further purified by gel filtration to remove aggregated and unfolded protein and buffer exchange. Briefly, the gel filtration column (GE Healthcare; Superose 6 prep grade resin, XK 16/70 column; 125 ml column volume, 62.6 cm bed height, 13,561 plates/m) was equilibrated with 2 column volumes of running buffer, HBS-EP (10 mM HEPES, 150 mM NaCl, 30 mM EDTA, 0.05% polyoxyethylenesorbitan 20, pH 7.4, filtered and degassed under vacuum) before applying the combined fractions to the column (approximately 1.5% of column volume), followed by washing with running buffer at a flow rate of 1 ml/min. Fractions (1.2 ml) were collected after approximately 45 ml of running buffer (equivalent to the void volume of the column) had passed through the column. The concentration of peak fractions was estimated by absorbance at 280 nm using *in silico* predicted extinction co-efficients (Gill and von Hippel, 1989).

2.6.3 Quantification by ELISA

Expression of recombinant proteins produced with a biotin ligase substrate peptide tag were quantified by ELISA using streptavidin-coated 96-well plates (Nunc Immobilizer) to capture biotinylated ligand and a monoclonal antibody that binds the CD4d3+4 tag, OX68.

Briefly, streptavidin-coated detection plates were rinsed briefly with PBST and

then blocked for at least 1 hour in 0.5% bovine serum albumin (BSA) in PBS. The detection plate was washed with PBS. Serial dilutions of each protein tested (in 0.2% BSA, PBS) were added to the detection plate in triplicate and left to incubate at room temperature for 30 minutes. The detection plate was washed repeatedly with PBS, followed by incubation with OX68 antibody (1:700, 0.2% BSA, PBS; Serotec) for 1 hour at room temperature. After repeated washing with PBS, the detection plate was incubated with alkaline phosphatase-conjugated anti-mouse antibody (1:5000, 0.2% BSA, PBS; Sigma) for 1 hour at room temperature. The detection plate was washed with PBS and then detected with *p*-nitrophenyl phosphate substrate (Sigma). Fluorescence was measured at 420 nm using a plate reader (PHERAstar plus; BMG Labtech).

2.6.4 Surface plasmon resonance

Surface plasmon resonance (SPR) was used to identify interactions between all six family members in both possible orientations of immobilised ligand and soluble analyte (figure 2.3).

Each biotinylated ligand was immobilised to a flow cell demarcated on a streptavidin-coated sensor chip (Series S Sensor Chip SA; GE Healthcare) in a molar equivalent amount to biotinylated CD4d3+4 immobilised to the control flow cell of the same chip (see Chapter 5, figure 5.3). The total amount of protein immobilised in each flow cell does not affect the kinetic parameters derived from collected data, but does influence the magnitude of response observed for an interaction. Both chips were stored in HBS-EP buffer at 4°C between experiments.

After purification, increasing concentrations of an analyte were passed over the flow cells of each of the two sensor chips at a high flow rate (100 µl/min), zebrafish physiological temperature (28°C), with real-time changes in surface plasmon resonance recorded at a frequency of 10 Hz using a Biacore T100 SPR machine (GE Healthcare). This process was repeated for each analyte.

2.6.5 Data analysis

An interaction was deemed to occur between the ligand and analyte tested if there was an increase in the response in the query flow cell during the injection phase, above that of the control flow cell tested in parallel. To determine this, the real-time SPR data of the control flow cell was subtracted from that of the query flow cell for each experiment, with correction for delay of sample delivery between flow cells.

In addition, the magnitude of change in response must increase with respect to rising analyte concentration, eventually reaching saturation, to demonstrate binding.

This was not possible for all interactions, likely because some interactions have a low K_D, *i.e.* to saturate binding required a higher concentration of analyte than was available.

To determine the dissociation rate constant (k_d) for each interaction, dissociation phase data for three mid-range concentrations of analyte were normalised and plotted as percent bound against time, with 100% bound at t = 0. The dissociation curves were averaged and then equations of the form:

$$y = Ae^{-k_d \cdot t}$$

were fitted to the data. The fitted curves demonstrated a R^2 > 0.9. The determined dissociation rate constants were used to calculate interaction half-lives, a concentration independent comparative measure:

$$t_{½} = \frac{\ln 2}{k_d}$$

Interactions in which a preliminary estimate of k_d was ≥ 6.9 were not considered for full analysis because of a lack of data. The half life of such an interaction is below the frequency of detection of the instrument used.

To determine if the quantified interactions were first order, the natural logarithm of the averaged normalised dissociation phase data for each interaction was plotted against time. First-order interactions are characterised by a straight line, with a gradient of $-k_d$.

All analysis was performed using Microsoft Excel 2007.

Table 2.1 Oligonucleotide sequences.

Name	Sequence
0141	CTA ATA CGA CTC ACT ATA GGG CAA GCA GTG GTA TCA ACG CAG AGT
0142	CTA ATA CGA CTC ACT ATA GGG C
0178	ACC TGG GGT ATC TGA AGG GT
0511	TGT ATG GAG GAG AGC ACA CAC GCA TCT
0512	AGT GGC AGT GGG CTC TAA AGG GGA AAA CAC
3268	GGA TCC TAA TAC GAC TCA CTA TAG GGA GGC CGT GAT GGA GGT CGA CGG CG
3269	ACA GGT GTC CAC TCC CAG GTC CAA G
3408	CCC CTG GAC ACA GAG ACT TCA TCA
3409	ACA CGA CCC ACA GGT ACA GTT CCA
3489	GTC AGC AGT CGC AAT CCT AAA GTG G
3490	TTT GTA CCA GGT GTA GAC GGC AGG T
3503	CTG GTG CTC TTC TAC TGG CTG TGT A
3504	AAC GCT TTC CCT GGT GCT CTT CTA C
3505	GCA TCC TCT TTC TTT ACC GAC CGG A
3506	GAT GAC GAA GGA GGA TTT GTG GCG A
3533	CTA AAC CTG CAT GTG AAA CAG CGG C
3534	ACC TTC TGA TAC TGA ACG CC
3538	CAG TTC AGT GCT TGA ACC CA
3565	GTG CGG ACC TAG CAA ATA AAC AGC TG
3566	CGG GTA ACA TTT GAA ACG CAT ACC G
3595	GCG GCC GCC ACC ATG GCG TTC GGC CGT CAA ACG CTT TCC CT
3596	GGC GCG CCC ACA ATG TCC AAG TCA TAC ACT TCC
3597	GCG GCC GCC ACC ATG GTG ACT TTA GTC TTT GTG TGT CTC TC
3598	GGC GCG CCA CTG CTG TCT ACA TCA TAA ACT TCC
M13F	TGT AAA ACG ACG GCC AGT
M13R	CAG GAA ACA GCT ATG ACC
B3-1	TTC TGT AAT TTG CTG CAA CG
B3-2	TGT AAA ACG ACG GCC AGT TGC TGA TGA CCG TTA AAC AC
B3-3	CAG GAA ACA GCT ATG ACC AGG GTT GGT GTC TTT CTC AG
B3-4	CCA TAG TAG ACG AAG GAC ACG
C5-1	GAG GAA ACC TCT GAA ACT GC
C5-2	TGT AAA ACG ACG GCC AGT ACT GAG TCG CTG TAA TGG TG
C5-3	CAG GAA ACA GCT ATG ACC AGC AGA TTC TCC TCA TGT CTG
C5-4	GGC ACT GAG TAC AAA TGG TG

Chapter 3

Cloning and homology of the zebrafish *jam* family

Summary

In this chapter I describe the evolutionary relationships between all members of the zebrafish *jam* family. Using BLAST searching of the zebrafish genome, I identified an additional two members of the family and cloned them by RT-PCR and 3′ RACE. I used the amino acid sequences of the conserved immunoglobulin-like domains from all of the zebrafish and mammalian JAM proteins to generate an alignment and a phylogenetic tree. This demonstrated that the zebrafish genome contains two orthologues of each of the three *JAM* genes in the mouse and human genomes. A cross-species analysis of local genome structure and evolutionarily conserved sequences indicate the genomic regions likely to have derived from genome duplication in zebrafish and which of those loci more closely resemble the ancestral loci.

3.1 Introduction

Mammalian genomes contain three *JAM* family members – *JAM-A*, *JAM-B* and *JAM-C*[†]. Prior to commencement of this project, four zebrafish *jam* family proteins had been identified. The zebrafish homologue of *JAM-A*, named *jama*; the *JAM-B* orthologues *jamb* and *jamb2*; and one *JAM-C* homologue, *jamc*, were identified from IMAGE consortium cDNA clones (Lennon *et al*, 1996). I sought to identify any other members of the family present in the zebrafish genome. The basic structural determinants of JAM family proteins are that they are type I transmembrane proteins with an N-terminal signal peptide, two immunoglobulin-like domains, a single transmembrane region and a short, apparently unstructured, cytoplasmic region ending in a type II PDZ-domain binding motif: ΦXΦ-COOH (figure 3.1).

The *JAM* genes have a conserved intron-exon structure over the regions encoding the extracellular protein domains, but the cytoplasmic domain-encoding exons of each *JAM* differ between family members (figure 3.2). Similarly, the amino acid sequence of the extracellular domains appears much more conserved than that of the cytoplasmic regions. Each immunoglobulin-like domain has a canonical disulfide bridge between B and F β-strands. Unusually, the membrane-proximal immunoglobulin-like domains of JAM-B and JAM-C each contain an additional, conserved, non-canonical disulfide bridge between A and G β-strands; the functional consequences of this feature are unknown. The JAM family proteins are predicted to be glycosylated and have conserved putative N-linked glycosylation sites: 'NX(S/T)'. The structures of recombinant ectodomains of murine and human JAM-A have been solved by X-ray crystallography (Kostrewa *et al*, 2001; Prota *et al*, 2003, respectively). In addition to the features already mentioned, both studies found the conformation of the immunoglobulin-like domains to be at an angle of 125° as a result of extensive hydrogen bonding between main chain atoms and hydrophobic interactions with the conserved linker peptide: 'VXV'. This conformation allows for the formation of homodimers *in cis*, which interact through the concave surface formed by the GFCC′ β-strands of the membrane-distal domain. An important motif within the

[†] There is considerable confusion of the nomenclature of the *JAM* family in the literature. For the sake of clarity, I have adopted the naming scheme suggested by Muller, 2003 that is now widely used by researchers. I have differentiated between zebrafish paralogues with a suffixed '*2*' for later discovered paralogues. This runs contrary to the guidelines given by the Zebrafish Nomenclature Committee, but is more useful for those researching the *JAM* family. Table 3.1 presents the gene names, aliases and Ensembl identifiers for each gene in the human, mouse and zebrafish genomes.

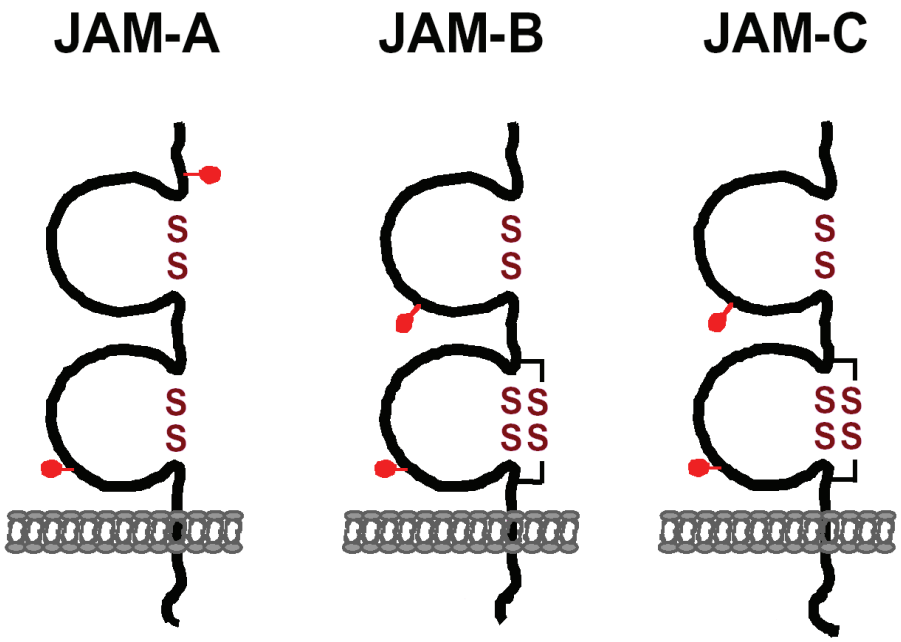

Figure 3.1 The mammalian JAM family.

Cartoon showing the basic structural features of all three mammalian JAM family proteins. Each JAM protein is a type I membrane protein with two extracellular, glycosylated, immunoglobulin-like domains and a short cytoplasmic domain ending in a type II PDZ-binding motif. Modified from Ebnet *et al* (2004), without permission.

Table 3.1 Nomenclature of the *JAM* family. Official gene symbols are marked in bold.

Name	Species	Synonyms	Gene identifier
JAM-A	Human	***F11R**, JAM-1, JAM, KAT, CD321, PAM1, JCAM*	ENSG00000158769
Jam-A	Mouse	***F11r**, Jam, Jcam, Jam-1, Ly106*	ENSMUSG00000038235
jama	Zebrafish	***f11r**, jam*	ENSDARG00000017320
jama2	Zebrafish		ENSDARG00000068114
JAM-B	Human	***JAM2**, CD322, VE-JAM, PRO245*	ENSG00000154721
Jam-B	Mouse	***Jam2**, Jam3, Vejam, Jcam2*	ENSMUSG00000053062
jamb	Zebrafish	***jam2**, vejam, cd322*	ENSDARG00000058996
jamb2	Zebrafish		ENSDARG00000079071
JAM-C	Human	***JAM3***	ENSG00000166086
Jam-C	Mouse	***Jam3**, Jam2*	ENSMUSG00000031990
jamc	Zebrafish	***jam3**, jam3b*	ENSDARG00000061794
jamc2	Zebrafish		ENSDART00000092689

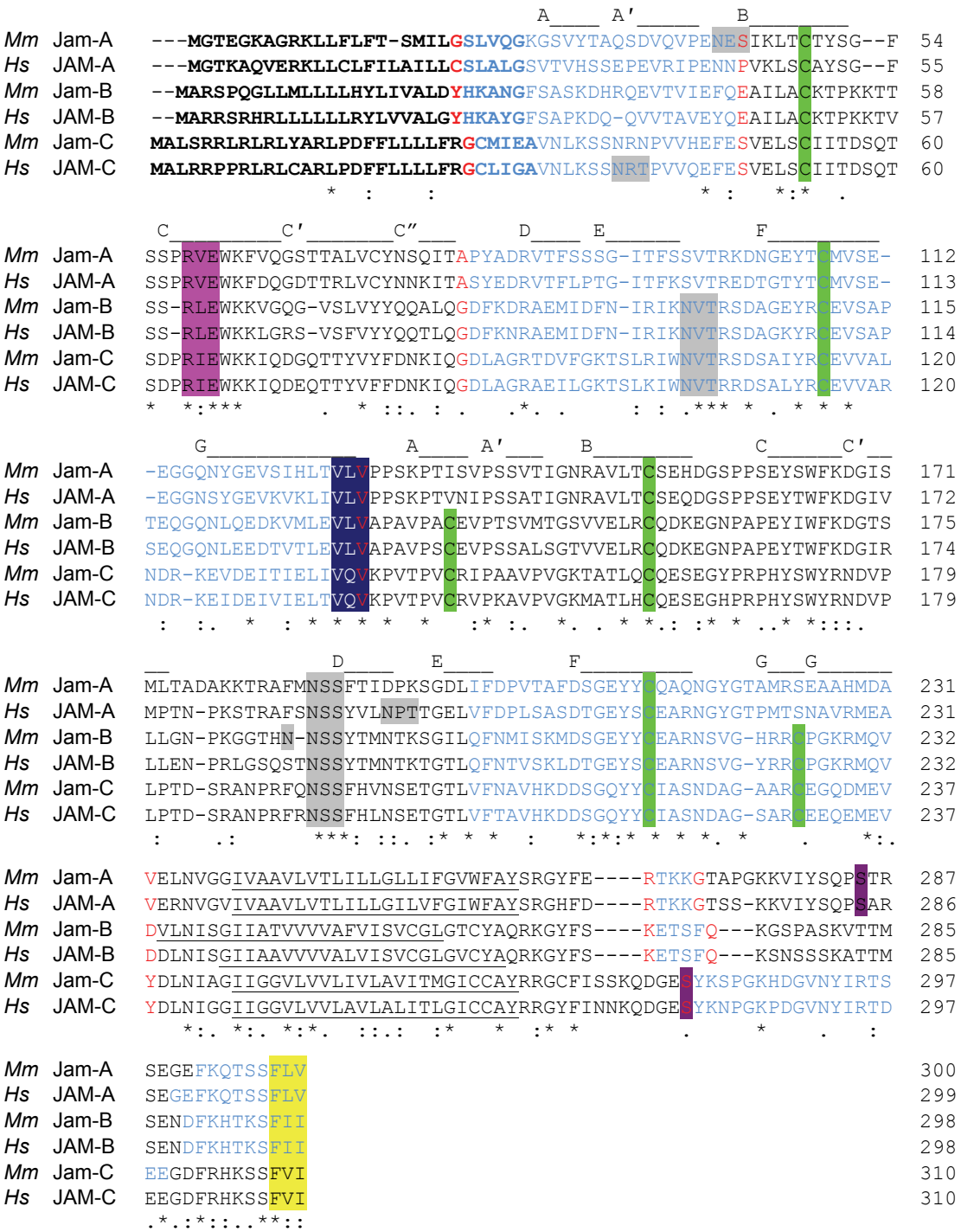

Figure 3.2 Conserved protein features of the mammalian JAM family.

ClustalW alignments of all human (*Hs*) and mouse (*Mm*) JAM family proteins, with key features highlighted. Exons – alternating blue/black colours, red – a cross-exon codon; bold – predicted signal peptide; green – disulfide bridge forming cysteines; lilac – binding interface residues; grey – putative N-linked glycoslyation sites; dark blue – linker sequence; underlined – predicted transmembrane helices; purple – phosphorylated serine; yellow – type II PDZ domain binding motif. The β-strands are indicated above the alignments.

C β-strand of this surface is 'R(V/I/L)E … Y' as these residues are important for forming salt bridges between monomers.

The cytoplasmic domain of JAM-A contains putative phosphorylation sites and some evidence for *in vivo* modification exists in activated platelets (Sobocka *et al*, 2000). Localisation of JAM-C to tight junctions seems to be regulated by phosphorylation of serine-281 in a cancer cell line (Mandicourt *et al*, 2007). The role of post-translational modification in the function of JAM-A, or the relevance to other members of the family, remains unexplored.

With the possibility of additional zebrafish *jam* family members that might be redundant with *jamb* and *jamc*, I searched the zebrafish genome for sequences with similarity to paralogues previously identified. I found two additional *jam* family genes and established their homology to mammalian *JAM-A* and *JAM-C* through sequence alignments and synteny.

3.2 Identification and cloning of *jama2* and *jamc2*

Putative paralogues of *jama* and *jamc* were identified in the zebrafish genome using TBLASTN searching of the zebrafish genome at the Ensembl website. The amino acid sequences of the extracellular immunoglobulin-like domains of Jama and Jamc were used as queries, as these regions were expected to be the most conserved between paralogues.

The best candidate paralogue of *jama* was a predicted gene found to be approximately 5.5 kbp upstream of *jama* on the same strand of chromosome 5. The protein sequence identity between the predicted gene product (hereafter referred to as Jama2) and Jama was very high across the immunoglobulin-like domains: approximately 79% by ClustalW alignment. However, careful manual searching of the genomic region downstream of *jama2* failed to reveal potential transmembrane and cytoplasmic domains. In order to establish that this putative paralogue is transcribed during development and to confirm the structure of the gene, 3′ RACE was performed, using nested primers specific to the predicted 5′ UTR of *jama2* (figure 3.3) and cDNA constructed from RNA extracted from 24 h. p. f. wildtype embryos, primed using a 3′ RACE primer. The major PCR product, approximately 1.5 kbp long, was purified, subcloned and sequenced. This *jama2* sequence included a small portion of the predicted 5′ UTR, the full open reading frame, including a stop codon, and 3′ UTR (figure 3.4). This sequence was compared to the genome and translated *in silico* and aligned against Jama (figure 3.5). The immunoglobulin-like domains of Jama2 are very closely matched to those of Jama and retain important protein

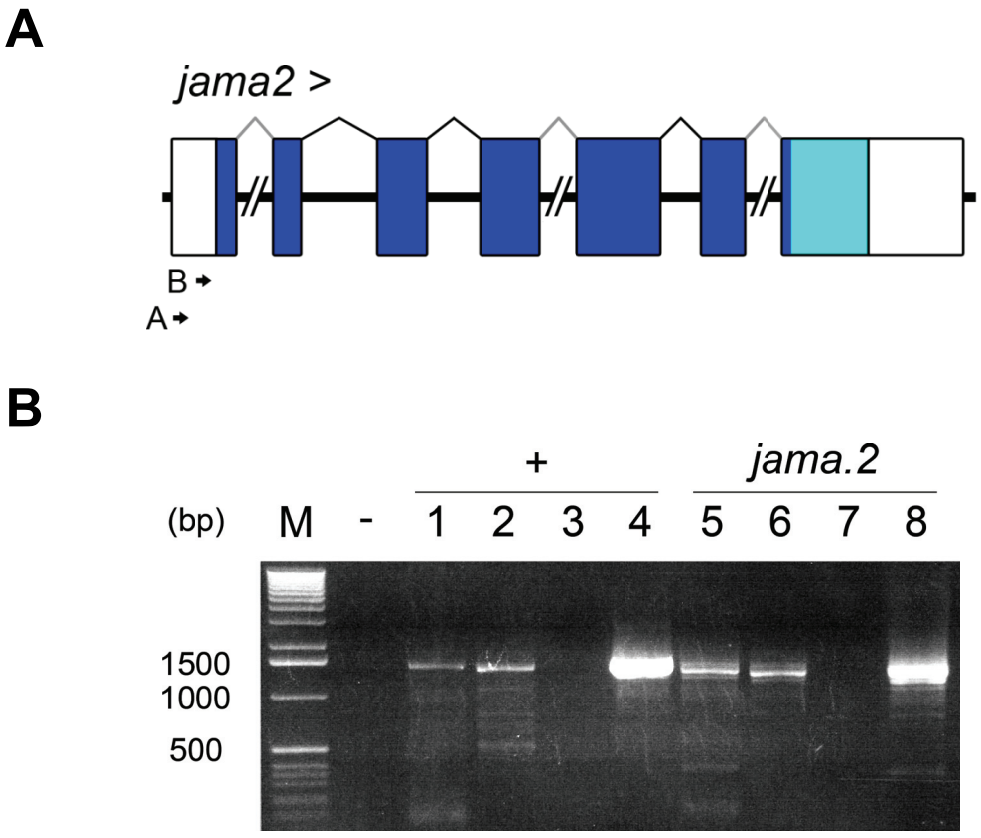

Figure 3.3 *jama2* is expressed at 24 h. p. f. as determined by 3′ RACE.

A. Scale diagram of the *jama2* loci, as determined sequence comparison between the 3′ RACE product and the zebrafish genome. Arrows indicate the position of the primers used in 3′ RACE experiments. Portion of gene cloned and used for protein production is indicated in dark blue. Introns larger than 500 bp were truncated for clarity, as indicated. **B.** Gel of 3′ RACE experiment using 24 h. p. f. cDNA. Lane descriptions as follows: '-' – negative control (no primers); *igsf11* positive control experiments: 1 & 2 - 5′ PCR primers, 3 – nested PCR control (no template), 4 – nested PCR; *jama2* experiments: 5 - 5′ primer A, 6 – nested 5′ primer B, 7 – nested PCR control (no template), 8 – nested PCR. M – DNA ladder, size of selected bands (in bp) shown to the left of the gel.

```
        10        20        30        40        50        60        70        80
cgggtaacatttgaaacgcataccgtggaaaaccttctatcatttcagactggaaATGTTGACTTTAGTCTTTGTGTGTC
                                                      M  L  T  L  V  F  V  C

        90       100       110       120       130       140       150       160
TCTCTTTTTCACTCACAGGCCTACATGCTTCCTTTTCAGTGGCTGTTAATGGTCCCGTAGTAAAAGTGAAGGAGAATGAG
L  S  F  S  L  T  G  L  H  A  S  F  S  V  A  V  N  G  P  V  V  K  V  K  E  N  E

       170       180       190       200       210       220       230       240
GGAGTTGACTTGCAATGTTCCTACACCGCTGACTTTGGAGCAACACCCAGAGTAGAATGGAAGTTCAGAAATCTGAAGGG
 G  V  D  L  Q  C  S  Y  T  A  D  F  G  A  T  P  R  V  E  W  K  F  R  N  L  K  G

       250       260       270       280       290       300       310       320
CTTTCAGTATTTCATCTACTTTAATAACAAACCAACTGTTGAATATGAACAGCGCATCACTGTGTACGCTGGAGGACTGA
  F  Q  Y  F  I  Y  F  N  N  K  P  T  V  E  Y  E  Q  R  I  T  V  Y  A  G  G  L

       330       340       350       360       370       380       390       400
GATTTCAAAAAGTAACGCGAGCAGACGCTGGAGATTATAACTGTGAGGTTTCTGGAAACGGTGGATATGGAGAGAATACC
R  F  Q  K  V  T  R  A  D  A  G  D  Y  N  C  E  V  S  G  N  G  G  Y  G  E  N  T

       410       420       430       440       450       460       470       480
ATCAAACTTGTAGTCTCTGTTCCTCCTTCCAAGCCTGTATCCAGCATTCCTTCATCAGTCACAACAGGCAGTAACGTCCG
 I  K  L  V  V  S  V  P  P  S  K  P  V  S  S  I  P  S  S  V  T  T  G  S  N  V  R

       490       500       510       520       530       540       550       560
CCTGACTTGCTTTGACCCAGTTGGCTCTCCTCCATCCACCTATGAGTGGTACAAAGACAACAACCTCCTCCCTGAGGACC
  L  T  C  F  D  P  V  G  S  P  P  S  T  Y  E  W  Y  K  D  N  N  L  L  P  E  D

       570       580       590       600       610       620       630       640
CAACCAAGTTTCCCATTTTTAAGAACCTCACATATAAGATGAATGCTTTCAATGGAAACCTGGAGTTCTTGAGTGTGTCT
P  T  K  F  P  I  F  K  N  L  T  Y  K  M  N  A  F  N  G  N  L  E  F  L  S  V  S

       650       660       670       680       690       700       710       720
AAGTGGGATGCTGGCTCATATTTTTGTGTGGCCAGTAATGAAAACGGTGTCTCTCAGCATGGTGATGCAGTGAAGATGGA
 K  W  D  A  G  S  Y  F  C  V  A  S  N  E  N  G  V  S  Q  H  G  D  A  V  K  M  E

       730       740       750       760       770       780       790       800
AGTTTATGATGTAGACAGCAGTcaagtgctggatgtgaagagcaacttgagcatggagacacacaacattccaggcaaga
  V  Y  D  V  D  S  S  Q  V  L  D  V  K  S  N  L  S  M  E  T  H  N  I  P  G  K

       810       820       830       840       850       860       870       880
tcaccaacagccacataatggaaaaacagtatggtgtgttcatgttgcaggaggtgaaactaaaactagagatccagaaa
I  T  N  S  H  I  M  E  K  Q  Y  G  V  F  M  L  Q  E  V  K  L  K  L  E  I  Q  K

       890       910       920       930       940       950       960       970
ctggaattagaagtgaccaagctaaagctggagctgcaaaaacttggacatgaagtgtagatgatatcattcatcattac
 L  E  L  E  V  T  K  L  K  L  E  L  Q  K  L  G  H  E  V  *

       980       990      1000      1010      1020      1030      1040      1050
tgctataagtcaaagaacttatttcatgtgctgatttcagatgttattgtaattacatttgtttttatacagctggggtc

      1060      1070      1080      1090      1100      1110      1120      1130
tgtttttcatacctcacttaaaagatctgtgatgatttgacagatatggatttttttcaggatatccgtgtggtcttaaa

      1140      1150      1160      1170      1180      1190
gtcttaaatctcaaaaactcaaatttaagccttaaagtgtctttaatcttctaaaaaaaa
```

Figure 3.4 Sequence of *jama2* mRNA as determined by 3′ RACE.

The mRNA sequence of the *jama2* 3′ RACE product and translation of the open reading frame. The 5′ and 3′ UTR elements, as determined by genomic alignment, are indicated in orange. Alternate exons within the open reading frame are indicated by alternate black and blue text. The region of cDNA cloned for protein expression is indicated by underlined capital letters.

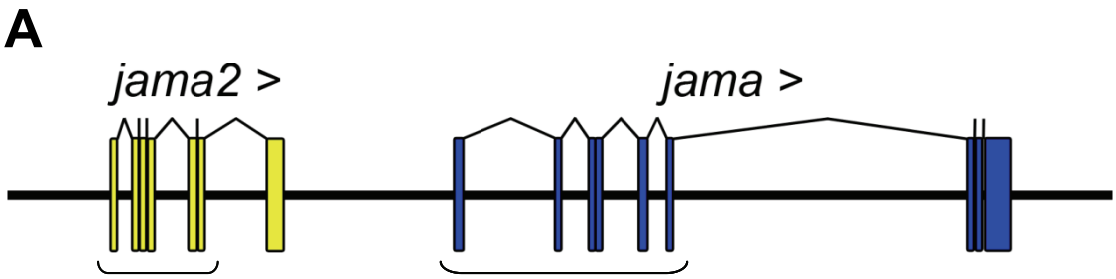

B

```
Dr Jama     MLTFAFVCFSLFVTGIHG-FQVTVTSP-VKVKENEGVDLQCSYTSDFGATPRVEWKFKDL   58
Dr Jama2    MLTLVFVCLSFSLTGLHASFSVAVNGPVVKVKENEGVDLQCSYTADFGATPRVEWKFRNL   60
            ***:.***:*: :**:*. *.*:*..* ****************:************::*

Dr Jama     KGSQTLVYFDGKPTGQYTGRVTMYDKGLRFNKVTRADTGDYDCEVSGSGGYGENTIKLTV   118
Dr Jama2    KGFQYFIYFNNKPTVEYEQRITVYAGGLRFQKVTRADAGDYNCEVSGNGGYGENTIKLVV   120
            ** * ::**:.*** :*  *:*:*  ****:******:***:*****.**********.*

Dr Jama     LVPPAKPVSRIPSSVTTSSNVRLTCFDPVGSPPSTYKWYKDNTPLPEDPTKFPAFKNLTY   178
Dr Jama2    SVPPSKPVSSIPSSVTTGSNVRLTCFDPVGSPPSTYEWYKDNNLLPEDPTKFPIFKNLTY   180
             ***:**** *******.******************:*****. ********* ******

Dr Jama     KMNVFNGNLEFPSVSKMDTGSYFCEASNGEGVPQRGDEVKMEVRDLN---VGGIVAGVIV   235
Dr Jama2    KMNAFNGNLEFLSVSKWDAGSYFCVASNENGVSQHGDAVKMEVYDVDSSQVLDVKSNLSM   240
            ***.******* **** *:***** *** :**.*:** ***** *::   * .: :.: :

Dr Jama     ALLAVGLLLFGLWYASKKGYLPKLSETKQKPQAVYTQPQTDDVDEANGFRQKSSFVV      292
Dr Jama2    ETHNIPGKITNSHIMEKQYGVFMLQEVKLK---LEIQKLELEVTKLKLELQKLGHEV      294
                :   : .    .*:  :  *.*.* *   :  *    :* : :   ** .. *
```

Figure 3.5 Genomic alignment of *jama2* cDNA sequence and comparison of the translated open reading frame with Jama.

A. The cDNA sequence of the *jama2* 3′ RACE product was compared to the zebrafish genome using BLAT at Ensembl. The cDNA matches the genomic sequence very close to *jama,* as shown in this schematic of the loci. The exons encoding the immunoglobulin-like domains in both genes are bracketed. The figure is drawn to scale. **B.** ClustalW alignment of the amino acid sequence of Jama and Jama2, as translated from the cDNA sequence. 58% of residues are identical over the whole alignment, rising to 79% over the immunoglobulin domains alone. Feature annotations as in figure 2.

features (such as signal peptide, cysteine residues for disulfide bridges, salt bridge residues of the dimerisation interface and glycoslyation site). The predicted intron-exon structure also matches very closely with that of *jama*, except just after the final immunoglobulin-like domain encoding exon. Unsurprisingly, a hidden Markov model analysis of the protein sequence (TMHMM v2.0; Krogh *et al*, 2001) failed to identify any possible transmembrane region within the *in silico* predicted protein, suggesting that Jama2 is a secreted protein (data not shown). In the absence of identification of any transmembrane or cytoplasmic domain, and for the sake of consistency, I chose to clone only the immunoglobulin-like-domain-encoding region of the *jama2* gene for later expression and analysis (figure 3.4, underlined; see Materials and Methods for experimental details).

The most likely candidate paralogue of *jamc* was found on chromosome 15; a predicted gene with a similar intron-exon structure and a closely matching predicted protein sequence (approximately 63% over the two immunoglobulin-like domains). The different predictions and EST evidence were contradictory in parts and even included a small portion of a likely downstream gene. To resolve the structure of the open-reading frame, I designed pairs of primers within different regions of the gene predictions and EST evidence and attempted to amplify the gene by RT-PCR from cDNA prepared from RNA extracted from 24 h. p. f. wild-type embryos (figure 3.6). Having confirmed the structure of the *jamc2* gene, I subsequently amplified the cDNA using a primer within the 5′ UTR region and the 3′ primer at the end of the coding sequence. A single product of approximately 1 kbp was purified, subcloned and fully sequenced. Comparing this sequence to the zebrafish genome identified some 5′ UTR and nearly 900 bases of open reading frame (figure 3.7). This was translated *in silico* and used in alignments with Jamc (figure 3.8). The high level of amino acid identity and the predicted intron-exon structure confirms this gene as a member of the *jam* family and the paralogue of *jamc* and is therefore referred to as *jamc2*. Analysis of the translated sequence predicted a transmembrane domain (TMHMM v2.0 Krogh *et al*, 2001), followed by a short cytoplasmic domain (figure 3.8). The cytoplasmic domain of Jamc2 contains conserved residues that may represent a type II PDZ motif, if they are indeed the C-terminal residues, as predicted from sequence alignment. The cDNA product did not include a stop codon, although there is a stop codon present in the genome immediately after the end of the aligned sequence, suggesting it is the true 3′ end of the gene. The complete extracellular domain-encoding region of *jamc2* was cloned for later expression and analysis (figure 3.7; see Materials and Methods for experimental details).

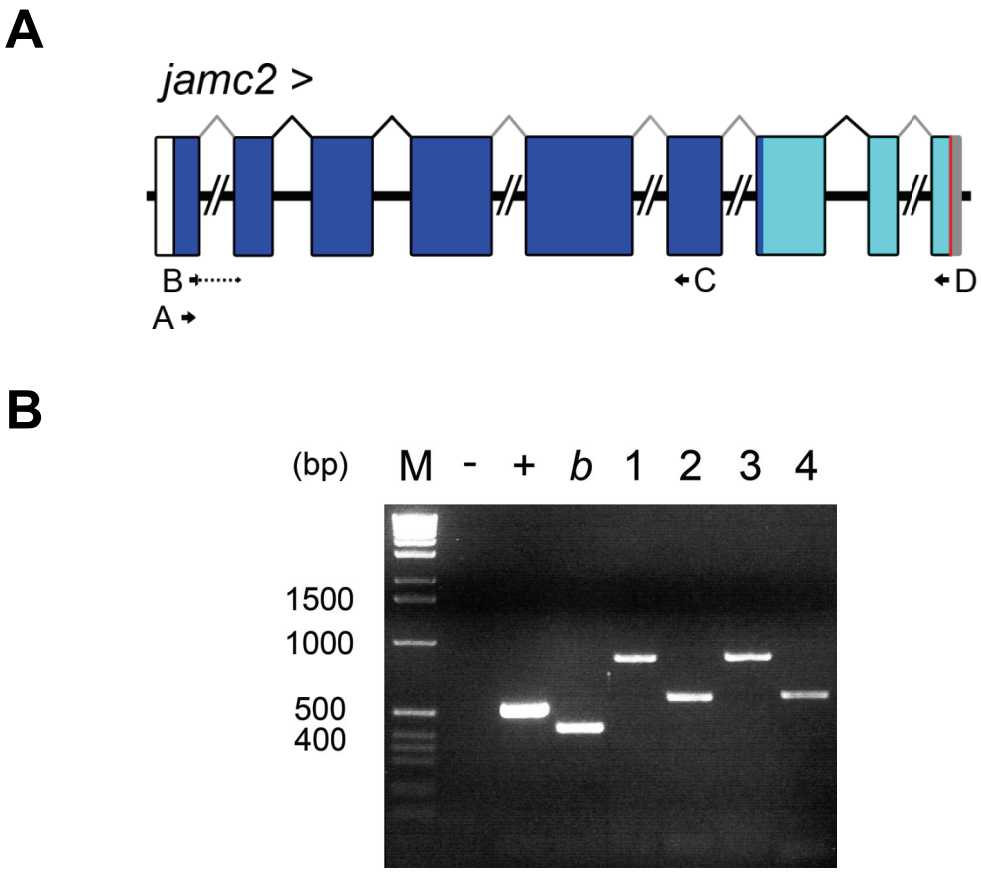

Figure 3.6 Structure of *jamc2* mRNA as determined by RT-PCR.

A. Scale diagram of the jamc2 loci, predicted from EST and gene prediction data and subsequently determined by comparison of sequenced RT-PCR products and the zebrafish genome. The true 3′ end of the gene remains to be formally established, but an in-frame stop codon is present in the genome sequence, directly adjacent to the aligned RT-PCR product sequence (red line). The 3′ UTR is likely to extend beyond this (region in grey) as no splice donor site is present nearby. Arrows indicate the position of primers used in RT-PCR experiments. Portion of the gene cloned and used in protein production is highlighted in dark blue. Introns larger than 500 bp were truncated for clarity, as indicated. **B.** Gel showing products of RT-PCR experiments. Lane descriptions as follows: '-' – negative control (no template), '+' - *ef1α* positive control, *b* – *jamb* positive control, 1 – primers B and D, 2 – primers B and C, 3 – primers A and D, 4 – primers A and C. M – DNA ladder, size of selected bands (in bp) shown to the left of the gel.

```
        10        20        30        40        50        60        70        80
ctaaacctgcatgtggaaacagcggctcaaaATGGCGTTCGGCCGTCAAACGCTTTCCCTGGTGCTCTTCTGCTGGCTGT
                                  M  A  F  G  R  Q  T  L  S  L  V  L  F  C  W  L

        90       100       110       120       130       140       150       160
GTAACAGTGCTGCCTTTGCTGTAATACTCCGAACAACTGAGAAATCTGTGTGGGCAAATGAATTTGAGTCAATCGAACTG
C  N  S  A  A  F  A  V  I  L  R  T  T  E  K  S  V  W  A  N  E  F  E  S  I  E  L

       170       180       190       200       210       220       230       240
ACCTGCTTGATAGAGTCCATTTCTACAAACAATCCTCGAATTGAATGGAAGAAAATAAAAAACGGTGTACCCAGTTATGT
 T  C  L  I  E  S  I  S  T  N  N  P  R  I  E  W  K  K  I  K  N  G  V  P  S  Y  V

       250       260       270       280       290       300       310       320
GTACTTTCAAAACAAAATATCAGGTGACCTGGAGCACAGGGCTTTGCTGCGAGAACCTGCAAACCTTCTGATACTGAACG
  Y  F  Q  N  K  I  S  G  D  L  E  H  R  A  L  L  R  E  P  A  N  L  L  I  L  N

       330       340       350       360       370       380       390       400
CCAGCAGATCAGACACAGCACAGTATCGCTGCGAGGTGGCCGCCATTGATGACCAGAAGCCTTTTGACGAAATATTAATC
A  S  R  S  D  T  A  Q  Y  R  C  E  V  A  A  I  D  D  Q  K  P  F  D  E  I  L  I

       410       420       430       440       450       460       470       480
AGTCTAGCTGTAAGAGTGAAGCCGGTAATCCCCAGATGTAGTGTGCCAGATGCAGTTAATGTGGGTTCAAGCACTGAACT
 S  L  A  V  R  V  K  P  V  I  P  R  C  S  V  P  D  A  V  N  V  G  S  S  T  E  L

       490       500       510       520       530       540       550       560
GCGATGTATTGAGAACGAAGGCTTTCCTCAGTCACAGTACCAGTGGTTCAAAAACAGCGAGGAGCTGCCCGAGGACCCAA
  R  C  I  E  N  E  G  F  P  Q  S  Q  Y  Q  W  F  K  N  S  E  E  L  P  E  D  P

       570       580       590       600       610       620       630       640
AAACCAGCAGCAAGTTCTACAATTCCTCATACATCATGAACATTGAGACTGGCTCTCTGAAATTCCGGTCGGTAAAGAAA
K  T  S  S  K  F  Y  N  S  S  Y  I  M  N  I  E  T  G  S  L  K  F  R  S  V  K  K

       650       660       670       680       690       700       710       720
GAGGATGCGGGTGAATATTATTGCCAGGCCAGAAATGAAGCCGGATGGTCAAAATGTATTCGACAGAGCATGGAAGTGTA
 E  D  A  G  E  Y  Y  C  Q  A  R  N  E  A  G  W  S  K  C  I  R  Q  S  M  E  V  Y

       730       740       750       760       770       780       790       800
TGACTTGGACATTGTGGGaatatttctgaaggttttgggtggagttgcagcatttatttttgtcattgtgggaatttgtc
  D  L  D  I  V  G  I  F  L  K  V  L  G  G  V  A  A  F  I  F  V  I  V  G  I  C

       810       820       830       840       850       860       870       880
aaattcagaaaagtggttactgttcctgcaaagatcacagagaaaccaactacaaagtaccccaacatgaaaacaggatg
Q  I  Q  K  S  G  Y  C  S  C  K  D  H  R  E  T  N  Y  K  V  P  Q  H  E  N  R  M

       890       900       910       920       930
gagtacaccactccagatgagggacattttcgccacaaatcctccttcgtcatc
 E  Y  T  T  P  D  E  G  H  F  R  H  K  S  S  F  V  I
```

Figure 3.7 Sequence of *jamc2* mRNA as determined by RT-PCR.

The cDNA sequence of the *jamc2* RT-PCR product and translation of the open reading frame. The 5′ UTR, as determined by genomic alignment, is indicated in orange. Alternate exons within the open reading frame are indicated by alternate black and blue text. The region of cDNA cloned for protein expression is indicated by underlined capital letters.

Figure 3.8 Comparison between Jamc and Jamc2 highlights conserved features.

ClustalW alignment of the amino acid sequence of Jamc and Jamc2, as translated from the cDNA sequence. 59% of residues are identical over the whole alignment, rising to 70% over the immunoglobulin-like domains alone. Feature annotations as in figure 2.

3.3 Evolutionary relationships of zebrafish *jam* family orthologues

To confirm the identity and family membership of the newly identified genes, I performed a phylogenetic analysis. I generated a clustalW alignment of the amino acid sequences of the immunoglobulin-like domains of all zebrafish, mouse and human *JAM* family genes. The immunoglobulin-like domains were used exclusively because of uncertainty about the true 3′ sequences of some of the family members and the strongly divergent nature of the unstructured C-terminal cytoplasmic domains. The closely-related cell surface, two immunoglobulin-like-domain containing proteins ESAM (mouse and human), A33 (mouse and human), CAR (mouse, human and zebrafish) and Jam4 (mouse only) were also included to test the robustness of paralogue assignments. This alignment was then used to generate a phylogenetic tree (figure 3.9). As expected, each of the putative paralogues was confirmed as *JAM* family members, distinct from the other immunoglobulin superfamily members. Both Jama and Jamc were also confirmed as either an 'A' type or 'C' type JAM family member, respectively.

Comparing human, mouse and zebrafish *JAM-A* loci suggest that this very small region has undergone duplication in the teleost lineage (figure 3.10). Only the gene immediately upstream of *jama* and *jama2*, *usf1l*, appears conserved between fish and mammals[†]. The lack of a transmembrane domain and cytoplasmic region in *jama2* suggest it is the derived allele. Only the exon sequences of the immunoglobulin-like domains have been conserved.

In contrast, *jamc2* appears to have a considerable amount of conservation of local gene structure, with local genes, *igsf9b*, *vps26b*, *acad8* and *thyn1* present in the same order and orientation with respect to *Jam-C* in the mouse and chick genomes (figure 3.11). An intervening gene in the mammalian and avian genomes, *Ncapd3*, is apparently missing from the *jamc* loci in zebrafish, but is present elsewhere in the zebrafish genome. This suggests that it has been deleted or transposed in teleosts, or inserted into the *Jam-C* locus in the mammalian lineage. The first *JAM-C* paralogue to be identified, *jamc*, is close to an *igsf9b* orthologue but apparently no other genes that are present in the *jamc2*, mouse or chicken loci. The apparent lack of gene conservation suggests that *jamc* is the derived allele of an ancient duplication of the genomic region bounded at one end by the ancestral *jamc*. Despite

[†] The chicken genome was not included in this analysis as no homologue of *JAM-A* could be found by BLAST search. I attempted to find the appropriate locus by finding homologues of other genes at the human *JAM-A* locus, but without success.

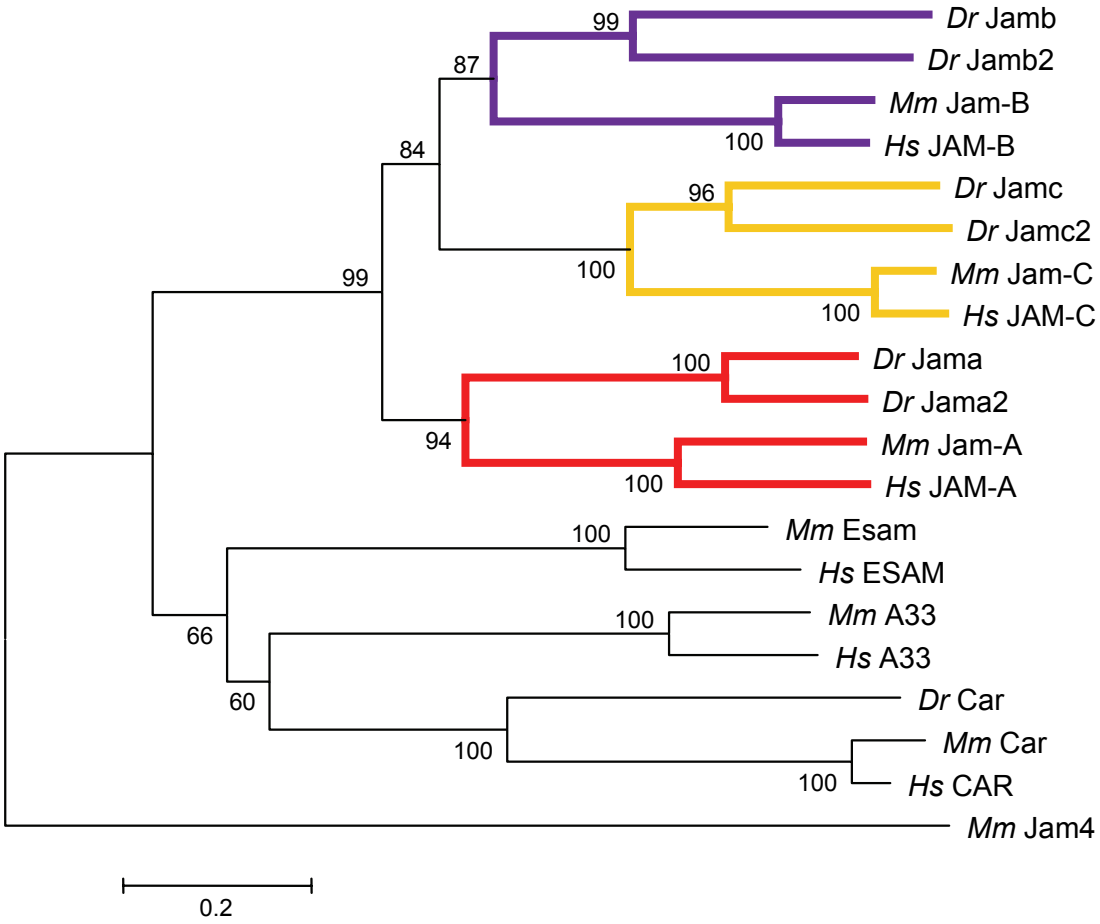

Figure 3.9 Zebrafish *JAM* family genes are distinct from related IgSF proteins and share a common ancestor with human and mouse *JAM* family genes.

Phylogeny generated by MEGA from ClustalW alignment of amino acid sequences of immunoglobulin-like domains from all human (*Hs*), mouse (*Mm*) and zebrafish (*Dr*) JAM family proteins and a selection of related transmembrane proteins. Values at nodes indicate percentage of bootstraps showing the same branching relationship (n = 500). Relative evolutionary distances are estimated by branch length; scale shown below tree.

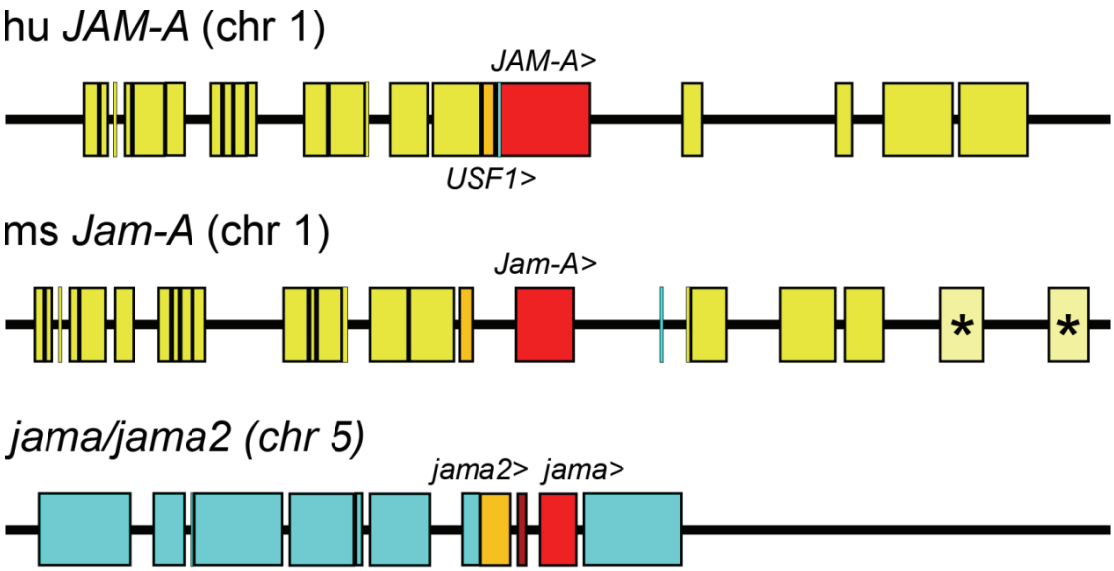

Figure 3.10 Multi-species comparison of *JAM-A* loci reveals limited conservation of local gene structure between zebrafish and mammals.

Schematic showing the arrangement of annotated genes (coloured boxes) within 0.5 Mb of sequence from the human, mouse and zebrafish genomes centered on *JAM-A* orthologues (red boxes). Genes conserved between these loci are highlighted by yellow boxes – only one example, *usf1l*, exists at the zebrafish *jama*/*jama2* loci. Genes that are present at only one locus are highlighted by blue boxes. The mouse genes highlighted with an asterisk (from left to right: *CD48* and *Slamf7*) are present at this loci in the human genome, but are outside the 0.5 Mb window presented here. The figure is drawn to scale.

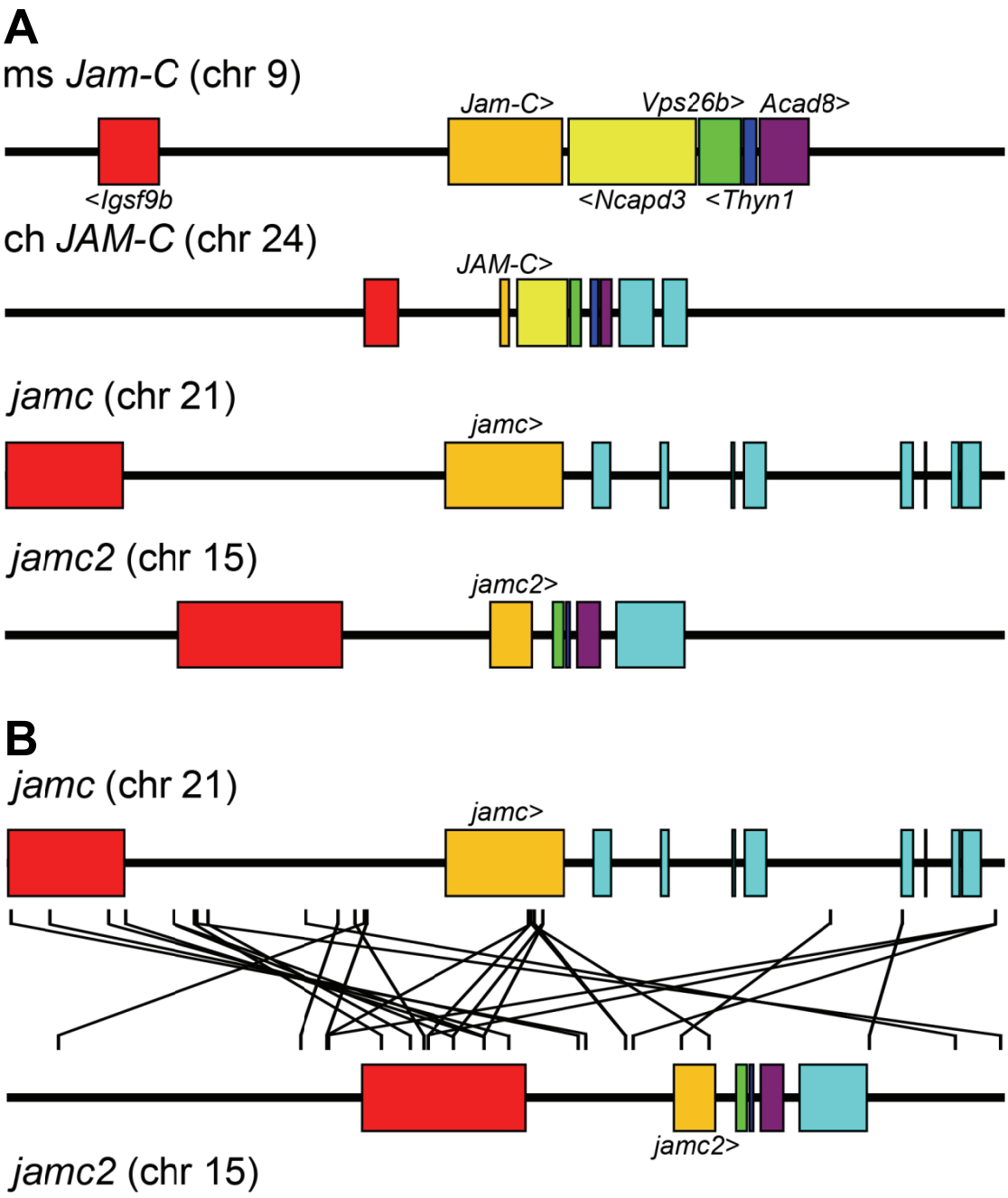

Figure 3.11 Multi-species comparison of *Jam-C* loci suggest *jamc* is the derived allele from an ancient genome duplication.

A. Schematic of the arrangement of annotated genes (coloured boxes) within 0.5 Mb of sequence from the mouse, chicken and zebrafish genomes centered on *Jam-C* orthologues (orange boxes). Genes conserved between these loci are colour-coded according to identity. Genes that are present at only one locus are highlighted by blue boxes. **B.** Schematic (as in A) of evolutionary conserved regions (ECRs) between zebrafish *jamc* and *jamc2* loci. ECRs are sequences at least 100 bp long with 70% identity or greater, as identified by BLASTz. The figure is drawn to scale.

this, the amino acid sequence of the extracellular domain of Jamc appears to be more conserved than that of Jamc2 in comparison to mouse Jam-C - 52% vs 45% identity respectively. I performed a more detailed comparison between the *jamc* and *jamc2* loci using zPicture (Ovcharenko *et al*, 2004), an interactive Blastz tool for genomic comparisons (figure 3.11). The resulting alignments suggest a more confusing relationship between the loci at the sequence level, with many sequences aligning in multiple positions within either region. As expected, the majority of the non-coding sequence alignments are between the region containing the *jamc* and *igsf9b* orthologues, although there are a few alignments outside this region. Many of these elements align with many different regions across the genome and might perhaps contain promoter or protein-binding sequences or as yet unidentified repetitive elements.

A multispecies comparison between zebrafish, chicken and mouse suggests a much less complicated evolution of the *Jam-B* loci (figure 3.12). The zebrafish *jamb* locus contains most of the genes present in the mouse and chicken loci (*adamts-1*, *cyyr1*, *appa*, *atp5j* and *mrpl39*), in the correct order and orientation. One clear difference is the apparent lack of an orthologue of *Gabpa*. In contrast, this gene is one of very few to be retained at the *jamb2* locus along with the *App* orthologue *appb*. It seems likely that the *jamb2* locus is derived from a duplication event and the *jamb* locus has retained ancestral characteristics. Both proteins are the least well conserved zebrafish Jams when compared by alignment (figure 3.13). Between paralogues, 46% of residues are identical across the immunoglobulin-like domains; this falls to 38% (Jamb) and 36% (Jamb2) in comparison to mouse Jam-B. Jamb2 also appears to lack all N-linked glycosylation sites, while Jamb has a novel site in the membrane-distal immunoglobulin-like domain, near the 'VLV' linker peptide. The cytoplasmic domains of the zebrafish JAM-B orthologues have diverged significantly from each other and the mammalian JAM-B. There appears to be an extra exon inserted into the cytoplasmic domain-encoding region of *jamb*, meaning the intracellular region is significantly longer than Jamb2 or mouse Jam-B (figure 3.13). Only the few residues close to the C-terminal PDZ-domain binding motif are conserved.

3.4 Discussion

Given that many orthologous genes in the zebrafish genome appear to have been duplicated (reviewed in Volff, 2005 and Ravi and Venkatesh, 2008), I undertook a search for any remaining unidentified *JAM* family genes. I identified two genes

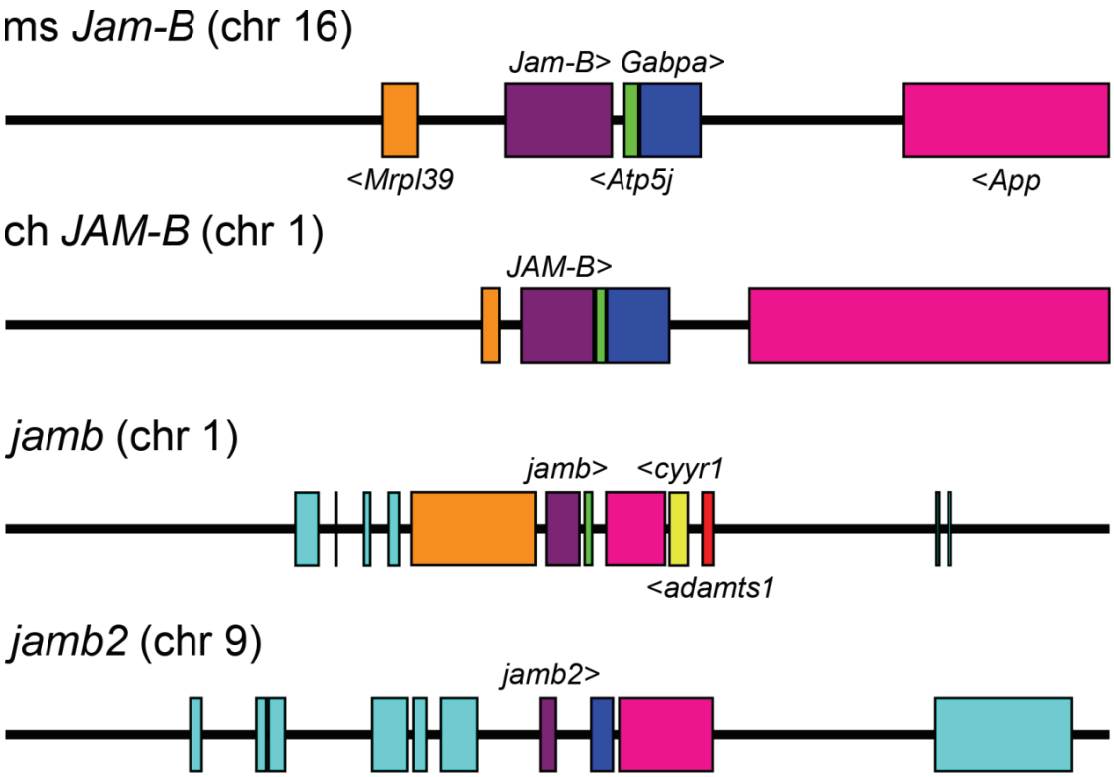

Figure 3.12 Multi-species comparison of *Jam-B* loci suggests *jamb2* is the derived allele of an ancient genome duplication event.

Schematic of the arrangement of annotated genes (coloured boxes) within 0.5 Mb of sequence from the mouse, chicken and zebrafish genomes centered on *Jam-B* orthologues (purple boxes). Genes conserved between these loci are colour-coded according to identity. Two genes present at the *jamb* locus, *cyyr1* (yellow) and *adamts1* (red), are conserved at the murine and chicken loci, but outside of the 0.5 Mbp genomic region presented here. Genes that are present at only one locus are highlighted by blue boxes. The figure is drawn to scale.

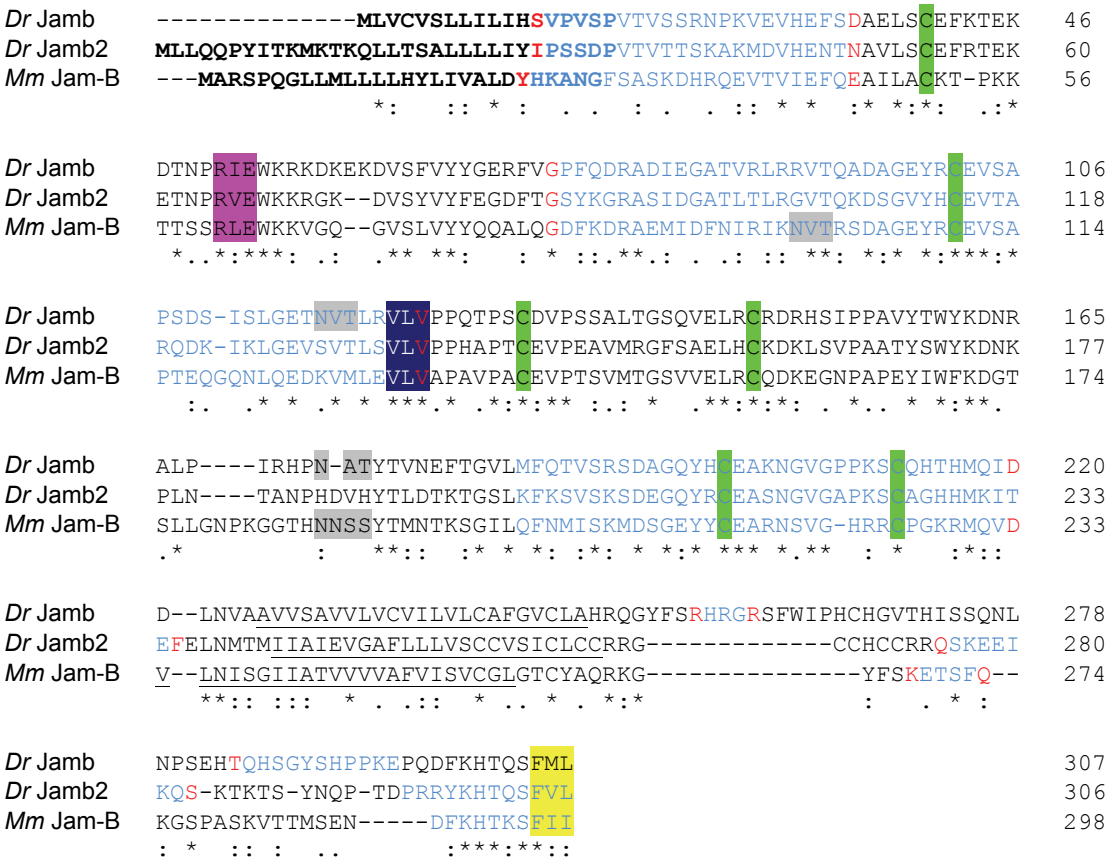

Figure 3.13 Comparison between Jamb, Jamb2 and Jam-B highlights conserved features and divergent cytoplasmic domains.

ClustalW alignment of the amino acid sequence of Jamb, Jamb2 and mouse Jam-B. 44% of residues are identical over the whole alignment of Jamb and Jamb2, rising to 46% over the immunoglobulin-like domains alone. 37% and 34% of residues are identical over the whole alignment between Jamb or Jamb2 and mouse Jam-B, respectively. Feature annotations as in figure 2.

encoding proteins with the appropriate structural features of JAM proteins and confirmed their relationship with the family by alignment, phylogeny and cross-species genome comparison. The presence of paralogous *JAM* genes has important implications for studying the function of any member of the family and relating those experimental results to human biology. Each paralogous gene may retain the same functions as the ancestral gene i.e. be functionally redundant; may have retained different ancestral functions, i.e. undergone sub-functionalisation; or may have diverged to take on different functions, i.e. neo-functionalisation. Gene expression may also be affected by duplication. Important promoter, enhancer and repressor sequences may also have been duplicated; may have been duplicated but subsequently mutated; or may have been lost from the duplicated gene entirely, resulting in a novel pattern of expression. Recombination may also bring the duplicated genes under the control of different regulatory elements. In this chapter, I have attempted to establish the evolutionary relationships between paralogues using a simple bioinformatics approach in order to address some of those questions.

There are two *JAM-C* orthologues in the zebrafish genome, the previously identified *jamc* on chromosome 21 and *jamc2* on chromosome 15. Both genes encode proteins with all the conserved features of JAM family proteins and the additional features of JAM-C - the additional disulfide bridge in the membrane-proximal immunoglobulin-like domain, both glycosylation sites and the transmembrane/cytoplasmic domain encoded by three exons instead of four. Comparing the extracellular domains of both zebrafish proteins with the mouse protein indicates that Jamc is better conserved. However, a multispecies analysis of synteny suggests that the *jamc* locus is derived from the ancestral duplication event. There is strong conservation of gene order at the *jamc2* locus in comparison to the chicken and mouse loci. Comparing both zebrafish loci using zBLAST demonstrates that there is good conservation of non-coding regions between the *jamc* and *igsf9b* orthologues, but few unique alignments outside of this region. This suggests that *jamc* marks the boundary of the duplicated region.

Similarly, there are two *JAM-B* orthologues in zebrafish: *jamb* on chromosome 1 and *jamb2* on chromosome 9. These are the least well conserved members of the zebrafish *jam* family. They retain the important characteristics of the JAMs, but have some interesting differences, in particular the divergent cytoplasmic domains. The C-terminal PDZ domain-binding motif remains intact in the paralogues, but the length and composition of the intracellular region is quite different, in terms of amino acid sequence and splicing of the appropriate regions of mRNA. The implication is a

divergence in intracellular function, but whether or not these changes represent sub-functionalisation is impossible to determine bioinformatically.

The existence of two *JAM-A* orthologues in the zebrafish genome is controversial. I identified a gene, close to *jama* on chromosome 5, encoding two immunoglobulin-like domains that are very highly conserved with those of Jama (79%) and reasonably well conserved with the human and mouse JAM-A (~40%). This appears to have arisen from a duplication of quite a small genomic region that may have included only part of the ancestral *jama* gene. The resulting duplicate acquired novel 3′ exons from local sequences, and as a result lacks any exons encoding a transmembrane domain or anything similar to the cytoplasmic domain of a JAM-A orthologue. As such, it lacks some important structural determinants of the JAM family; most notably, it does not encode a type I cell surface protein with a short cytoplasmic domain ending in a PDZ-domain binding motif. The protein is predicted to have a signal peptide and should therefore be secreted. There is no suggestion that such an arrangement exists in the *Gasterosteus aculeatus* (stickleback) or *Takifugu rubripes* (fugu) genomes (data not shown), implying that the duplication is restricted to the zebrafish sub-lineage of teleost fish. The amino acid sequence of the immunoglobulin-like domains of Jama2 are very well conserved, but there is little or no conservation of introns of *jama* and *jama2*. Given the level of conservation of exons and that the open reading frame was cloned from cDNA, it is unlikely that *jama2* is a pseudogene. It is possible that the *jama2* sequence is from a mis-spliced transcript, but extensive searching of the region 3′ to the immunoglobulin-like domain encoding exons revealed no candidate transmembrane or cytoplasmic domain exons. The significant change in the characteristics of *jama2* and the level of conservation suggest that the paralogue has taken on novel functions.

In summary, the zebrafish *jam* family has been duplicated in the teleost lineage, resulting in six *jam* genes with strong conservation of protein coding sequence between paralogues and orthologues in avians and mammals. The extracellular regions of the paralogues are well conserved, but the intracellular domains are much more divergent. Almost all loci have a local gene structure that is conserved through to mammals, except for *jama* and *jama2*, which are neighbouring genes in a small region with very little similarity to that of other species.

Chapter 4

Expression patterns of the zebrafish *jam* family during development

Summary

In this chapter I describe the embryonic expression patterns of all six zebrafish *jam* family genes during the first 48 hours of development post fertilization, as determined by RNA *in situ* hybridisation. Both *jamb* and *jamc* are co-expressed by myoblasts in the developing myotome. The expression patterns of the other family members do not overlap with those of *jamb* and *jamc* in space or time, suggesting no functional redundancy between paralogues. Jamb protein is present on the cell surface of myoblasts and muscle fibres during development. Expression of *jamc* is repressed by *prdm1*, a transcription factor that regulates slow muscle fate, suggesting a function for the gene that is specific to fast muscle myogenesis.

4.1 Introduction

Spatio-temporal data concerning the embryonic expression of *JAM* family genes in any model organism is sparse and disorganised. All three *JAM* genes are expressed during murine development, as determined by RT-PCR and real time PCR, in whole embryos at embryonic stages between 9.5 – 16.5 days post conception (d. p. c.; Sakaguchi *et al*, 2006; Gitton *et al*, 2002). Expression of the *JAM* genes does not appear to be restricted to any of the germ layers.

Embryonic *Jam-A* expression has been documented by use of a *LacZ* knock-in reporter line (Parris *et al*, 2005). Throughout embryogenesis, *Jam-A* expression is observed in the vasculature, inner ear and nasal placode, brain and choroid plexus, kidney, lung, gut and skin. RNA *in situ* hybridisation at 14.5 d. p. c. also demonstrates widespread expression of *Jam-A*. Expression in the pancreas has been detected between 11.5 – 18.5 d. p. c. by RT-PCR (Hoffman *et al*, 2008). Immunohistochemistry studies at very early stages of embryonic development reveal expression of Jam-A from as early as the 8-cell stage, where it is thought to play a role in the timing of blastocoel cavity formation (Thomas *et al*, 2004).

Both Jam-B and Jam-C are known to be expressed in testes and spermatogonia, respectively, during development as demonstrated by immunohistochemistry and *Jam-C LacZ* reporter line (Gliki *et al*, 2004). RNA *in situ* hybridisation has detected expression of both genes in a wide range of tissues at 14.5 d. p. c., including, but not limited to, brain, spinal cord, retina, gut, liver, kidney, pancreas, ear, heart and of particular interest, tongue, diaphragm and skeletal musculature (Visel *et al*, 2004). Jam-B and Jam-C expression was also described in a recent mouse knockout screen for transmembrane and secreted proteins (Tang *et al*, 2010). Both genes are expressed in neural tissues between 8.5 and 11.5 d. p. c. and in the somites between 10.5 and 12.5 d. p. c., as determined by wholemount RNA *in situ* hybridisation. Before commencement of this project, wholemount *in situ* hybridisation performed by members of the laboratory demonstrated co-expression of *jamb* and *jamc* in the somites and developing myotome of zebrafish embryos, specifically, fast muscle precursor cells.

I sought to further characterise the expression of the zebrafish *jam* family genes over several stages of development through wholemount RNA *in situ* hybridisation, to identify potential sites of interaction. Better understanding of the biological context of expression of each of the identified *jam* family orthologues (Chapter 3) highlighted differences between the regulation of the family members and their respective roles

in development. Comprehensive analysis of embryonic expression reiterates the observation that *jamb* and *jamc* are likely to interact during muscle development and also suggests that the respective paralogues do not function redundantly.

4.2 Expression patterns of the *jam* family

To get a comprehensive understanding of the expression of each of the zebrafish genes during early development, I performed wholemount RNA *in situ* hybridisation of riboprobes for each gene at several stages representative of the consecutive periods of development: gastrulation (shield, 6 h. p. f.; figure 4.1), segmentation (10 – 13 somites, approximately 14 h. p. f. and 21 somites, approximately 19½ h. p. f.; figures 4.2 and 4.3 respectively), pharyngula (24 h. p. f.; figure 4.4) and hatching (48 h. p. f.; figure 4.5). The riboprobes used were derived from the immunoglobulin domain-encoding regions of each gene (see Chapters 2 and 3). Tissue annotations for each gene and developmental stage are listed in table 4.1.

The expression patterns of *jama* and *jama2* are nearly identical, both spatially and temporally. This may be a result of cross-hybridisation between riboprobes and their respective targets because there is a high level of identity between the coding sequence of the immunoglobulin domains of both genes (table 4.2). However, the *jama2* riboprobe does not detect expression in any tissue of the 10 - 13 somites stage embryos and only weakly in tissues of the later developmental stages. Another possible explanation is that both genes may be regulated by the same promoter and enhancer elements because of the close proximity of *jama* and *jama2* within the zebrafish genome (see Chapter 3).

There is little similarity between the expression patterns of the remaining closely-related paralogues. *jamb* is predominantly expressed in the somites during segmentation (figures 4.2 and 4.3). This is attenuated in rostral myotomes during the pharyngula period (figure 4.4), and is undetectable in the myotomes of hatching period embryos, but strongly expressed in craniofacial mesoderm and hypaxial, epaxial and pectoral fin muscles (figure 4.5). In contrast, *jamb2* is expressed most strongly in the epithelia over the yolk ball, lateral to the main axis of the embryo, from early segmentation through to the pharyngula period (figure 4.6). By the hatching period, *jamb2* expression is restricted to pectoral fin muscles and branchial/mandibular arch mesoderm. There is possible overlap between expression of *jamb* and *jamb2* in craniofacial mesoderm at this stage.

Similarly, there is little overlap of expression of *jamc* and *jamc2* observed using this technique during early development. Expression of *jamc* is similar to that of *jamb*.

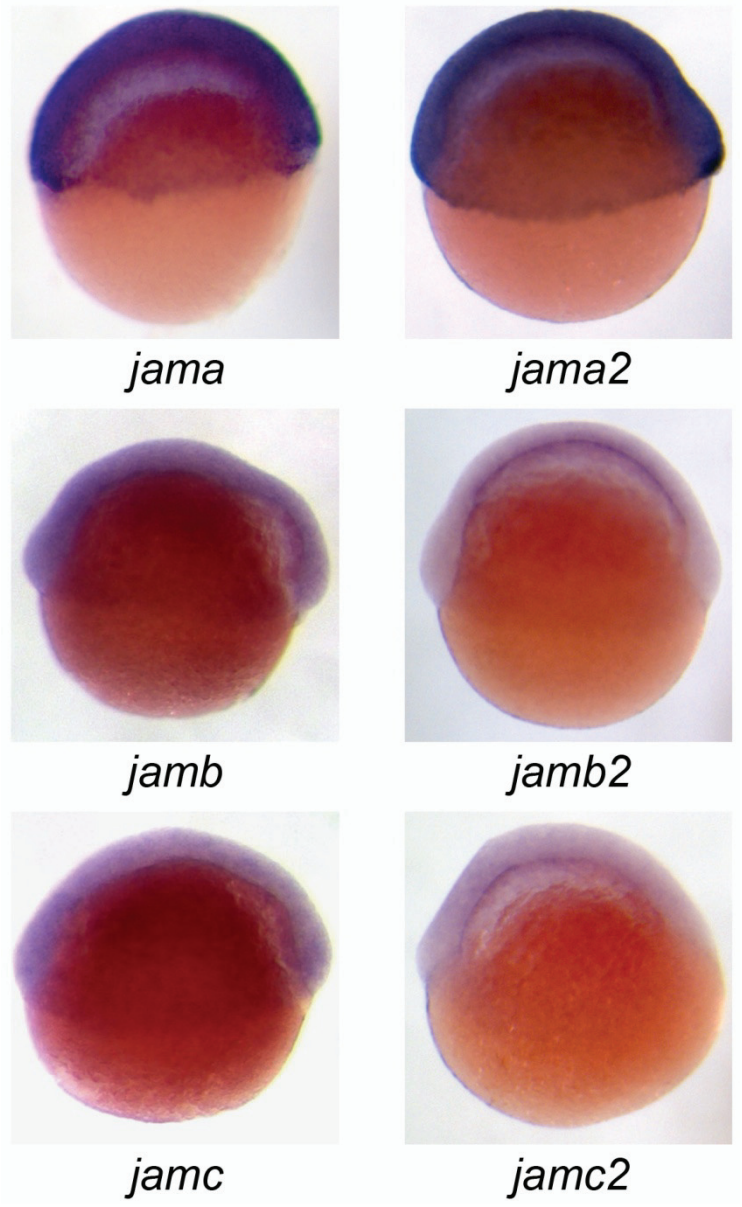

Figure 4.1 Expression patterns of *jam* family genes in the gastrula.

Wholemount RNA *in situ* hybridisation of shield stage embryos (6 h. p. f.), animal pole top, using riboprobes derived from the extracellular domain-encoding region of each *jam* family gene. There is uniform expression of *jama* and *jama2*, but no detectable expression of *jamb*, *jamb2*, *jamc* and *jamc2*.

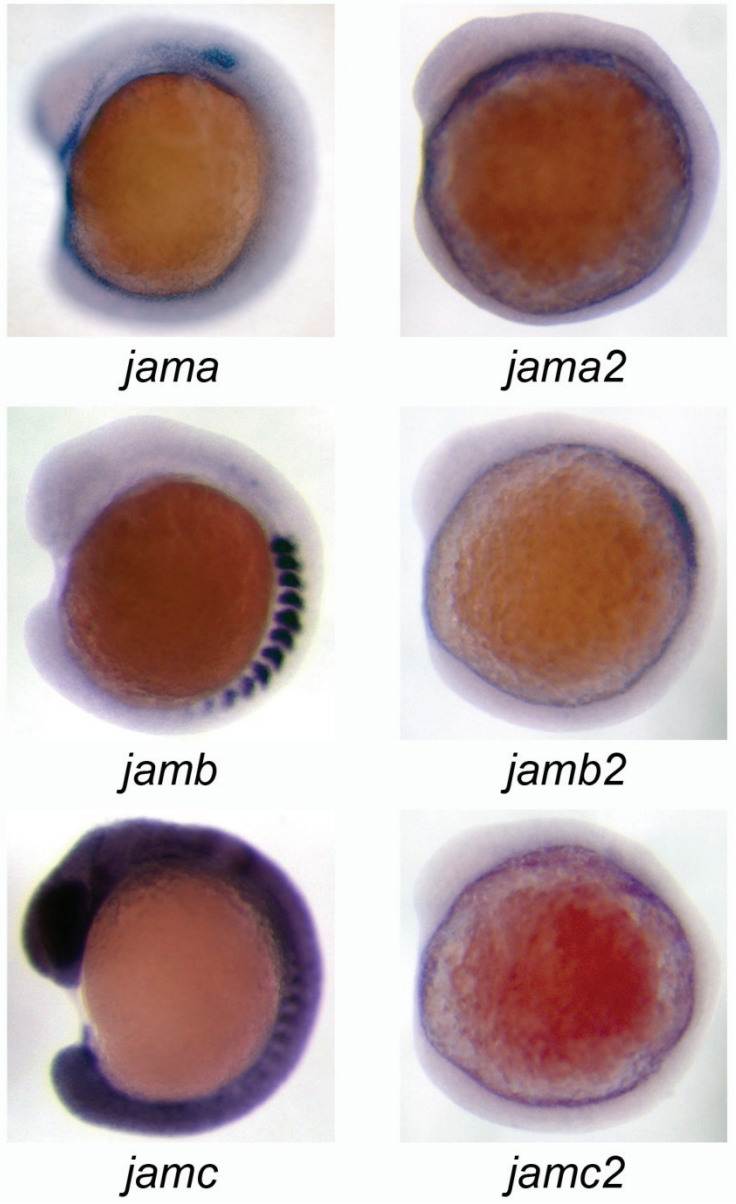

Figure 4.2 Expression patterns of *jam* family genes during early segmentation.

Lateral views of wholemount RNA *in situ* hybridisation expression patterns of 10 – 13 somites stage embryos (approximately 14 h. p. f.); anterior top. There is diversity between the regions of expression of each gene, with the exception of *jamb* and *jamc*. Both genes are expressed in mature somites. The closely-related paralogues are not expressed in similar regions within the developing embryo.

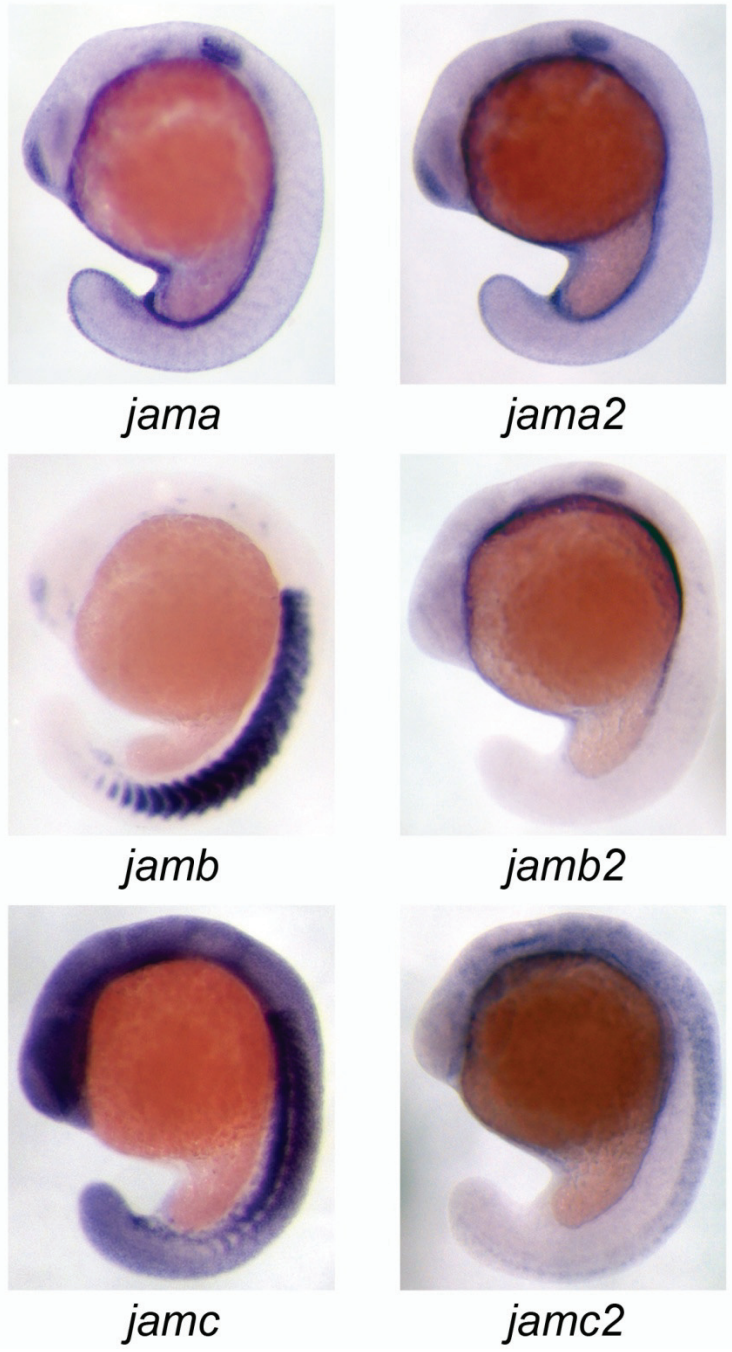

Figure 4.3 Expression patterns of *jam* family genes during late segmentation.

Lateral views of wholemount RNA *in situ* hybridisation patterns of embryos at 21 somites stage (19½ h. p. f.); anterior top. There are diverse, but overlapping, expression patterns of *jam* family genes. Both *jamb* and *jamc* continue to be expressed in anterior myotomes and caudal somites. Closely-related paralogues are expressed in different tissues of the embryo, with the exception of *jama* and *jama2*.

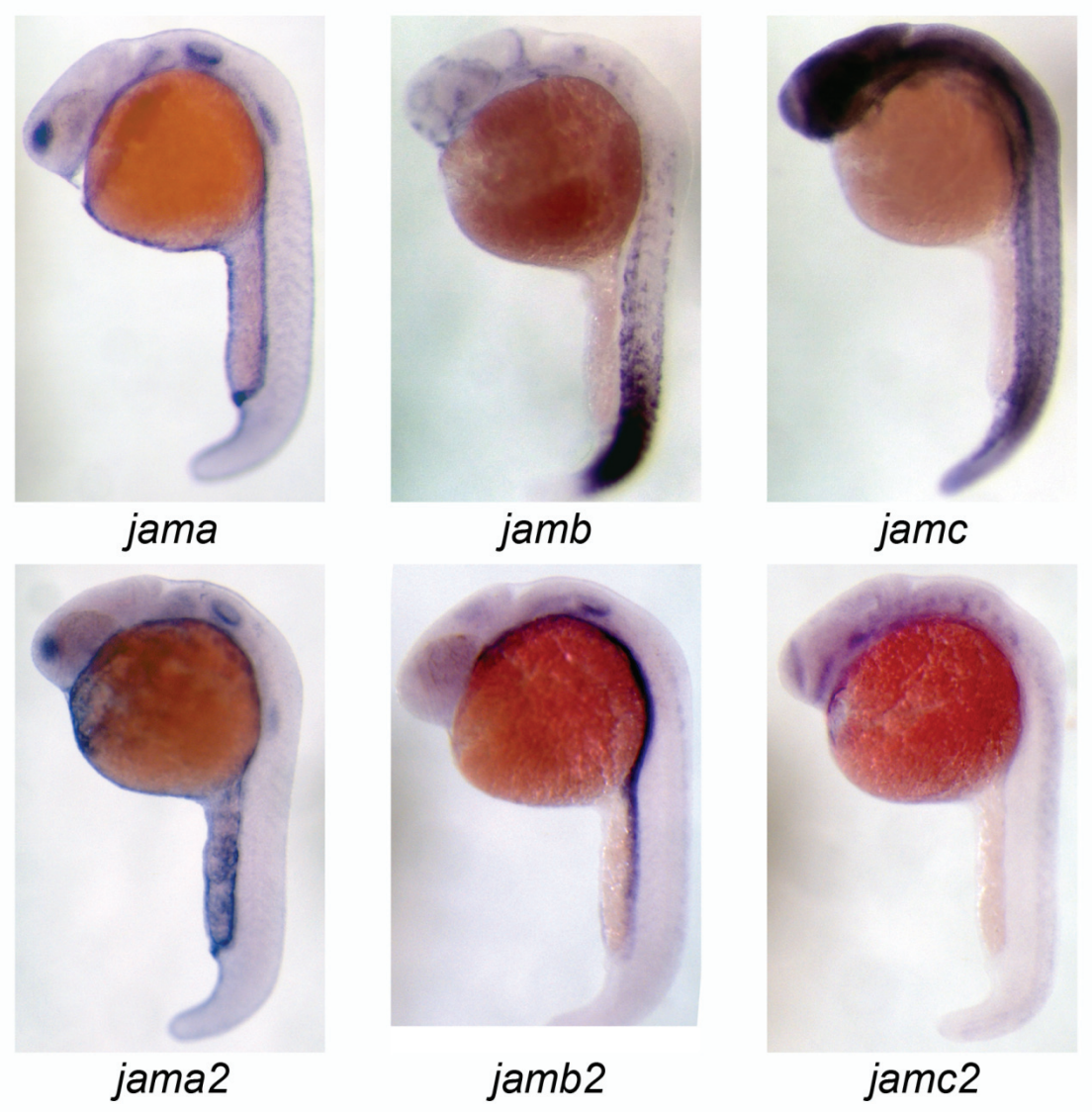

Figure 4.4 Expression patterns of *jam* family genes during the pharyngula period.

Lateral views of wholemount RNA *in situ* hybridisation of 24 h. p.f. embryos; anterior top. Co-expression of *jamb* and *jamc* is attenuated in all but the most caudal somites. The closely-related paralogues are expressed in different tissues, except for *jama* and *jama2.*

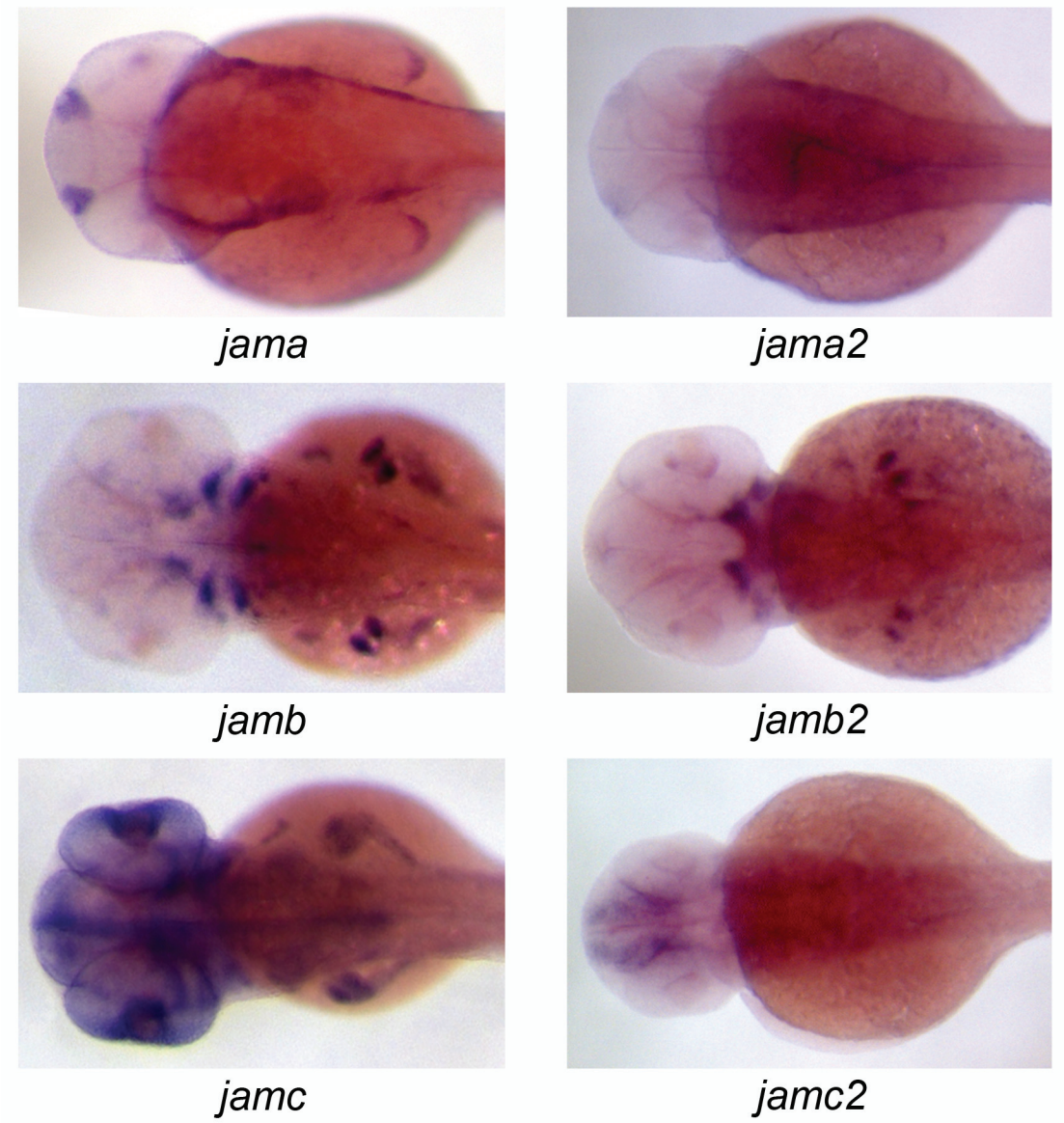

Figure 4.5 Expression patterns of *jam* family genes during hatching.

Dorsal views of head and trunk regions of wholemount RNA *in situ* hybridisation of 48 h. p. f. embryos; anterior left. Both *jamb* and *jamc* are expressed in craniofacial mesoderm, hypaxial, epaxial and pectoral fin muscles. *jamb2* is also expressed in pectoral fin muscles, and may overlap in expression with *jamb* in the head.

Figure 4.6 Expression pattern of *jamb2* between early segmentation and pharyngula periods.

Dorsal views of wholemount RNA *in situ* hybridisation of *jamb2* during development. There is strong expression of *jamb2* detected in the epithelia over the yolk ball, lateral to the main axis of the embryo, and yolk extension.

Table 4.1 Expression patterns of zebrafish *jam* family genes determined by wholemount RNA *in situ* hybridisation.

Gene	Stage									
	Shield		10 – 13 somites		21 somites		24 h. p. f.		48 h. p. f.	
jama	uniform	+++	**otic placode** nasal epithelium	+++ ++	epidermis eye lateral line primordium **otic vesicle** nasal epithelium pronephric ducts	+ + ++ +++ +++ +++	epidermis lateral line primordium **otic vesicle** nasal epithelium pronephric ducts	+ ++ ++ +++ +++	epidermis lateral line primordium **otic vesicle** nasal epithelium pronephric ducts pectoral fin	+ +++ ++ +++ +++ ++
jama2	uniform	+		-	epidermis eye **otic vesicle** nasal epithelium pronephric ducts	+ + + + +	epidermis lateral line primordium **otic vesicle** nasal epithelium pronephric ducts	+ + + ++ ++	**otic vesicle** nasal epithelium pectoral fin	+ + +
jamb		-	**anterior and posterior poles of otic placode** **posterior epithelium and mesenchyme of mature somites**	++ +++	**anterior and posterior poles of otic placode** **myotome/mature somites** **forebrain**	++ +++ ++	**otic vesicle** **caudal somites** **brain**	+ +++ +	**pectoral fin muscles** **hypaxial/epaxial muscles** **craniofacial mesoderm**	+++ +++ +++
jamb2		-	epithelium over yolk ball	++	**otic vesicle** epithelium over yolk ball	+ ++	**otic vesicle** epithelium over yolk ball	+ ++	**pectoral fin muscles** branchial/mandibular arches	++ ++
jamc		-	ubiquitous expression **rostral somites, posterior-medial foci** hindbrain	++ +++ +++	ubiquitous expression **dorsal/ventral myotome, caudal somites, posterior-medial foci**	++ +++	ubiquitous expression **caudal somites** **hindbrain/forebrain** eye	++ +++ +++ +++	ubiquitous expression **pectoral fin muscles** **hypaxial/epaxial muscles** **craniofacial mesoderm** eye	++ +++ +++ +++ +++
jamc2		-		-	neural tube anterior lateral line primordium	+ +	neural tube **brain**	+ +	**brain**	+

Some sites of expression are colour-coded by anatomical feature: **blue** - somites/myotome/muscle **green** – otic placode/vesicle **orange** - brain
Qualitative descriptors: '-' Absent '+' Weak (light staining after 4 hours or requiring overnight development) '++' Strong (clear, heavy staining after 2-4 hours of development) '+++' Very strong (very heavy staining after 2 hours of development)

It is strongly expressed in the somites throughout segmentation (figures 4.2 and 4.3) and is attenuated in the myotomes of the pharyngula (figure 4.4), remains absent in the trunk and tail of hatching period embryos but is strongly expressed in craniofacial muscle mesoderm and hypaxial, epaxial and pectoral fin muscles. There is also strong expression of *jamc* in the hindbrain at 10 – 13 somites stage (figure 4.2) and 24 h. p. f. (figure 4.4). In contrast, *jamc2* expression is not detected until late stages of segmentation (figure 4.3) and is restricted primarily to the neural tube until at least 24 h. p.f. (figure 4.4). *jamc2* is expressed in the brain throughout pharyngula (figure 4.4) and hatching periods (figure 4.5). There is strong ubiquitous expression of *jamc* evident in all developmental stages tested. I believe this represents the true pattern of *jamc* transcription because RNA *in situ* hybridisation performed using an independent riboprobe, derived from the 3′ UTR of *jamc*, yielded the same results.

There is overlap in expression of the *jam* family genes in the otic placode/vesicle from segmentation through to the pharyngula period, where *jamb*, *jamb2* and *jama*, *jama2* are expressed. Curiously, the expression of *jamb* seems to be limited to small foci at the anterior and posterior poles of the otic vesicle. There is also co-expression of *jamb*, *jamc* and *jamc2* within the brain of the pharyngula (figure 4.4). There is a strong and sustained co-expression of *jamb* and *jamc* within the somites from early segmentation stages (figure 4.2), continuing through late segmentation stages as the caudal-most somites transition into myotome (figure 4.3) before the attenuation of expression of both genes in all but the most rostral somites of the phyrangula (figure 4.4). During the hatching stages, both genes are co-expressed in the craniofacial, limb and abdominal musculature (figure 4.5).

4.3 Detailed expression patterns of *jamb* and *jamc*

While there is clear co-expression of *jamb* and *jamc* in the somites from early segmentation, there seems to be a more dynamic and spatially-restricted expression of *jamc*. Whilst *jamb* is expressed in all myoblasts within nearly all somites of the 10 – 13 somites stage embryo, *jamc* seems to be initially expressed in only a small sub-population of cells in the most rostral somites (figure 4.2). Flatmounts of 10 – 13 somites stage embryos further highlight the limited expression domain of *jamc* to medio-posterior myoblasts along the dorso-ventral axis (figure 4.7) in comparison to the expression of *jamb* in apparently all myoblasts. To better understand the dynamic nature of their expression, I observed expression of both *jamb* and *jamc* throughout early stages of segmentation by wholemount RNA *in situ* hybridisation (figure 4.7). The expression of *jamb* in the somites was first observed at 3 somites stage and

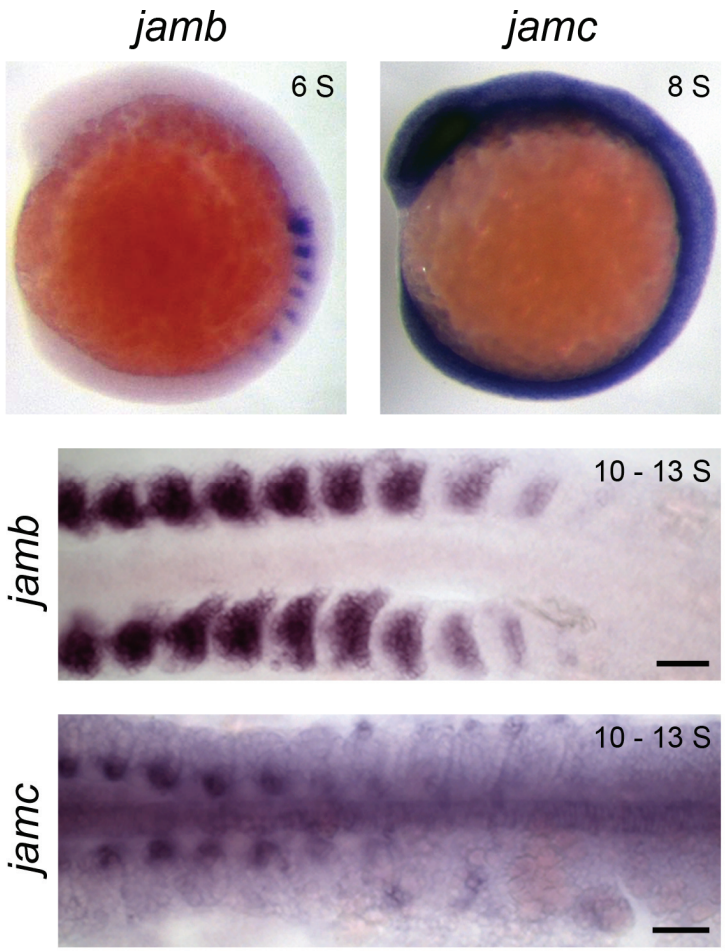

Figure 4.7 Detailed observation of *jamb* and *jamc* expression in somites.

Wholemount RNA *in situ* hybridisation of *jamb* and *jamc* during early segmentation reveals a difference in the timing of expression of both genes. *jamb* is expressed in each somite shortly after formation (top left) and is expressed in all myoblasts (middle). In contrast, *jamc* is not expressed in the somites (top right) until approximately the 10 – 13 somites stage, when it is expressed in a subpopulation of myoblasts in the rostral somites simultaneously (lower panel). Lateral views (top; anterior top) and flatmounts (middle and lower panel; dorsal, anterior left) of wholemount RNA *in situ* hybridisation against *jamb* and *jamc* during early segmentation, stages as indicated in panels. Scale bars represent 50 µm.

continued to be expressed in newly formed somites shortly after their formation. In contrast, *jamc* was not observed in the somites until approximately 10 – 13 somites stage. It was apparently expressed in the first few rostral somites simultaneously, in only a small medio-posterior sub-population of myoblasts. Thereafter, expression of *jamc* seems to appear in each somite shortly after its formation, in a similar fashion to *jamb*.

4.4 Regulation by *prdm1* suggests a fast muscle-specific function for *jamc*, but not *jamb*

Given the apparently static nature of *jamb* expression and the dynamic nature of *jamc*, I sought to find a cause of differential regulation between these genes in the fast muscle myoblasts. Upon examination of the literature, the muscle fate regulatory switch formed by *sox6* and *prdm1* seemed a likely source of regulation of *jamb* and *jamc*, principally because of the similarity of expression pattern between *sox6* and *jamc* (von Hofsten *et al*, 2008). Briefly, *prdm1* is a transcriptional repressor expressed in the adaxial cells of the zebrafish embryo. It represses expression of *sox6*, which would otherwise repress the expression of slow muscle-specific genes, and also directly represses fast muscle-specific genes in the adaxial cells. This combination of activity allows the adaxial cells to adopt a slow muscle fate. In the absence of *prdm1*, adaxial cells express fast muscle-specific genes and adopt a 'mixed' muscle fate.

To test whether either *jamb* or *jamc* are directly regulated by *prdm1*, I performed wholemount RNA *in situ* hybridisation of both genes in wild-type and *prdm1*^{tp39} mutant embryos (kindly provided by Dr Stone Elworthy). I also included a riboprobe against another fast muscle-specific gene, *kirrel*, which encodes a cell surface protein known to play an important role in myoblast fusion (Srinivas *et al*, 2007). Only *jamc* was misexpressed in the adaxial cells of *prdm1*^{tp39} mutants; both *jamb* and *kirrel* were only expressed in fast muscle myoblasts (figure 4.8). These results suggest that only *jamc* expression is repressed in slow muscle by *prdm1*.

4.5 Jamb is located on myoblast and myofibre membranes

To further characterise the expression of Jamb, I made use of a polyclonal antibody raised against the recombinant extracellular domain of Jamb (figure 4.9). Zebrafish muscle differentiation proceeds in a medial-to-lateral wave within each somite in relation to the migration of slow muscle fibres (Henry and Amacher, 2004). Accordingly, Jamb protein was detected on the cell surface of myofibres (medial) and

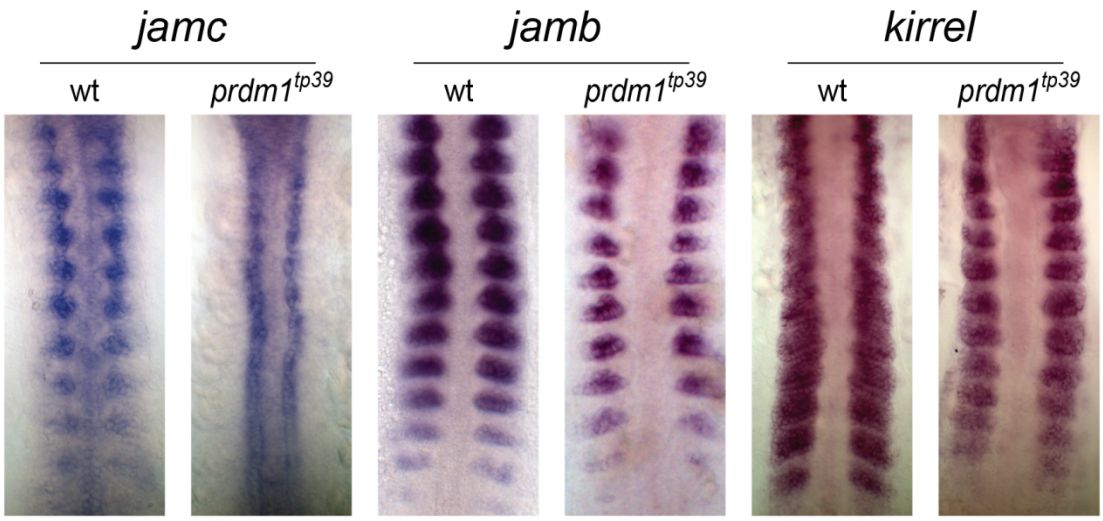

Figure 4.8 *jamc*, but not *jamb* or *kirrel*, is misexpressed in *prdm1*^{tp39} mutants.

Flatmounts of wholemount RNA *in situ* hybridisation of 10 – 13 somites stage wild-type and *prdm1*^{tp39} embryos for *jamc*, *jamb* and *kirrel*. *jamc*, but not *jamb* or *kirrel*, is misexpressed in the adaxial cells of *prdm1* mutant embryos, suggesting it is regulated by *prdm1*, a known repressor of fast muscle-specific genes.

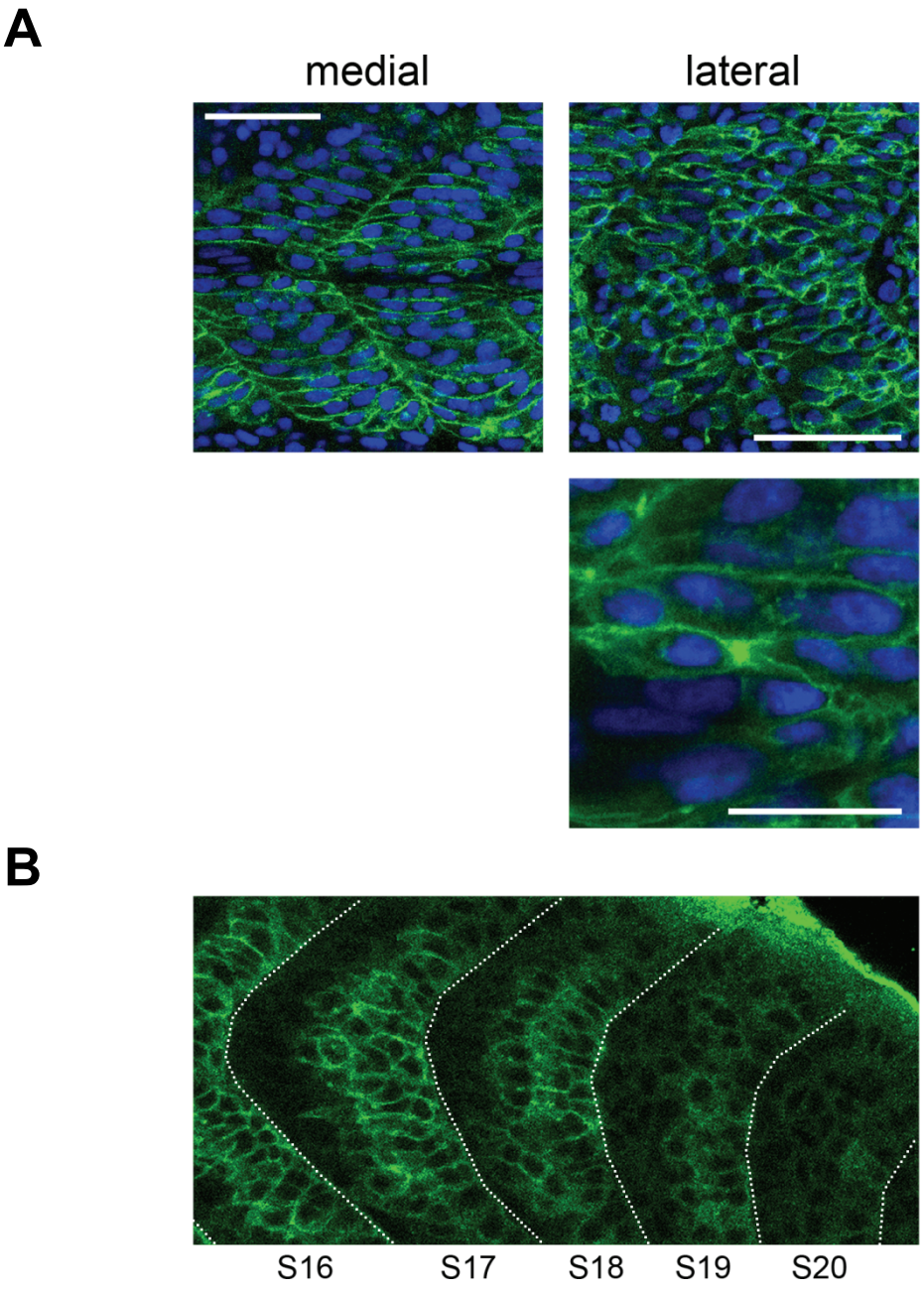

Figure 4.9 Jamb is expressed on the cell surface of myotubes and myoblasts.

A. Immunohistochemistry against Jamb (green) shows the presence of the protein on the cell surface of multinucleated medial myofibres (left) and lateral myoblasts (right). There is considerable enrichment of Jamb at sites of contact between myoblasts (bottom). Somites 8-9 of a 21 somites stage embryo counterstained with DAPI to highlight nuclei (blue), anterior left. Scale bars represent 50 μm in top panels, 20 μm in bottom panel. **B.** Jamb protein (green) is present on the cell membranes of myoblasts within somites shortly after their formation. Caudal somites of 21 somites stage embryo, anterior left. Dotted lines indicate somite boundaries.

myoblasts (lateral) in wild-type embryos during segmentation (figure 4.9). Jamb did not appear to be spatially restricted within the plane of the cell membrane, but was notably enriched at sites of contact between myoblasts. Detection of Jamb in the caudal somites demonstrate little time difference between the transcription and translation of *jamb* and confirm the observation that *jamb* is expressed in myoblasts shortly after the formation of each somite.

4.6 Discussion

To identify potential sites of interactions between Jam proteins and assess redundancy of expression between paralogues, I determined the expression patterns of all members of the zebrafish *jam* family during development by wholemount RNA *in situ* hybridisation.

The predominant example of spatio-temporal co-expression of *jam* family members is that of *jamb* and *jamc* in the somites, between early segmentation and pharyngula periods, coincident with primary myogenesis. In addition, both genes are later expressed in craniofacial, limb and abdominal musculature. Furthermore, Jamb protein was detected on the cell surface of myofibres and myoblasts during segmentation. Taken together, these results strongly suggest a function for the interaction between both proteins in muscle development.

Careful observations of *jamb* and *jamc* expression in the somites during early segmentation reveal interesting differences in the spatio-temporal nature of their regulation. Expression of *jamb* is stable throughout segmentation, beginning in each somite shortly after its formation and attenuated after it has matured into a myotome. In contrast, *jamc* is only expressed in the somites after approximately 10 – 13 somites have formed. It is simultaneously expressed in the most rostral somites and is subsequently upregulated in the remaining somites in an anterior-to-posterior wave. In addition, it is initially only expressed in a sub-population of myoblasts within the somite, a medio-posterior group of cells along the dorso-ventral axis. The expression domain of *jamc* within the somite expands medio-laterally over time. Like *jamb*, *jamc* is also attenuated as each somite matures into myotome. The dynamic expression of *jamc* in comparison to the stable expression of *jamb* suggests differential regulation between the two genes. The expression pattern of *jamc* is very similar to that of myogenin (Weinberg *et al*, 1996), an important transcription factor for terminal differentiation of muscle (reviewed in Pownall *et al*, 2002). It remains to be determined if *jamc*, but not *jamb*, is a target of myogenin.

Notably, *jamc* is misexpressed in the adaxial cells of *prdm1*^{tp39} mutants. This

suggests that *jamc*, but not *jamb* and *kirrel*, is repressed by *prdm1*. This observation is of particular interest because wild-type slow muscle is mononuclear (Roy *et al*, 2001) but *prdm1* mutant adaxial cells undergo fusion with other myoblasts (von Hofsten *et al*, 2008). Therefore, key components of myoblast fusion must be regulated by *prdm1*, directly or otherwise. Kirrel is orthologous to Dumbfounded and Roughest, cell surface proteins known to be critical for myoblast fusion in *Drosophila*. Loss-of-function of *kirrel* in zebrafish results in a near complete block of myoblast fusion (Srinivas *et al*, 2007). Given these observations, it is surprising to find that *kirrel* is not regulated by *prdm1*, but that *jamc* is. One possible hypothesis is that *jamc* is a critical regulator of myoblast fusion. Subsequent experiments demonstrate that this is likely to be the case (see Chapters 6, 7 and 8).

Previous analysis indicated a high level of conservation between the amino acid sequences of the extracellular domains of the zebrafish Jam family proteins, especially between paralogues (see Chapter 3). This suggested a possibility of cross-hybridisation between riboprobes and other *jam* transcripts, confounding the purpose of determining the expression patterns of each gene. The level of nucleotide conservation between the coding sequences of the extracellular domains is lower, as determined by clustalW alignments, but still very high between *JAM-A* paralogues, 82% (see table 4.2). The expression patterns of both *jama* and *jama2* genes are almost identical, although the relative expression of *jama2* does seem to be weaker. However, both genes are in close proximity in the zebrafish genome (see Chapter 3), and so may be regulated by the same promoter or enhancer elements. Further investigation with riboprobes derived from the dissimilar 3′ untranslated regions (UTR) of either gene would be necessary to differentiate between these possibilities. The distinct expression patterns between the *JAM-B* and *JAM-C* orthologues suggest that any overlap between them is unlikely to be a result of cross-hybridisation. It also suggests that there is little similarity in transcriptional regulation of the paralogues, with the obvious exception of *jama*/*jama2*, reducing the likelihood of redundancy amongst them.

In summary, analysis of expression of the zebrafish *jam* family indicates a role for *jamb* and *jamc* during primary myogenesis and lessens the likelihood of redundancy amongst family members that might otherwise confound analysis of the function of the interaction between Jamb and Jamc during development.

Table 4.2 Identity of coding sequence and amino acid sequence of immunoglobulin domains between *jam* family members. Percent identity of clustalW alignments; values ≥ 50% are highlighted in bold.

	jama	*jama2*	*jamb*	*jamb2*	*jamc*	*jamc2*	
jama		**75%**	35%	33%	29%	31%	Immunoglobulin domains (aa)
jama2	**82%**		33%	29%	31%	31%	
jamb	34%	7%		**50%**	36%	32%	
jamb2	30%	14%	**57%**		32%	31%	
jamc	31%	10%	49%	17%		**63%**	
jamc2	17%	22%	14%	26%	**63%**		
	CDS of immunoglobulin domains (nucleotides)						

Chapter 5

Determining the physical interactions within the zebrafish Jam family

Summary

In this chapter I describe the biochemical interactions between the soluble ectodomains of all identified members of the zebrafish Jam family and the implications for studying Jam family interactions during development in light of their spatio-temporal expression data. The cloned extracellular domain of each of the Jam family members was expressed by transient transfection of a mammalian cell line, purified and used in a surface plasmon resonance (SPR) -based biochemical interaction screen. The dissociation rate constants for each monomeric interaction was determined from the dissociation phase data and used to compare their relative strengths. Interactions amongst the Jam family members appear to be conserved between fish, mice and humans. The wide range of interaction strengths suggests that even closely related family members would be less able to act redundantly. In the context of spatio-temporal expression in early development, only heterophilic interactions between Jamb and Jamc seem likely, given co-expression in fast muscle myoblasts.

5.1 Introduction

Interactions between mammalian JAM family members have already been described (figure 5.1; reviewed in Weber *et al*, 2007), though rarely in a systematic or quantitative way. Crystallographic studies have suggested two different binding modes between mouse and human JAM-A ectodomains; homophilic binding *in cis* through conserved residues in the surface formed by GFCC' β-strands, and homophilic binding of homodimers *in trans*. A bioinformatic analysis of the zebrafish Jam family showed strong conservation of the putative binding site in the membrane-distal immunoglobulin-like domain in all homologues (see Chapter 3), suggesting similar binding capabilities. I sought to test whether biochemical interactions were conserved in the zebrafish Jam family and to evaluate the likelihood of other Jam family interactions with either Jamb or Jamc that might confound functional studies. In order to achieve these goals, I undertook a systematic and comparative surface plasmon resonance interaction study using soluble ectodomain fragments of each Jam family member.

Surface plasmon resonance (SPR) is a very sensitive method to detect physical interactions between an immobilised ligand and a soluble analyte in real-time (reviewed in van der Merwe and Barclay, 1996; figure 5.2). Under total internal reflection, light reflecting off a thin conducting film at the interface between two media with different refractive indices will generate an electrical field. This evanescent wave field has a very limited depth of penetration across the media. At a certain combination of angle of incidence (θ_i) and wavelength (λ), the incident light excites plasmons in the conducting film, resulting in a loss of reflected light at a corresponding angle of reflection (θ_r). Because the evanescent wave penetrates the media, the angle of incidence and wavelength necessary to cause this absorption of energy is dependent upon the refractive index of the media within the depth of penetration by the wave field. The Biacore technology uses sensor chips containing a thin film of gold (the conducting film) on a glass surface, over which a sample solution is passed by a microfluidic system. Changes in solute concentration within the depth of evanescent wave field change the refractive index of the media, and so the angle at which plasmons are excited in the gold film at a fixed wavelength (800 nm). The change in absorption angle is monitored in real time over a fixed range of θ_i/θ_r and recorded in arbitrary response units (RU). The ligand of interest is immobilised on the glass surface and analyte solutions are passed over the sample; any change in the SPR signal is recorded every tenth of a second (10 Hz, figure 5.3). An analyte that binds the immobilised ligand will change the SPR signal by changing

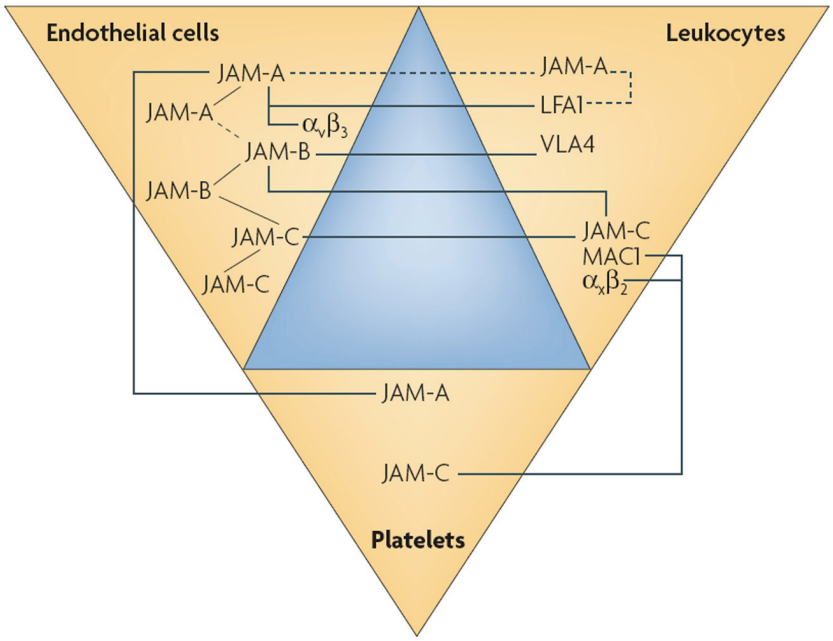

Figure 5.1 Known extracellular interactions of JAM family proteins.

Diagram illustrating known extracellular interactions between JAM family proteins and integrins expressed on the surface of mammalian endothelial and peripheral blood cells. Reproduced from Weber *et al* (2007), without permission.

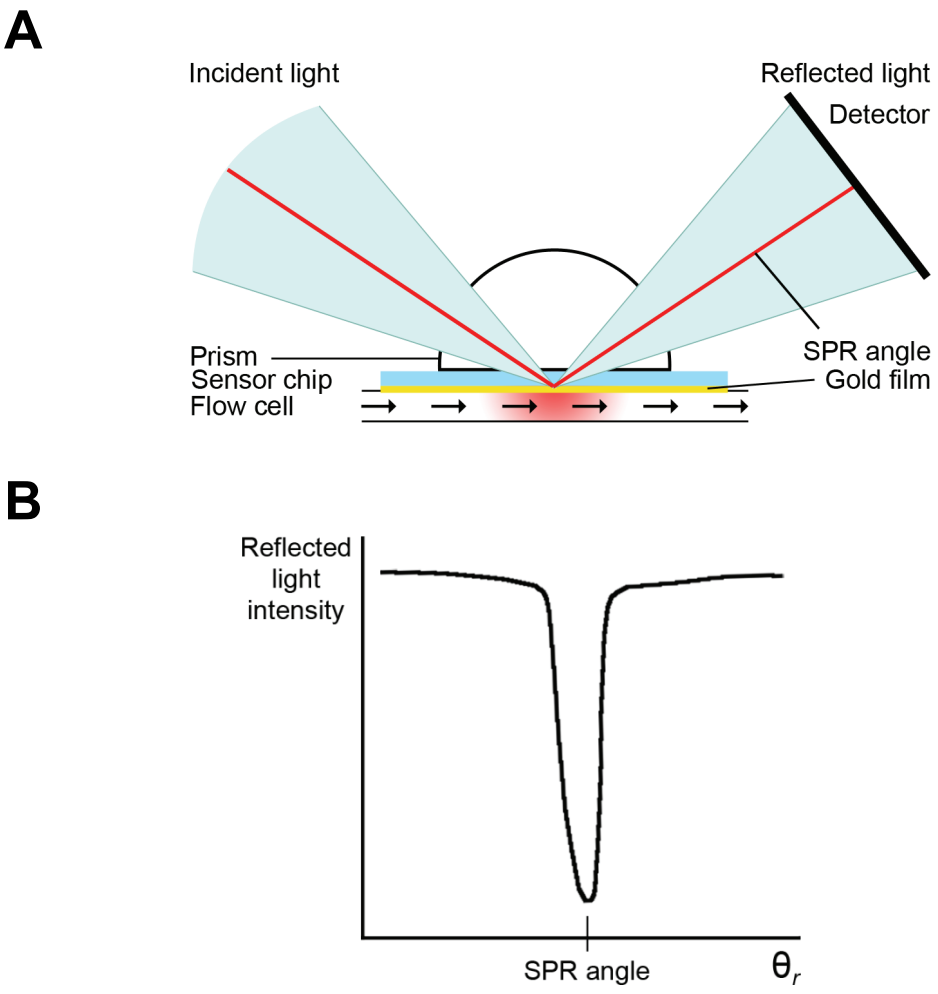

Figure 5.2 The surface plasmon resonance principle.

A. Schematic of Biacore technology used to detect protein interactions. Light (λ = 800 nm) at a fixed range of angle of incidence strikes a thin gold film, exciting plasmons and generating an evanescent wave field which penetrates the media within the flow cell. The light is reflected internally onto a detector which measures intensity. **B.** The intensity of reflected light drops at a particular angle that generates an evanescent wave field (the SPR angle). The SPR angle changes with respect to changes in the refractive index of the media passing through the flow cell. Modified from Biacore Sensor Surface Handbook, October 2003 edition, without permission.

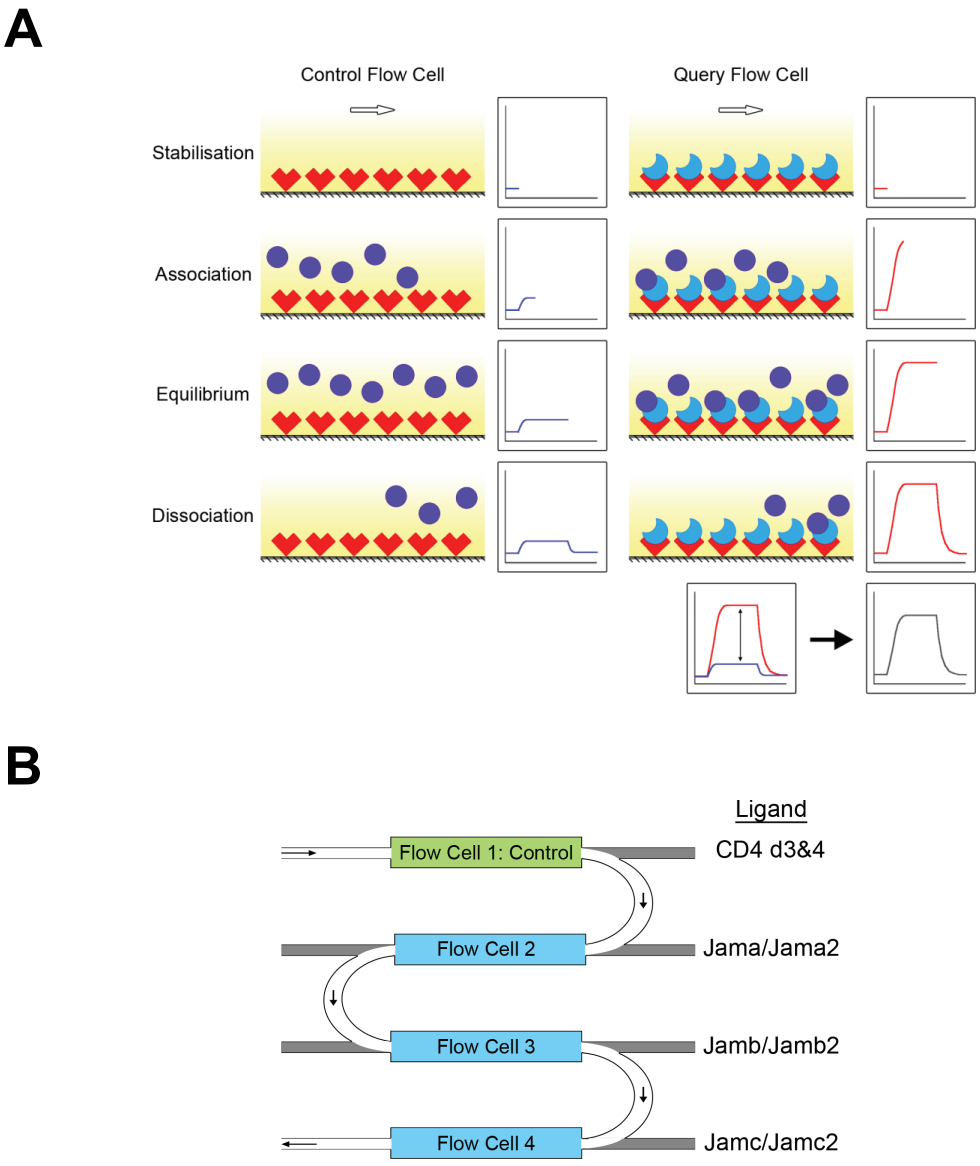

Figure 5.3 Real-time monitoring of protein interactions by surface plasmon resonance.

A. Schematic depicting real-time detection of interactions of an analyte (purple) with an immobilised ligand in a query flow cell (right, blue and red) but not in the control flow cell (left; red) in parallel over time: buffer stabilisation, association, equilibrium and dissociation (top to bottom). The changes in SPR responses plotted against time are displayed in the graphs to the right of each flow cell. Binding measurements are made by subtracting the control flow cell responses from the query cell responses. Arrows indicate the direction of flow. **B.** Schematic of the microfluidic chamber demonstrating arrangement of flow cells, the analyte flow path and the ligands immobilised in the flow cells of two sensor chips. A continuous flow of analyte allows each surface to be tested in parallel.

the refractive index of the media within the effective penetration depth of the evanescent wave field, approximately 20% of the wavelength of incident light (160 nm at θ_i = 800 nm). This increase in signal will be beyond the change in signal in the negative reference sample, tested in parallel. Binding is measured by subtracting the SPR response observed with the negative reference ligand from that observed with the query ligand. An analyte that doesn't bind the immobilised ligand will still change the SPR signal, as it has a different refractive index to the buffer used, but will not be beyond that observed in the negative reference.

The real-time monitoring of SPR signal allows for a quantitative analysis of the kinetics of binding. Comparing the half-lives of interactions is a useful and intuitive way to assess the relative strengths of similar binding events. For a simple interaction, the rate of decay of the interaction complex, assuming first-order dissociation kinetics, is defined as:

$$-\frac{d[A \cdot B]}{dt} = k_{\mathrm{d}}\,[A \cdot B]$$

where $[A \cdot B]$ is the concentration of the complex and k_{d} is the dissociation rate constant (s^{-1}). At t = ½, the concentration of the complex is halved:

$$\int_{[A.B]}^{\frac{[A.B]}{2}} \frac{d[A \cdot B]}{[A \cdot B]} = -\int_{t_0}^{t_{½}} k_{\mathrm{d}}\; dt$$

After integration and subsequent rearrangement:

$$t_{½} = \frac{\ln 2}{k_{\mathrm{d}}}$$

It is clear that the half-life depends on the dissociation rate constant (k_d) alone. This is useful, because determining the true concentration of active protein within a sample is notoriously difficult, particularly if the protein is known to bind itself, and can introduce a considerable source of error. Note also that true first order dissociation produces a linear plot when the natural logarithm of concentration of bound complex is plotted against time:

$$\ln[A \cdot B] = -k_{\mathrm{d}} \cdot t$$

with a slope equal to the inverse of the dissociation rate constant.

To assess the possibility of redundancy amongst zebrafish Jam family proteins I identified interactions amongst recombinant immunoglobulin domains using surface plasmon resonance. I identified many interactions with a range of strengths, suggesting little redundancy between the proteins with respect to biochemistry.

5.2 Jam family ectodomain production and purification

I tested all possible pairwise interactions amongst zebrafish Jam family proteins, using each protein as both immobilised ligand and soluble analyte. To do this, I expressed soluble recombinant ectodomains of each protein, fused to rat CD4 domains 3 and 4 (CD4-d3&4), in two forms using mammalian cell culture: one tagged with a C-terminal biotinylation peptide, the other with a C-terminal hexa-histidine tag (figure 5.4; see Materials and Methods for further details). The former were assessed by enzyme-linked immunosorbent assay (ELISA; figure 5.4) and immobilised on streptavidin-coated Biacore chips in molar amounts equivalent to the negative control ligand, CD4-d3&4 tag only (figure 5.3). The latter were purified using a nickel column, followed by gel filtration to remove impurities and exchange the protein into SPR buffer (figure 5.5). Analyte concentrations were estimated by absorbance at 280nm, based upon *in silico* predicted absorption co-efficients.

5.3 Using surface plasmon resonance to quantify Jam family interactions

To establish the network of interactions between the Jam family proteins, I performed an-all-against-all SPR screen using the recombinant proteins produced. After an analyte was purified, several dilutions were passed over each of the immobilised ligands at high flow rate to minimise re-binding effects. The SPR response in each flow cell was measured simultaneously and in real-time. The CD4-d3&4 tag negative control protein surface response was subtracted from the data collected in each flow cell in parallel and real-time. The data were corrected for a time lag in sample delivery between the flow cells which are connected in series (see Materials and Methods for full details; figures 5.3 and 5.6). Several biochemical interactions, of varying strengths, were identified within the family (figure 5.7).

5.4 Comparing Jam family interactions

To assess quantitative differences between interactions, I determined k_d and calculated half-lives from dissociation curves plotted from SPR data (tables 5.1 and 5.2). Each interaction was first shown to comply with first order dissociation kinetics by plotting the natural logarithm of specific binding against time (figure 5.8). Some interactions were not analysed because of limited data; where $t_{½}$ is below the frequency of detection of the instrument used (≤ 0.1 sec). Dissociation curves were then plotted for three different concentrations of analyte in each interaction and k_d estimated by fitting equations of the form:

A

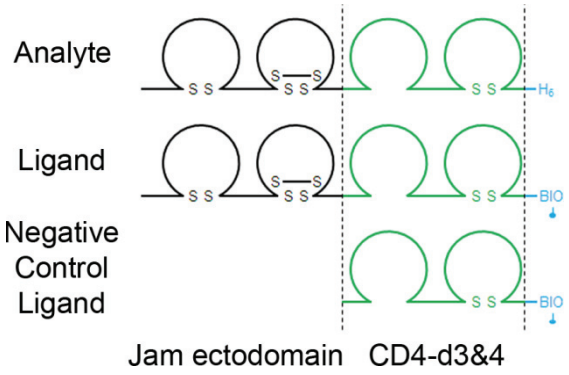

B

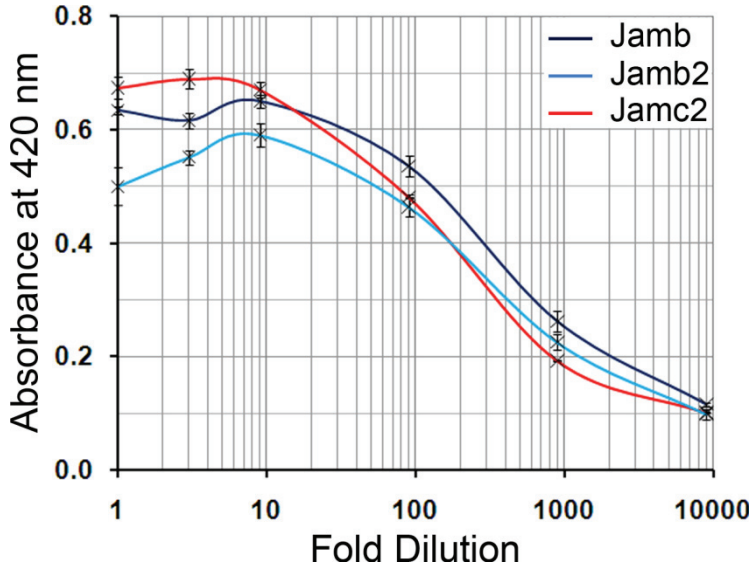

Figure 5.4 Production and quantification of biotinylated Jam family ectodomains.

A. Diagrams of fusion proteins produced for SPR screening. Jam ectodomains were fused to a CD4-d3&4 tag (green) and either a hexa-histidine tag (H_6; analyte) or a substrate peptide for the biotin ligase, BirA (bio; ligand). The negative control ligand was the CD4-d3&4 tag and the BirA substrate peptide only. **B.** Example ELISA assay to quantify production of ligands tagged with biotin by BirA, using streptavidin-coated plates to capture the biotinylated protein.

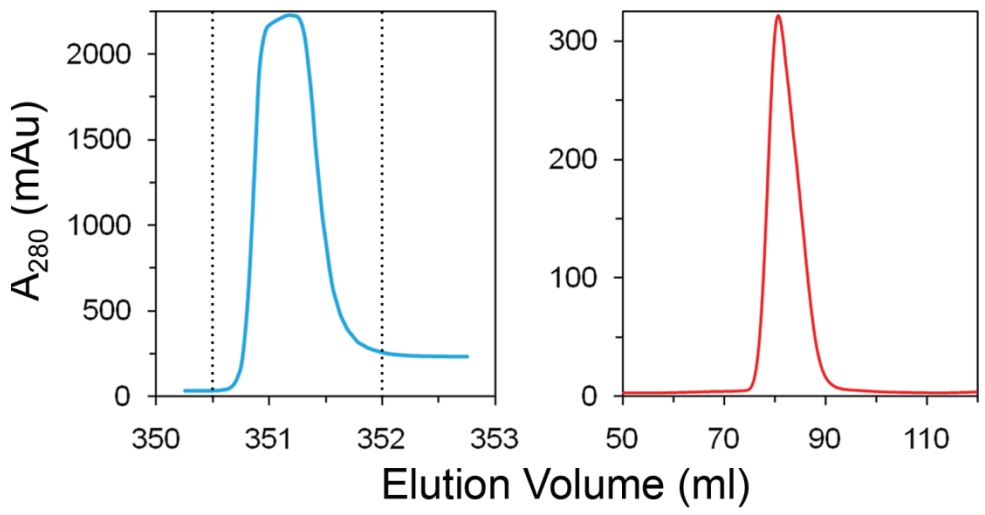

Figure 5.5 Purification of histidine-tagged Jam family ectodomains.

Example traces of purification of Jamc analyte by nickel column (left) followed by gel purification (right) as monitored by absorbance of flowthrough at 280 nm. The purified protein was eluted from a nickel column using imidazole and the combined peak fractions (dashed lines, left) were then purified by gel filtration (right). Peak fractions, eluted from the gel filtration column in SPR running buffer, were then used for SPR in serial dilutions.

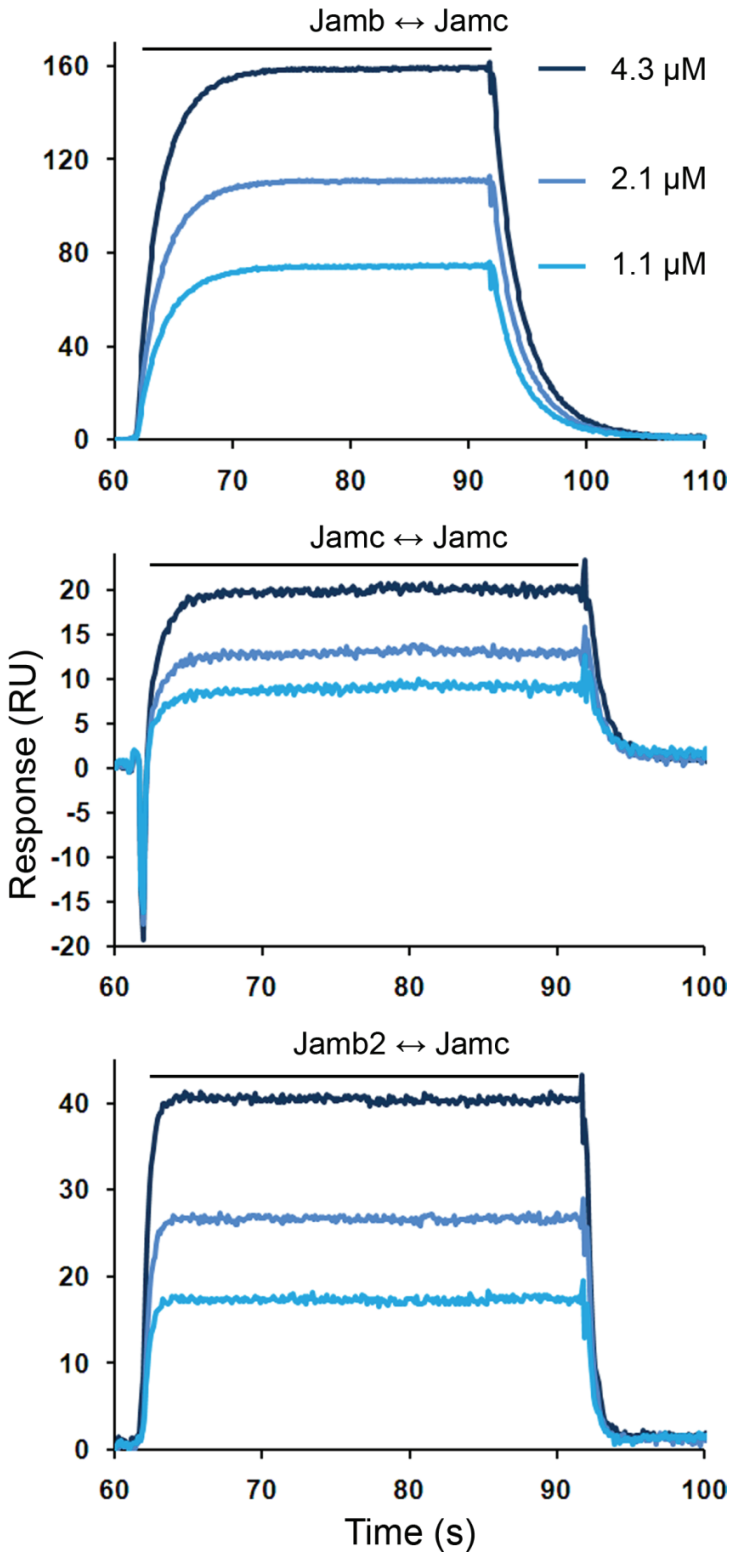

Figure 5.6 Example sensorgrams of detected interactions.

Sensorgrams demonstrating three interactions of differing affinity detected using the same analyte, Jamc, tested against immobilised Jamb, Jamc and Jamb2. Responses from experiments using three dilutions of analyte (4.2, 2.1 and 1.1 μM) are displayed for each interaction. Bar above sensorgrams represents injection phase.

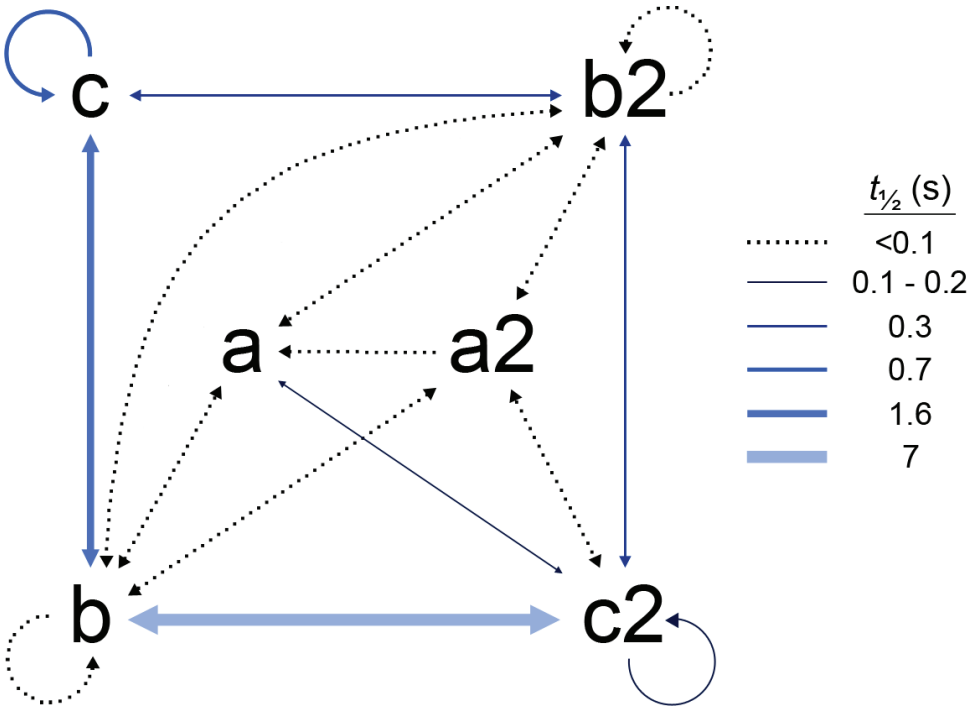

Figure 5.7 Network of interactions detected between Jam family proteins.

Schematic showing all interactions detected between Jam family extracellular domains in the surface plasmon resonance screen, colour-coded according to half-life. Double-headed arrows represent interactions detected in both orientations of immobilised ligand and analyte; single-headed arrows represent unreciprocated interactions.

Table 5.1 Dissociation rate constants for interactions amongst JAM family proteins. Dissociation rate constants are presented for each positive interaction observed. Interactions that were too weak to quantify are given the nominal value ≥ 6.9, equivalent to a half-life of 0.1 seconds. Interactions that could be quantified are presented as a mean ± S. D. (n = 3) and are highlighted in bold.

Ligand	Analyte					
	Jama	Jama2	Jamb	Jamb2	Jamc	Jamc2
Jama	-	-	≥ 6.9	≥ 6.9	-	**4.43 ± 0.95**
Jama2	≥ 6.9	-	≥ 6.9	≥ 6.9	-	≥ 6.9
Jamb	≥ 6.9	≥ 6.9	≥ 6.9	≥ 6.9	**0.37 ± <0.01**	**0.09 ± <0.01**
Jamb2	≥ 6.9	≥ 6.9	≥ 6.9	≥ 6.9	**2.44 ± 0.28**	**1.88† ± 0.05**
Jamc	-	-	**0.50 ± 0.04**	**2.86 ± 0.22**	**1.03 ± 0.09**	-
Jamc2	≥ 6.9	≥ 6.9	**0.11 ± <0.01**	**2.39† ± 0.30**	-	**6.22 ± 0.60**

† denotes an interaction that appears to display a two-phase dissociation - the dissociation rate constant is estimated from the first 0.9-1 seconds of dissociation (accounting for approximately 85-90% of specific binding) that fits a first order exponential decay model with an $R^2 \geq 0.97$.

Table 5.2 Calculated half-lives for interactions amongst JAM family proteins. Calculated half-lives are presented for each positive interaction observed. Interactions that were too weak to quantify are given the nominal value of ≤ 0.1 seconds. Half-lives are calculated using the average value of the dissociation rate constant for each interaction and the formula $t_{½} = \ln 2 / k_d$.

Ligand	Analyte					
	Jama	Jama2	Jamb	Jamb2	Jamc	Jamc2
Jama	-	-	≤ 0.1	≤ 0.1	-	**0.16**
Jama2	≤ 0.1	-	≤ 0.1	≤ 0.1	-	≤ 0.1
Jamb	≤ 0.1	≤ 0.1	≤ 0.1	≤ 0.1	**1.87**	**7.70**
Jamb2	≤ 0.1	≤ 0.1	≤ 0.1	≤ 0.1	**0.28**	**0.37**†
Jamc	-	-	**1.39**	**0.24**	**0.67**	-
Jamc2	≤ 0.1	≤ 0.1	**6.30**	**0.29**†	-	**0.11**

† denotes an interaction that appears to display a two-phase dissociation – the half-life was calculated from the dissociation rate constant estimated from the first 0.9-1 seconds of dissociation (accounting for approximately 85-90% of specific binding) that fits a first order exponential decay model with an $R^2 \geq 0.97$.

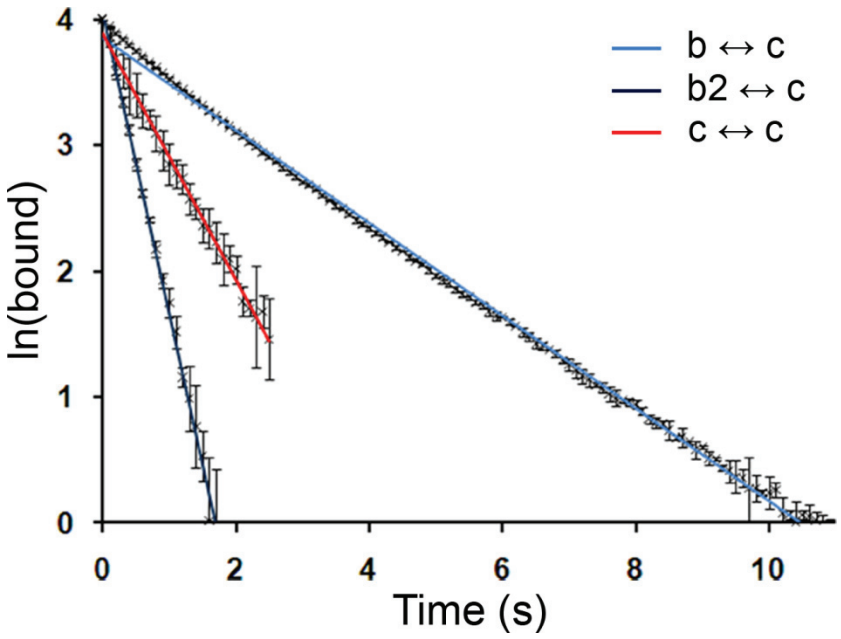

Figure 5.8 Example plots of dissociation phase data demonstrating first-order kinetics.

Three example plots of ln(bound) as a function of time for dissociation phase data of three interactions of differing affinity, demonstrating first-order dissociation kinetics. Each series represents the average of three experiments using different dilutions of Jamc analyte (4.2, 2.1 and 1.1 μM); error bars represent standard deviation.

$$y = Ae^{-k_d \cdot t}$$

to the data (figure 5.9, table 5.1). Estimates of k_d were then converted to half-lives, as previously described, and used for comparison (figure 5.9, table 5.2). A wide range of half-lives were determined, ranging from 7.7 seconds to 0.11 seconds. Estimates for k_d were slightly different depending on the orientation of ligand and analyte for a given interaction. This is likely to be because of rebinding effects, despite the high flow rate of analyte.

5.5 Discussion

To test the relative properties of each of the Jam family proteins I performed a quantitative all-against-all biochemical interaction screen using the conserved extracellular domains. The results described above demonstrate that the ectodomains do not appear to be biochemically equivalent with respect to binding kinetics or specificity *in vitro*.

The generalised scheme of protein interactions amongst family members seems to be conserved between zebrafish and mammals (compare figure 5.1 and figure 5.7). For example, zebrafish Jamb proteins interact with Jamc proteins. JAM-C is known to bind itself in mouse and human; similarly, each zebrafish JAM-C paralogue protein interacts homophilically. Some interactions have not been identified in previous studies, such as the weak interactions detected between Jamc2, *JAM-B* paralogues with both *JAM-A* paralogues. Curiously, Jamc and Jamc2 do not interact with each other, suggesting that they have diverged enough to no longer bind each other whilst retaining homophilic binding activity. Both JAM-C paralogue proteins also bind both Jamb proteins, with remarkably different affinities. In contrast, homophilic and heterophilic interactions were detected amongst Jamb proteins. Also, both Jamb paralogues were found to interact with Jama, but only one of the Jamc paralogues was found to, Jamc2. This suggests that whilst the JAM-C paralogues have diverged with respect to binding specificity, JAM-A and JAM-B paralogues have not, despite the high level of primary amino acid sequence conservation between the extracellular domains of paralogues in all 3 subgroups (see Chapter 3).

A defining characteristic of each of the JAM family proteins is a conserved binding site in the concave surface formed by the GFCC′ β-strands of the distal immunoglobulin-like domain. This motif, R(V,I,L)E ... Y, contains residues important for forming salt bridges between monomers *in cis*, as identified by crystallographic studies (Kostrewa *et al*, 2001; Prota *et al*, 2003). The core of the motif is completely conserved amongst all JAM proteins from zebrafish to humans, but other amino

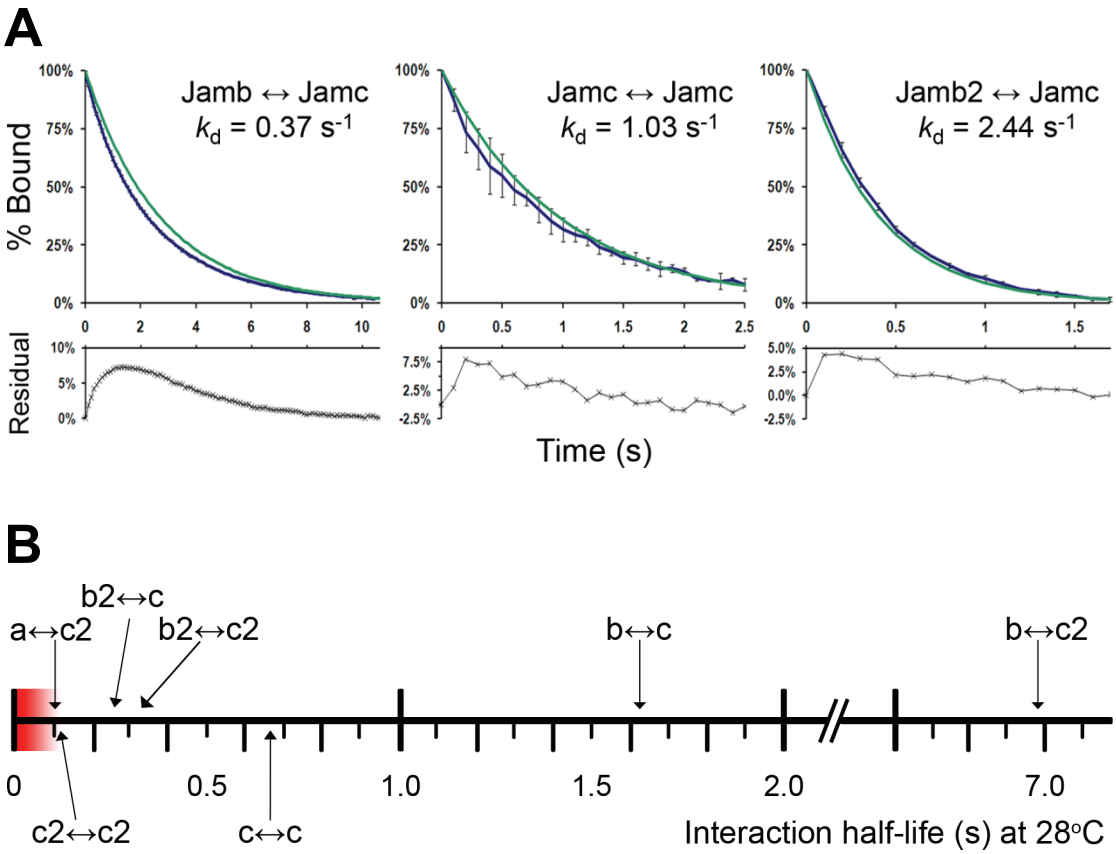

Figure 5.9 Comparing dissociation phase data reveals a wide range of interaction strengths within the Jam family.

A. Examples of observed dissociation curves (blue) and first order decay curves of the respective dissociation rate constants ($y = Ae^{-k \cdot t}$; green) demonstrating a goodness of fit for three interactions of differing strengths. Residuals represent the differences between observed and modelled data. Observed curves are the average of three experiments using different dilutions of Jamc analyte (4.2, 2.1 and 1.1 μM); error bars represent standard deviation. **B.** Scale showing the different half-lives for all interactions quantified; heterophilic interactions are grouped above the scale, homophilic interactions below. Region highlighted in red represents the detection limit of the instrumentation and materials used.

acids that form the binding surface are more variable. This comprehensive, quantitative study of the relative strengths of interactions demonstrates that there is great variability within the family. Crystallographic modelling suggests that the formation of dimers *in cis* through the GFCC′ surface is necessary for interactions *in trans* (Kostrewa *et al*, 2001; Prota *et al* 2003). However, each of the dissociations I studied conformed to first-order kinetics, suggesting no pre-requirement of homodimer formation *in cis* for interactions *in trans*.

Unfortunately, many of the interactions identified were refractory to quantitative analysis, likely because of high K_D i.e. the analyte protein concentration was below that required to saturate available binding sites in each case. Detection of the weakest interactions could be improved by deliberate multimerisation of the extracellular domains through a C-terminal tag such as the cartilage oligomeric matrix protein (COMP). This would increase the avidity of any interaction and add confidence to the detection of weak interactions (Bushell *et al*, 2008). However, any kinetic data would be difficult to interpret or compare to other interactions, as association and dissociation phases would likely be of a higher order.

In summary, the data presented here suggest clear biochemical differences between the Jam family proteins with respect to binding specificity and kinetics, despite strong conservation of primary amino acid sequence. Intra-family interactions are broadly conserved, but paralogues demonstrate differing binding kinetics when interacting with the same ligand. These results suggest it is unlikely that any of the Jam family proteins function redundantly.

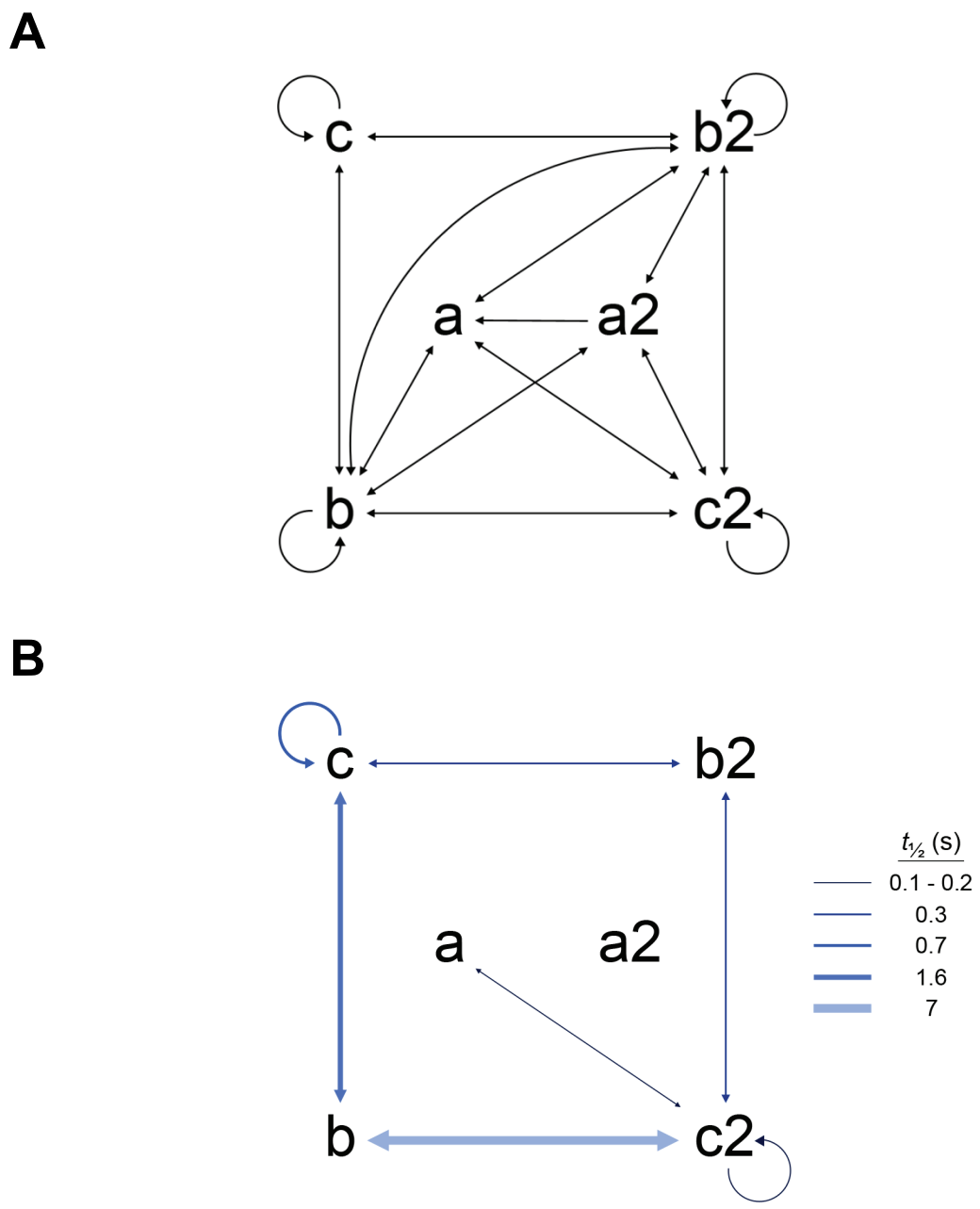

Figure 5.7 Schematics of the interactions detected between Jam family proteins.

A. Schematic showing all interactions detected between Jam family extracellular domains in the surface plasmon resonance screen. **B.** Schematic showing all quantified interactions, colour-coded according to half-life. Double-headed arrows

Chapter 6

Characterization of the *jamb* and *jamc* mutant phenotypes

Summary

In this chapter I describe the phenotype of mutant embryos homozygous for the *jamb*^{HU3319} nonsense allele or the *jamc*^{sa0037} missense allele. Disruption of either gene results in a complete lack of myoblast fusion, characterized by mononuclear fast-twitch muscle fibres with a striking regimented arrangement of centrally-positioned nuclei with respect to myotome boundaries. Mutant mononuclear fibres differentiate fully, as determined by expression of fast muscle myosin heavy chain, but appear to be delayed; the elongation of each fibre and concomitant arrangement of nuclei is not evident until approximately 32 h. p. f. There is a 1.8-fold and 1.6-fold increase in the number of fast muscle fibres in *jamb* and *jamc* mutant embryos, respectively. These phenotypic characteristics are inconsistent with the *Drosophila* founder cell paradigm of myoblast fusion, suggesting a different vertebrate-specific regulatory mechanism is used for this process.

6.1 Introduction

Loss-of-function experiments are crucial to the study of any biological system. The functions of JAM-B and JAM-C in mouse have been well-characterised using targeted knockout mutants generated through homologous recombination (see Chapter 1). Unfortunately, this technique is not yet available for the study of gene function in zebrafish.

Forward genetics screens were of key importance to the identification of critical genes involved in the early development of zebrafish (Driever *et al*, 1996). Briefly, chemical mutagenesis generated many mutant lines identified from assaying phenotypic defects in a biology of interest, for example, muscle motility (Granato *et al*, 1996). The causative allele of a given mutant is then later identified by positional cloning. This process is lengthy and resource intensive, but yields important long-term tools and relevant functional information. For example, the *candyfloss* mutant identified from a screen of muscle motility mutants (Granato *et al*, 1996) has been used to better understand the pathology of a major subgroup of congenital muscular dystrophies (CMD), the *laminin α2*-deficient CMD (MDC1A; Hall *et al*, 2007). Forward genetics screens are primarily limited by the difficulty of screening large numbers of embryos with ever more complicated phenotypic assays to identify rare phenotypes or mutations. With increasingly cheaper sequencing and the availability of complete genome sequences, more targeted reverse genetics methods for generating non-functional alleles are now widely used. Targeting Induced Local Lesions IN Genomes (TILLING) is an established method in zebrafish, first designed for use in studying *Aradopsis thaliana* (McCallum *et al*, 2000) and subsequently adapted for other organisms. Briefly, male zebrafish are chemically mutagenised and then mated to wild-type females to yield a library of F1 progeny. Genomic DNA is taken from F1 fish and analysed for mutations within a gene of interest by PCR and sequencing. Identified heterozygous carrier F1 fish are then outcrossed as many times as may be required to isolate the mutation of interest from other 'background' mutations, which may be closely linked. The random mutagenesis of an individual genome can result in an allelic series for a given gene from a single screen. However, disruption of haploinsufficient genes and mutations that result in a dominant lethal phenotype cannot be isolated by TILLING. Other reverse genetic methods which use different means of random mutagenesis have been developed, for example, retroviral insertions (Wang *et al*, 2007) or transposon-mediated gene trapping (Kawakami *et al*, 2004). These techniques require maintenance of large libraries of fish and are also resource intensive, making them less suitable for small scale laboratories.

A more recently developed genetic method for targeted loss-of-function in zebrafish makes use of customised zinc finger nucleases (ZFN; reviewed in Urnov *et al*, 2010), originally applied to *Drosophila melanogaster* (Bibikova *et al*, 2002). Briefly, customised proteins, containing three zinc finger domains and the catalytic domain of FokI nuclease, are designed to bind specific inverted 9 base pair DNA sequences flanking a site of interest, separated by 4-6 base pairs. FokI nuclease is only active upon dimerisation. Once bound to both sites within the genomic DNA, in the correct orientation, the FokI domains can dimerise and induce a double-strand break. Repair of this lesion by non-homologous end joining can result in a small insertion or deletion that disrupts the targeted gene. This is an exciting technology, with a potential for gene modification or addition through homology-directed repair. The main drawback, however, is the lengthy and complicated process to produce specific nucleases that are active *in vivo* and have the desired effect of yielding a targeted mutant line.

In the absence of rapid genetic methods for gene disruption in zebrafish, morpholinos have been widely used in functional studies (reviewed in Bill *et al*, 2009). Morpholinos are antisense oligonucleotides in which the phosphoribose backbone has been replaced with a phosphorodiamidate backbone. This modification yields higher affinity binding to RNA and prevents enzymatic degradation of the oligomer *in vivo*. Morpholinos are injected into zebrafish embryos to block the translation or splicing of a specific target mRNA. The oligomer binds to the translation start site or a splice donor site, inhibiting translation or splicing by steric hindrance. While morpholinos have proved to be useful reagents, there has been considerable difficulty in controlling toxicity and off-target binding effects (reviewed in Eisen and Smith, 2008). Previously, a morpholino targeting *jamc*[1] was included in a functional screen of cell surface and secreted proteins in zebrafish (Pickart *et al*, 2006). The morpholino-injected embryos displayed a marked defect in pigmentation. At 24 h. p. f., morpholino-injected embryos lacked differentiated melanophores until approximately 48 h. p. f. No other phenotype was described for this morpholino. It is important to note, however, that only 15 of the 25 nucleotides of the sequence are found to match the very 5′ end of the annotated *jamc* 5′ UTR. No full-length matches were identified through BLAST searches of the entire nucleotide collection at the NCBI. Given these difficulties, it is highly unlikely that this phenotype is a result of the

[1] This morpholino was incorrectly annotated as targeting *jam2* (referred to here as *jamb*). A BLAST search of the morpholino sequence against the zebrafish genome reveals its target as *jamc*. It is not similar to any other zebrafish *jam* family members.

loss-of-function of *jamc*.

To get the best and most unequivocal results of loss-of-function studies of *jamb* and *jamc*, I sought out TILLING mutants from two different resources available to other zebrafish researchers: the Hubrecht Laboratory and the Wellcome Trust Sanger Institute Zebrafish Mutation Resource. Very shortly after obtaining these mutants, it became obvious that loss-of-function of both genes results in a near-complete loss of myoblast fusion. To highlight the phenotypic consequences of disruption of myoblast fusion genes in different model organisms, I will briefly describe results from functional studies of the guanine exchange factor *myoblast city* (*mbc*) in *Drosophila* and its orthologues *Dock1* and *Dock5* in zebrafish and mouse.

Loss-of-function of *mbc* in *Drosophila* results in a complete block of myoblast fusion (Rushton *et al*, 1995). All null alleles of *mbc* are recessive and embryonic lethal, as the mutant larvae are unable to hatch from the vitelline membrane. Within the hemisegment of a *mbc* mutant larvae, there are two phenotypically different populations of unfused myoblasts. One is a large population of rounded, myosin-expressing myoblasts that are phagocytosed by macrophages, decreasing in number from around 13 hours after egg laying (AEL). The other is a small population of myoblasts that also express myosin, but persist until 17 hours AEL, migrate to positions of body wall muscles and elongate and attach to the epidermis. These sub-populations are referred to as fusion-competent myoblasts (FCMs) and founder cells, respectively (see Chapter 1).

In contrast, morpholino knockdown of zebrafish homologues *dock1* or *dock5* results in a significant increase in mononucleate fibres at 26 – 28 h. p. f., but the majority of myocytes elongate to span each somite (Moore *et al*, 2007). Simultaneous knockdown of *dock1* and *dock5* does not result in any significant enhancement of the phenotype of either morpholino used individually. This suggests that disruption of both genes only partially suppresses myoblast fusion.

Investigation of *Dock1* null embryos in mouse reveals a similar phenotype. At embryonic day 13.5 – 14.5 the majority of myosin heavy chain-expressing fibres are elongated and mononuclear throughout the embryo (Laurin *et al*, 2008). Primary myoblasts isolated from embryonic day 18.5 *Dock1* null mice reveal a significant defect in myoblast fusion in culture; 80% of desmin-expressing *Dock1* null myoblasts remain mononucleate, in contrast to 20% of wild-type myoblasts. It is important to note, however, that the isolated null primary myoblasts remained rounded in cell culture, but elongate and align to form muscle bundles in the embryo. The *Dock1* null allele is lethal, likely because newborn pups fail to breathe. In contrast, a *Dock5* null

allele is viable and seems morphologically normal. However, an incompletely penetrant muscle phenotype was observed in *Dock1*$^{+/-}$, *Dock5*$^{-/-}$ embryos, suggesting some functional redundancy between the orthologues.

Clearly, *myoblast city* activity in myogenesis is conserved between invertebrates and vertebrates, and is critical for myoblast fusion. However, the phenotypic consequences of loss-of-function are different in the different models. Upon blocking myoblast fusion in the vertebrate models, the majority of myocytes elongate and form mononucleate fibres, but only a rare sub-population do so in fruitflies. This suggests a different, vertebrate-specific process for fusion. The gross phenotypic consequences of disrupting myoblast fusion between the vertebrate models highlights the relative merits and drawbacks of studying muscle development in zebrafish. Importantly, the accessibility and translucence of zebrafish embryos makes it easy to detect and quantify myoblast fusion defects in the embryo *in situ*. In mice, studies of myoblast fusion have largely been limited to extraction of primary myoblasts or immortalised myoblast cell lines which might not behave the same in culture (Cornelison, 2008). Interestingly, very few studies of genes reported as playing a role in myoblast fusion in cell culture have demonstrated any effect of gene disruption in the embryo. For example, M-cadherin has been implicated in myoblast fusion in cell culture (Charrasse *et al*, 2007), but no similar phenotype has been described in M-cadherin null embryos (Hollnagel *et al*, 2002). It is worth noting, however, that simultaneous knockdown of *dock1* and *dock5* in zebrafish didn't completely disrupt myoblast fusion, unlike the *Dock1*$^{-/-}$ or *Dock1*$^{+/-}$, *Dock5*$^{-/-}$ embryos, suggesting the genes involved and their relative roles in this process may be different between vertebrate models.

To understand the function of *jamb* and *jamc* during muscle development, I characterised the development of the axial musculature in wild-type, *jamb*^{HU3319} and *jamc*^{sa0037} zebrafish embryos. Myoblast fusion was completely blocked in both mutants, resulting in an overabundance of fast muscle fibres. These results suggest that Jamb and Jamc act as a receptor:ligand pair, and that the majority of myoblasts are able to form muscle fibres. This observation is inconsistent with the founder cell paradigm for myoblast fusion, suggesting a different vertebrate-specific mechanism.

6.2 General characteristics of the *jamb*^{HU3319} and *jamc*^{sa0037} alleles and mutants

Mutant alleles of *jamb* and *jamc* were isolated from two separate TILLING screens. The *jamb*^{HU3319} allele, identified and supplied by the Hubrecht Institute

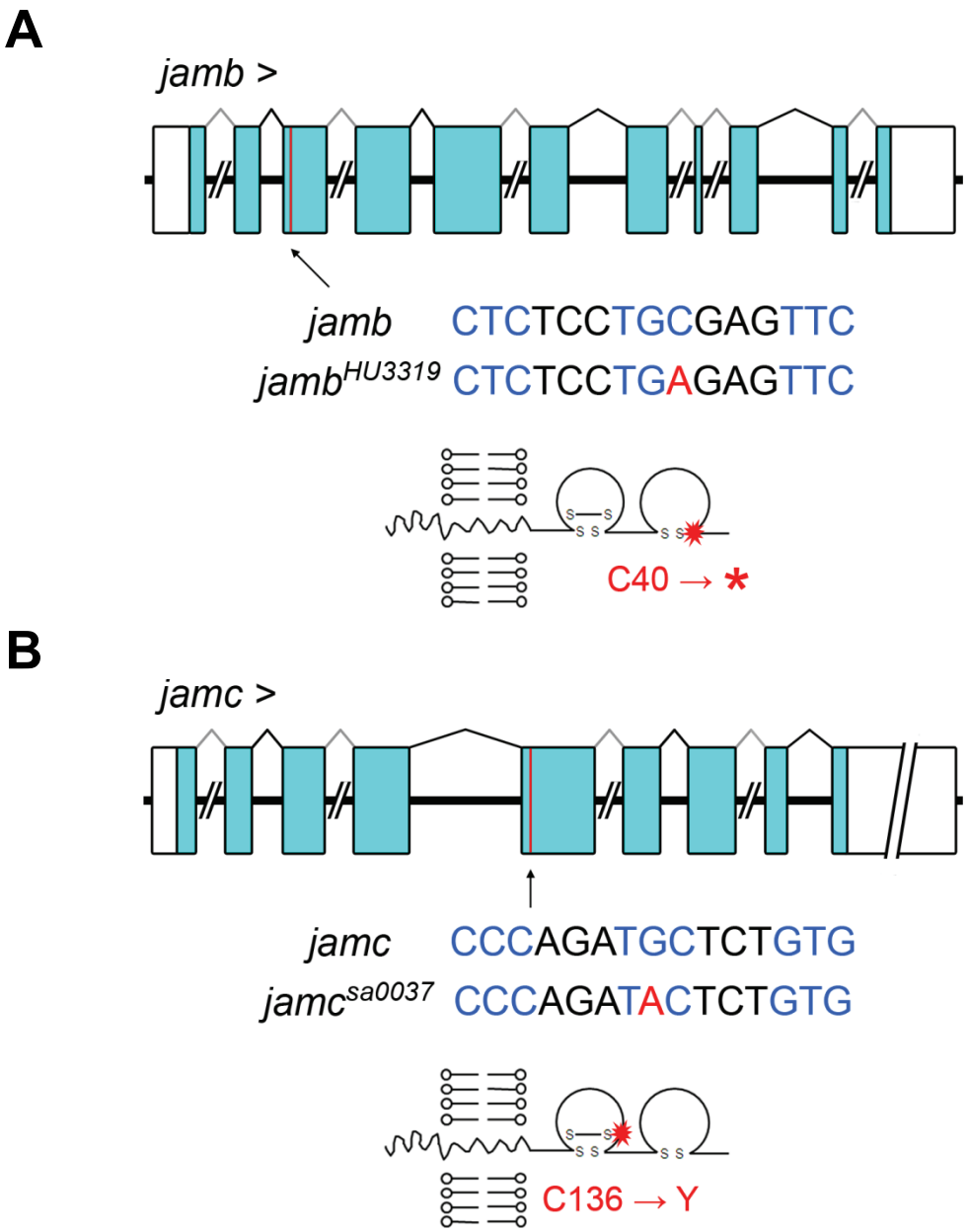

Figure 6.1 The molecular nature of *jamb*^{HU3319} and *jamc*^{sa0037} alleles.

A. Diagram illustrating the structure of the *jamb* loci. The *jamb*^{HU3319} allele contains a nonsense mutation in exon 3 (red line), introducing a stop codon (shown below the diagram) and truncating the protein (schematic below sequence) in the membrane-distal immunoglobulin-like domain (red star). **B.** Diagram illustrating the structure of the *jamc* loci. The *jamc*^{sa0037} allele contains a missense mutation in exon 5, changing a codon encoding cysteine to a codon encoding tyrosine (shown below the diagram) and disrupting a conserved disulphide bond in the membrane-proximal immunoglobulin-like domain (red star, schematic below sequence). Diagrams are drawn to scale; introns or untranslated regions larger than 400 bp were truncated for clarity, as indicated.

(Utrecht, Netherlands), contains a nonsense mutation in exon 3 of *jamb* (figure 6.1). The premature stop codon truncates the Jamb protein in the B β-strand of the N-terminal immunoglobulin-like domain (figure 6.1). This mutation results in a complete lack of Jamb expression, as determined by immunohistochemistry (figure 6.2) using a polyclonal antibody raised against the extracellular domain of Jamb. The *jamc*^{sa0037} allele, isolated from a library raised at the Wellcome Trust Sanger Institute Zebrafish Mutation Resource (Hinxton, U. K.), contains a missense mutation in exon 5. This alters the codon for cysteine-136 to tyrosine (figure 6.1). The mutation disrupts the non-canonical, but conserved, disulphide bridge between Cys-136 and Cys-222 on the A and G β-strands of the membrane-proximal immunoglobulin-like domain. It is reasonable to assume that this disruption would seriously affect the folding and function of Jamc and the allele was subsequently shown to be a strong hypomorph.

Mutant embryos homozygous for either allele are viable and fertile in our aquarium, but do not thrive. There is significant transmission bias of either allele, likely because of poor survival of homozygote embryos, although the gross morphology of 5 day larvae before transfer to the aquarium is normal. Current generations of *jamc*^{sa0037} adult fish grow slowly and present a wide range of morphological defects, unlike *jamc*^{sa0037}/+ siblings, suggesting the existence of other recessive background mutations. Female *jamc*^{sa0037} adults become egg-bound quickly without regular spawning and male *jamc*^{sa0037} adults seem reluctant or unsuccessful mates; spawning events are often spread over a long time period from initial light stimulus. Size and fertilization rates of clutches do not appear different between mutant and wild-type fish. Adult *jamb*^{HU3319} fish appear normal in gross morphology and behaviour. Initial breeding of *jamb*^{HU3319}/+ fish identified a recessive pigment defect, but this was not linked to *jamb* genotype (figure 6.3 and table 6.1).

6.3 *jamb*^{HU3319} and *jamc*^{sa0037} mutants display a complete block in myoblast fusion

Both *jam* mutant embryos show a near complete lack of myoblast fusion in the fast muscle myotomes along the trunk and tail, as highlighted by labelling of all cell membranes by transient expression of membrane-targeted red fluorescent protein (mRFP; figure 6.4). At 48 h. p. f. mutant fast muscle is composed of mononuclear fibres with a characteristic arrangement of nuclei equidistant from either myotome boundary, in stark contrast to the multinucleated wild-type myofibres. This phenotype is not evident in mutants until approximately 32 h. p. f. (figure 6.4) and persists until at least 5 days (figure 6.5). Embryos injected with morpholinos that prevent the

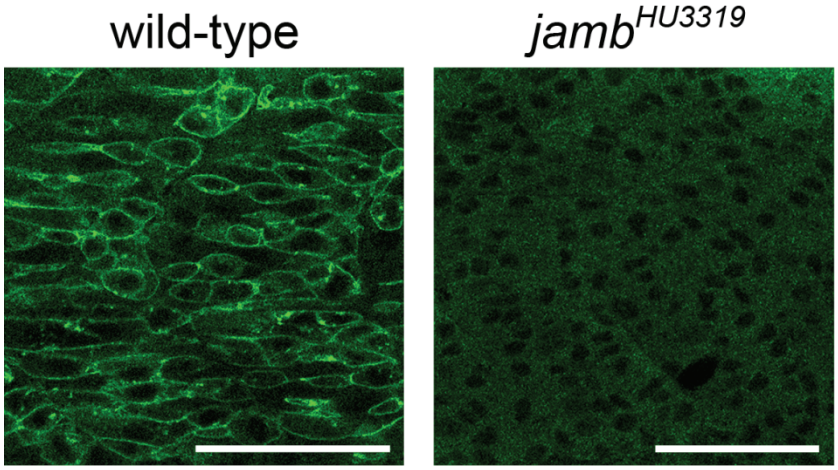

Figure 6.2 Jamb is not detected in *jamb*^{HU3319} mutant embryos.

Immunohistochemistry against Jamb (green) detects the protein on the cell surface of myoblasts and myotubes in wild-type, but not *jamb*^{HU3319} mutant, siblings. Confocal microscopy images of mid-trunk somites of 21 somites stage siblings from a *jamb*^{HU3319}/+ incross. Anterior left; scale bars represent 50 μm.

Figure 6.3 A pigment defect in *jamb*^{HU3319}/+ incross progeny is recessive.

Microscopy images of examples of *jamb*^{HU3319}/+ incross progeny at 48 h. p. f., showing normal pigmentation in 75% of embryos and an apparent lack of melanin pigmentation (*pig*) in the remaining 25%, suggesting a causative recessive mutation. This phenotype is not observed in all *jamb*^{HU3319}/+ incross clutches, suggesting it is not caused by the *jamb*^{HU3319} allele.

Table 6.1 Pigment defect is not linked to *jamb*^{HU3319} allele. Percent frequency of *jamb* genotype and pigment defect phenotype in embryos from a single *jamb*^{HU3319}/+ incross clutch.

Phenotype	Genotype			Total
	wild-type	*jamb*^{HU3319}/+	*jamb*^{HU3319}	
wild-type	17.3%	38.5%	19.2%	75%
unpigmented	3.8%	15.4%	5.8%	25%
Total	21.1%	53.9%	25%	100%

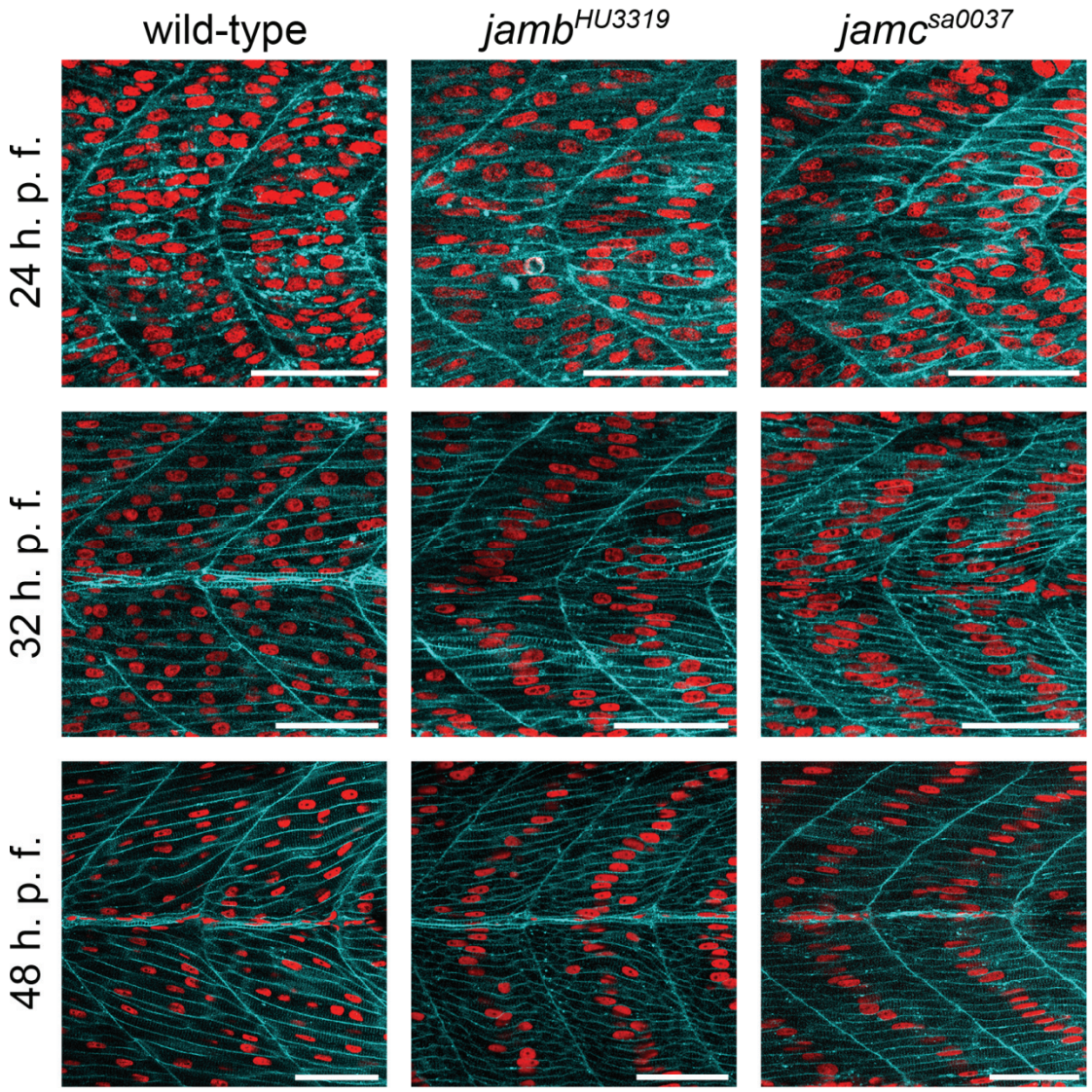

Figure 6.4 Fast muscle fibres are mononuclear in *jamb*^{HU3319} and *jamc*^{sa0037} mutants.

Confocal microscopy images of myotomes 12-13 in wild-type, *jamb*^{HU3319} and *jamc*^{sa0037} mutant embryos at 24 h. p. f. (top row), 32 h. p. f. (middle row) and 48 h. p. f. expressing membrane-targetted RFP (cyan) and counterstained with DAPI to highlight nuclei (red). In wild-type embryos, most myoblasts have fused to form multinucleated fast muscle fibres which thicken and express sarcomeric proteins. In both *jamb*^{HU3319} and *jamc*^{sa0037} mutants, most myoblasts have elongated by 24 h. p. f., but appear undifferentiated until approximately 32 h. p. f., at which time, fast muscle fibres thicken and a characteristic chevron arrangement of nuclei becomes evident. Anterior left; scale bars represent 50 μm.

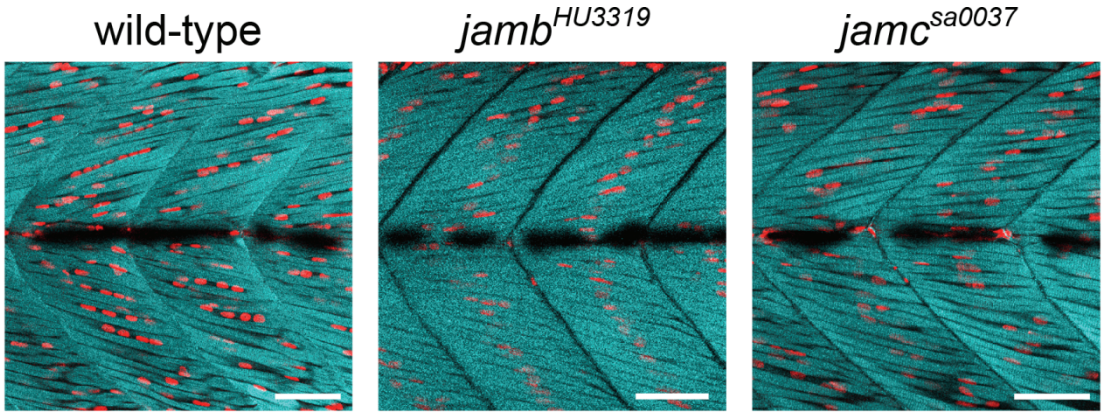

Figure 6.5 Fast muscle fibres are mononuclear in 5 day old *jamb*^{HU3319} and *jamc*^{sa0037} mutants

Mononuclear fast muscle fibres persist until at least 5 days of development. Confocal microscopy images of myotomes 12-13 in wild-type, *jamb*^{HU3319} and *jamc*^{sa0037} mutant embryos at 120 h. p. f., stained for F-actin (cyan) and nuclei (red) with phalloidin-Alexa 488 and DAPI, respectively. Anterior left; scale bars represent 50 µm.

translation of either gene, phenocopy the mutants (figure 6.6), demonstrating that the phenotype can be attributed to the *jamb*^{HU3319} and *jamc*^{sa0037} mutant alleles and not another mutation closely linked to either allele. The phenotype does not result from an overabundance of axial slow muscle, which is mononucleate in zebrafish (Roy *et al*, 2001), as the number and position of slow muscle fibres is the same as wild-type, as determined by immunohistochemistry against slow muscle myosin heavy chain (sMyHC; figure 6.7). As expected, mutant mononuclear fibres express fast muscle myosin heavy chain (fMyHC) and are supernumary compared to wild-type (figure 6.8). Muscle fibre differentiation is delayed in mutant embryos by several hours because elongated fibres are not evident until approximately 32 h. p. f., 6-8 hours after wild-type embryos (figure 6.4).

6.4 Fast muscle fibres are overabundant in *jamb*^{HU3319} and *jamc*^{sa0037} mutants

To quantify the overabundance of fast-twitch myofibres, I counted mRFP-labelled fast muscle fibres in optical cross-sections of wild-type and mutant embryos between 24-48 h. p. f (figure 6.9 and table 6.2; see Chapter 2). There is a statistically significant increase of myofibre number by approximately 1.8 and 1.6 -fold in *jamb*^{HU3319} and *jamc*^{sa0037} embryos, respectively, at 32 and 48 h. p. f., compared to wild-type (tables 6.2 and 6.3). The difference between the two mutants is likely because of the hypomorphic nature of the *jamc*^{sa0037} allele. Subsequent experiments demonstrate that approximately 5% and 15% of fibres are multinucleate in *jamb*^{HU3319} and *jamc*^{sa0037} embryos, respectively, compared to 97% in wild-type embryos (see Chapter 7, table 7.1: *jamb*^{HU3319} donor, *jamb*^{HU3319} host, *jamc*^{sa0037} donor, *jamc*^{sa0037} host and wild-type donor, wild-type host). These results show that in the absence of myoblast fusion, the majority of myoblasts are able to undergo differentiation to form functional muscle fibres.

6.5 Myoblast proliferation is repressed in *jamb*^{HU3319} and *jamc*^{sa0037} embryos

The average number of nuclei in each fibre at 48 h. p. f. in wild-type embryos is approximately 3 (Moore *et al*, 2007). In light of this result, one would expect a much higher number of mononucleate fibres in both mutants compared to wild-type. One possible explanation for the apparent lack of fast muscle fibres is apoptosis of unfused myoblasts in mutant embryos. To assess this, wild-type, *jamb*^{HU3319} and *jamc*^{sa0037} embryos were treated with acridine orange between 24 and 32 h. p. f.

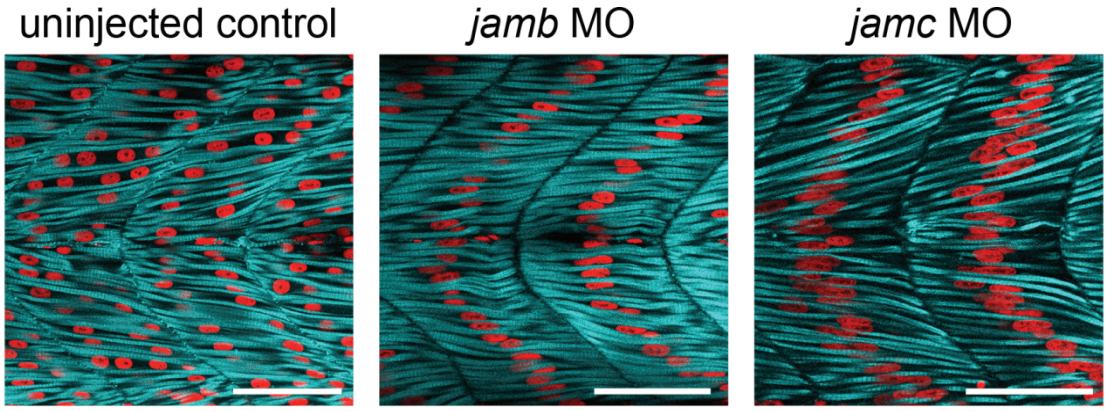

Figure 6.6 Morpholinos targeted to *jamb* and *jamc* phenocopy mutant alleles.

Confocal miscroscopy images of myotomes 12-13 in uninjected, *jamb* and *jamc* morpholino-injected wild-type embryos at 48 h. p. f., stained for F-actin (cyan) and nuclei (red) with phalloidin-Alexa 488 and DAPI, respectively. Anterior left; scale bars represent 50 µm.

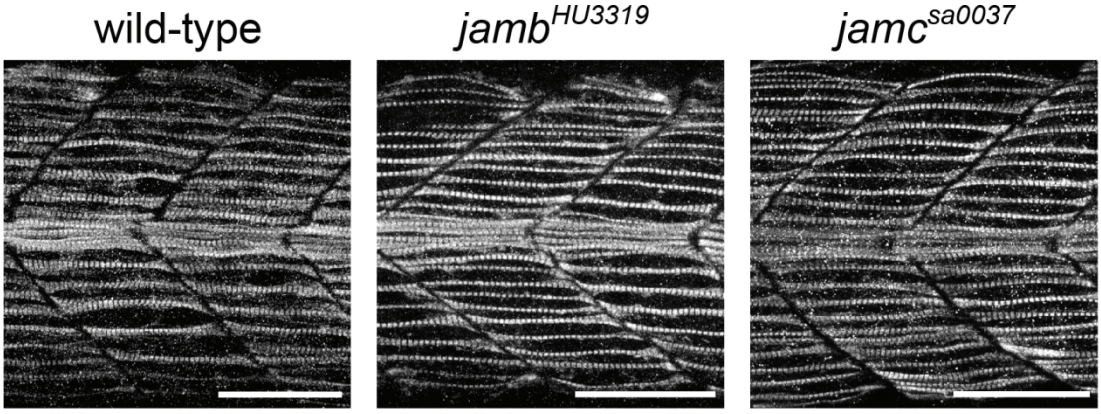

Figure 6.7 Slow muscle develops normally in *jamb*^{HU3319} and *jamc*^{sa0037} mutants.

Confocal microscopy images of myotomes 12-13 in wild-type, *jamb*^{HU3319} and *jamc*^{sa0037} 24 h. p. f. embryos, stained for slow muscle-specific myosin heavy chain (sMyHC). Slow muscle is superficial and develops normally in both mutants compared to wild-type. Anterior left; scale bars represent 50 μm.

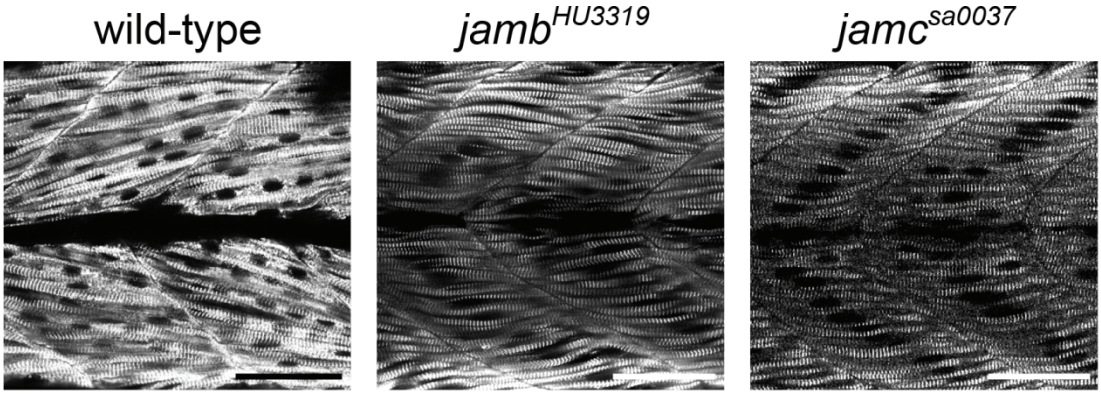

Figure 6.8 Fast muscle fibres are fully differentiated in *jamb*^{HU3319} and *jamc*^{sa0037} mutants.

Confocal microscopy images of myotomes 12-13 in wild-type, *jamb*^{HU3319} and *jamc*^{sa0037} 48 h. p. f. embryos, stained for fast muscle-specific myosin heavy chain (fMyHC). Mononucleate fast muscle fibres are differentiated and supernumary in both mutants compared to wild-type. Anterior left; scale bars represent 50 μm.

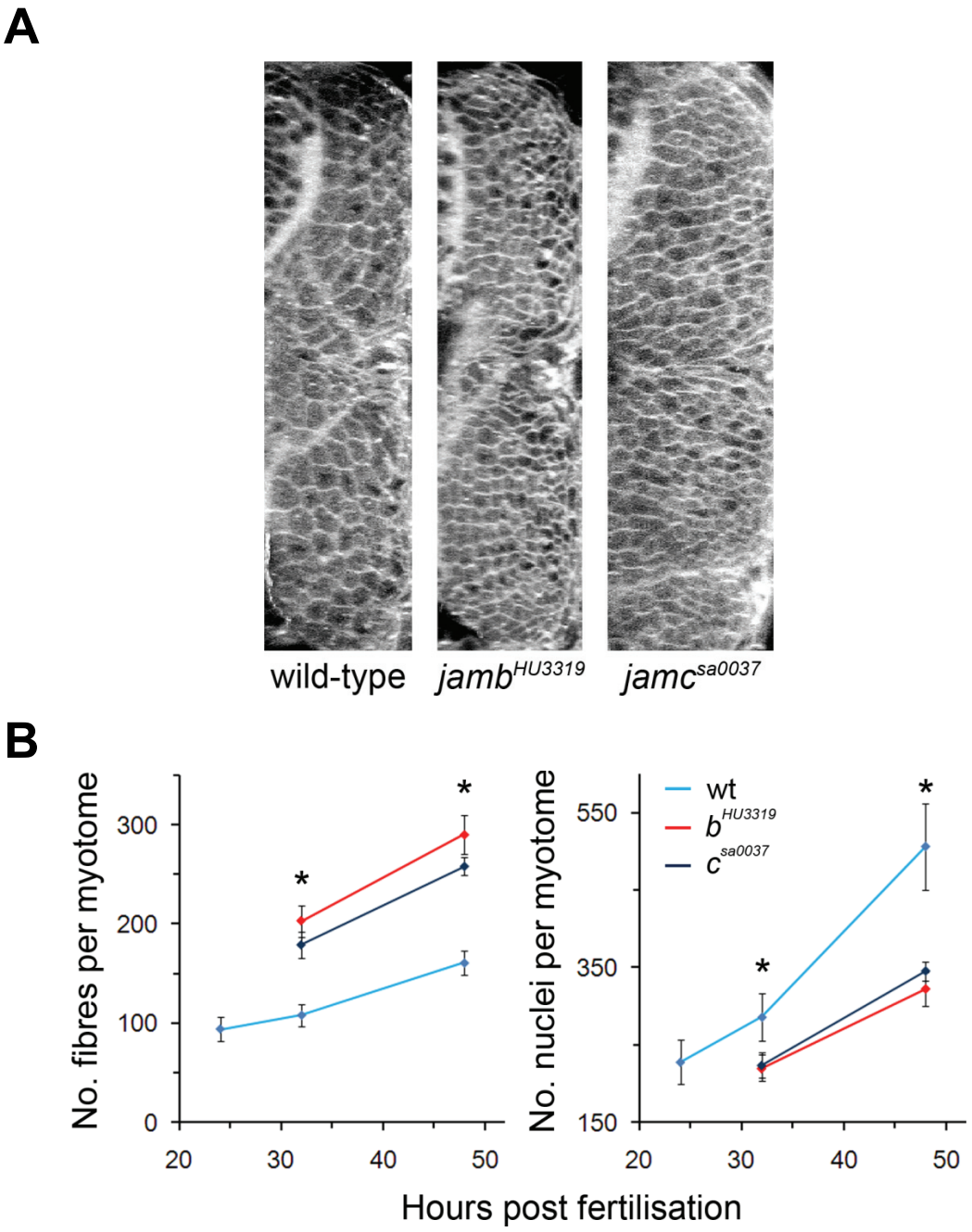

Figure 6.9 Quantification of supernumary fast muscle fibres in both *jamb*^{HU3319} and *jamc*^{sa0037} mutant embryos.

A. Cross-sections of myotomes from wild-type, *jamb*^{HU3319} and *jamc*^{sa0037} 48 h. p. f. embryos expressing membrane-targetted RFP (mRFP). Images were generated from confocal microscopy z-stack images. Dorsal, top. **B.** Graphs showing the average number of fast muscle fibres per myotome at different stages of development (left) and the estimated average number of nuclei per myotome at different stages of development (right) in wild-type, *jamb*^{HU3319} and *jamc*^{sa0037} embryos. Error bars represent standard deviation.

Table 6.2 Quantification of number of fast muscle fibres per myotome in wild-type, *jamb*^{HU3319} and *jamc*^{sa0037} embryos. Average number of fast muscle fibres per myotome in wild-type and mutant embryos at different developmental stages. Values presented as mean ± S. D., n = number of embryos tested.

Time (h. p. f.)	Genotype							
	wild-type		*jamb*^{HU3319}			*jamc*^{sa0037}		
	no. fibres	n	no. fibres	ratio to wt	n	no. fibres	ratio to wt	n
24	94 ± 12	12	-	-	-	-	-	-
32	108 ± 11	10	203 ± 16	1.9	6	179 ± 13	1.7	5
48	159 ± 17	8	290 ± 20	1.8	11	258 ± 9	1.6	6

Table 6.3 Statistical significance of comparisons between fast muscle fibre number in wild-type, *jamb*^{HU3319} and *jamc*^{sa0037} embryos. One-tailed probability values from t-tests adjusted to account for unequal variances and sample sizes.

Time (h. p. f.)	Comparison		
	wild-type – *jamb*^{HU3319}	wild-type – *jamc*^{sa0037}	*jamb*^{HU3319} – *jamc*^{sa0037}
32	2.0×10^{-6}	2.2×10^{-5}	0.01
48	3.7×10^{-12}	1.3×10^{-9}	2.4×10^{-4}

There was no qualitative increase in apoptosis observed in mutants compared to wild-type embryos (figure 6.10).

Another possible explanation is a reduction of myoblast proliferation in mutant embryos after the completion of primary myogenesis at 24 h. p. f. The rate of increase in fibre number is the same in mutant and wild-type embryos between 32 – 48 h. p. f. (figure 6.9), yet the number of fast muscle fibre nuclei must increase much more quickly in wild-type embryos than mutants, as each new muscle fibre requires many more myoblasts. To address this possibility I estimated the relative numbers of nuclei per myotome and developmental stage (figure 6.9, tables 6.4 and 6.5). The number of fast muscle fibres at each stage (f_h, where h represents developmental stage, h. p. f.) was multiplied by the average number of nuclei per fibre (n_h), reported in Moore *et al* (2007). This number was adjusted for the percentage of multinucleate fibres (m) observed in subsequent transplant experiments (wild-type - 97%, *jamb*^{HU3319} – 5%, *jamc*^{sa0037} – 15%; see Chapter 7) as follows:

$$\text{number of nuclei per myotome} = mf_h n_h + (1 - m)f_h$$

As expected, there is a statistically significant difference in the number of nuclei per myotome in wild-type embryos compared to both mutants, and this difference increases over time. These results suggest there is a decrease in myoblast proliferation in both *jamb*^{HU3319} and *jamc*^{sa0037} mutant embryos. Thus, while there is a clear overabundance of fast muscle fibres in both *jam* mutants, this increase is smaller than expected because of limited myoblast proliferation.

6.6 Discussion

Both *jamb*^{HU3319} and *jamc*^{sa0037} mutant embryos display the same phenotype: delayed, overabundant, mononucleate fast muscle fibres in the axial musculature. This phenotype is recapitulated in morpholino knockdown embryos, indicating it is specific to the loss-of-function of either gene. These results demonstrate that Jamb and Jamc are likely to be a vertebrate-specific receptor:ligand pair and are necessary for fusion between myoblasts during primary myogenesis in the zebrafish myotome. Further experiments performed to test this hypothesis are described in Chapter 7.

The differences in phenotype between myoblast fusion mutants in *Drosophila* and the *jam* mutants reveal interesting differences in the process of muscle development. In *Drosophila*, early specification of rare muscle founder cells determines the absolute number and nature of muscles formed in each hemisegment, irrespective of the occurrence of myoblast fusion (Ruiz-Gomez *et al*, 2000). In contrast, the absence of myoblast fusion in either *jam* mutant results in an

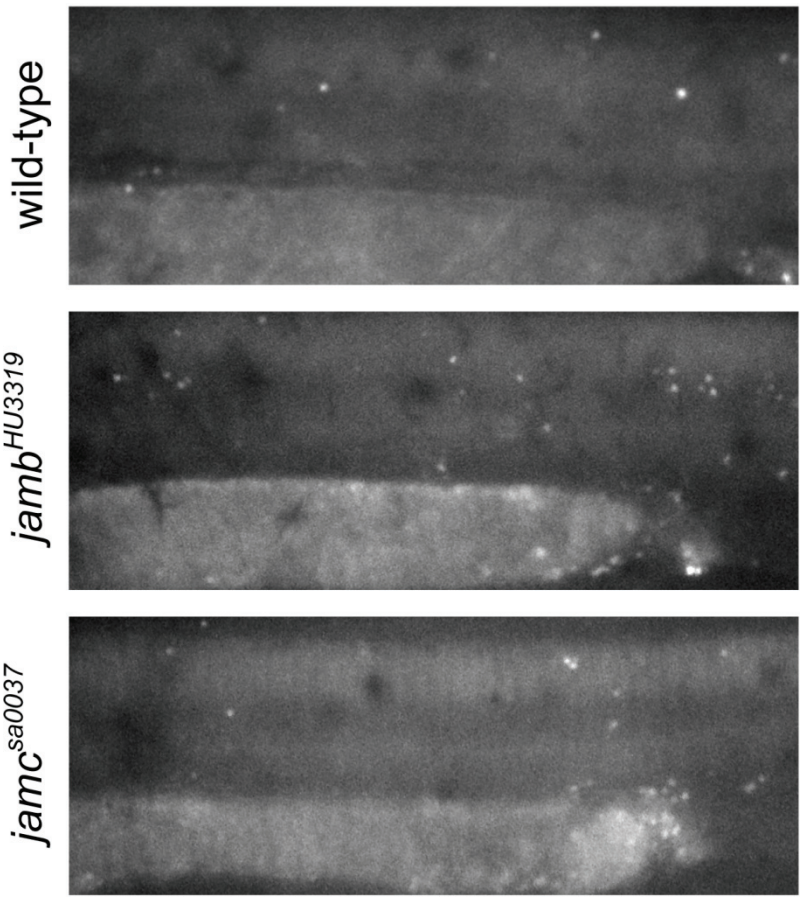

Figure 6.10 Apoptosis does not increase in the absence of myoblast fusion.

Example images of wild-type, *jamb*^{HU3319} and *jamc*^{sa0037} mutant embryos incubated in acridine orange at 32 h. p. f. showing no qualitative increase in mutant embryos relative to wild-type. Anterior left.

Table 6.4 Calculated number of nuclei per myotome in wild-type, *jamb*^{HU3319} and *jamc*^{sa0037} embryos. Average number of nuclei per myotome, calculated from number of fast muscle fibres per myotome in wild-type and mutant embryos at different developmental stages. Values presented as mean ± S. D., number of embryos tested as in table 6.2.

Time (*h*; h. p. f.)	Average no. nuclei per fibre (n_h)*	Genotype				
		wild-type	*jamb*^{HU3319}		*jamc*^{sa0037}	
		no. nuclei	no. nuclei	ratio to wt	no. nuclei	ratio to wt
24	2.48	228 ± 29	-	-	-	-
32	2.70	286 ± 30	220 ± 17	0.8	224 ± 16	0.8
48	3.23	506 ± 56	322 ± 22	0.6	345 ± 12	0.7

* Values from Moore *et al*, 2007

Table 6.5 Statistical significance of comparisons between number of nuclei per myotome in wild-type, *jamb*^{HU3319} and *jamc*^{sa0037} embryos. One-tailed probability values from t-tests adjusted to account for unequal variances and sample sizes.

Time (h. p. f.)	Comparison		
	wild-type – *jamb*^{HU3319}	wild-type – *jamc*^{sa0037}	*jamb*^{HU3319} – *jamc*^{sa0037}
32	4.2×10^{-5}	1.1×10^{-4}	0.35
48	1.1×10^{-5}	5.0×10^{-5}	7.2×10^{-3}

increase in the number of fast muscle fibres. This suggests that in zebrafish myogenesis, the majority, if not all, myoblasts are capable of forming a myofibre. While the overabundance of fast muscle fibres is clear, it is not as high as might be expected in light of the average number of nuclei in wild-type myotome. There is no obvious increase in apoptosis of myoblasts before differentiation, discounting this as a possible explanation. An analysis of muscle fibre growth suggests a reduction of myoblast proliferation in mutants compared to wild-type over time, which might explain the apparent lack of fibres. It is difficult to speculate on a link between proliferation of dermomyotome cells, which are likely to be the source of new myoblasts for myotome growth (Hammond *et al*, 2007), and myoblast fusion mediated by *jamb* and *jamc*. One possibility that remains to be assessed is whether proliferation of mutant myoblasts before differentiation results in an excess of fast muscle fibres. Differentiation of mutant myoblasts is delayed by approximately 6 – 8 hours compared to wild-type. Whether or not these cells are post-mitotic or proliferative during this delay is unknown.

Another important aspect of regulation in *Drosophila* is the more ubiquitous fusion competent myoblast population. They act as a substrate that fuses to muscle founders to increase the bulk of each fibre (Ruiz-Gomez *et al*, 2002). In the absence of fusion they persist as rounded cells, weakly express myosin heavy chain and eventually undergo apoptosis (Rushton *et al*, 1995). Similarly, in zebrafish *kirrel* morpholino-injected embryos, a large population of myoblasts fail to form fibres, remain rounded, express myosin heavy chain although how long these cells persist, or if they do form mononucleate fibres is uncertain (Srinivas *et al*, 2007). These cells are described as being lateral to slow muscle fibres, possibly impeding their migration from the midline to a lateral superficial position. However, no such phenotype was observed in either $jamb^{HU3319}$ or $jamc^{sa0037}$ mutants. It is difficult to rationalise the difference in phenotype between *kirrel* morpholino-injected embryos and both *jam* mutants. One possibility is that the *kirrel* morpholino directly affects the development of slow muscle, as noted by Srinivas *et al* (2007), and this in turn affects the development of fast muscle myoblasts (Henry and Amacher, 2004). Whilst appropriate controls were performed by the authors of the study of *kirrel*, the possibility of toxic side-effects of injected morpholinos remains to be fully explored in this context. It would be interesting to establish the veracity of the morpholino phenotype by using a loss-of-function allele, but none have been reported to date.

In summary, characterisation of mutant alleles of *jamb* or *jamc* show that a loss-of-function of either gene results in a complete block of myoblast fusion. As a

consequence, the majority of myoblasts within each somite form a mononucleate fibre, resulting in a significant overabundance of fast muscle. These results are not consistent with a founder cell model of myogenesis, in which the number of muscle fibres remains constant in the absence of fusion because each of them is predefined by a rare sub-population of 'founder' cells.

Chapter 7

Physical interaction between Jamb and Jamc is necessary for myoblast fusion

Summary

In this chapter I describe a series of transplant experiments designed to further elucidate the function and mechanism of the interaction between Jamb and Jamc during the process of myoblast fusion. As expected, both Jamb and Jamc are found to be necessary for fusion and do not act as homophilic receptors. Cellular complementation and double deficient donor transplants demonstrate that Jamb and Jamc interact *in trans* and that it is the interaction between these receptors that is essential for myoblast fusion.

7.1 Introduction

The results from experiments described so far have strongly suggested Jamb and Jamc interact and that this interaction is necessary for myoblast fusion. Both genes are expressed by myoblasts during primary myogenesis in the zebrafish embryo (see Chapter 4); Jamb and Jamc are able to interact heterophilically and homophilically *in vitro* (see Chapter 5) and furthermore, mammalian homologues have been identified as binding partners in different biological contexts (see Introduction); *jamb*^{HU3319} and *jamc*^{sa0037} mutant embryos display the same phenotype, principally a near-complete lack of myoblast fusion, suggesting they act in the same pathway (see Chapter 6). These results have not distinguished between different possible mechanisms for the function of either gene. For example, Jamb and Jamc could act as independent homophilic receptors. To further demonstrate and characterise the importance and mechanism of the interaction between Jamb and Jamc in muscle development *in vivo*, I performed a comprehensive series of transplant experiments using wild-type and mutant genotypes.

Transplant experiments have been widely used for characterising the function of genes; for example, this approach demonstrated that the transcription factor *spadetail* was found to act exclusively in the mesoderm of developing embryos (Ho and Kane, 1990). The concept and practicalities of a transplant experiment are simple (see figure 7.1). Essentially, the experiment mixes genotypically different cells within an embryo and assays their respective properties during development. The donor cells are labelled for later analysis, in this instance, using a fluorescent dextran dye. By doing so, a transplant experiment tests whether a gene functions within the cell alone, such as a transcription factor would, or outside the cell, like a secreted growth factor. Do mutant cells continue to function abnormally in a background of wild-type cells and *vice versa*? If so, the gene is considered to be cell autonomous; that is, the phenotype of the mutant cell is solely dependent on its genotype. For example, *spadetail* mutant cells were found to be unable to converge during gastrulation in a wild-type host (Ho and Kane, 1990). Are wild-type cells affected by mutant cells, or *vice versa*? If so, the gene is considered to be non-cell autonomous; the phenotype of the mutant cell is independent of its genotype. For example, wild-type donor cells transplanted into the mesodermal region of *no tail*/*brachyury* mutants could rescue formation of paired posterior somites, despite only being present on one side of the embryo (Martin and Kimelman, 2008). Neither classical definition is useful when considering the function of some cell surface proteins, as they may affect transplanted cells and neighbouring host cells simultaneously. For example, wild-type

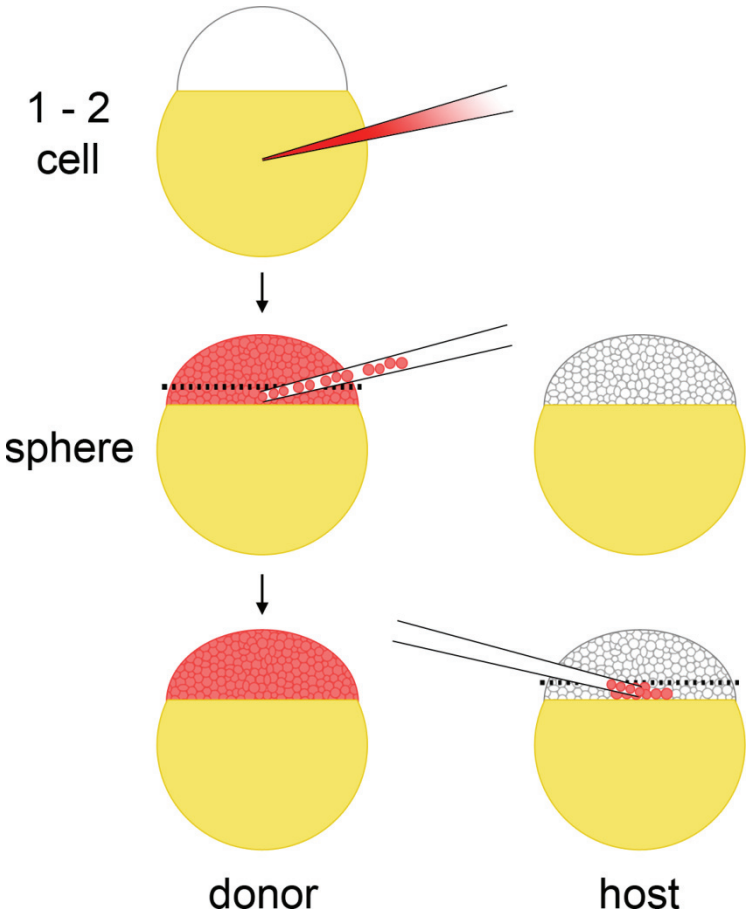

Figure 7.1 Schematic of zebrafish transplant experiments.

Schematic outlining the process of transplant experiments performed to assess the function of *jamb* and *jamc* during muscle development. Donor embryos are microinjected with a solution of fluorescently-labelled dextran at the 1-2 cell stage and allowed to develop to the sphere stage. Labelled mesoderm cells from the margin of the donor embryo (below dotted line) are then transplanted into the margin of a host embryo.

donor cells affect surrounding cells in host zebrafish embryos injected with morpholinos that target *notch1a* and *notch3*, whilst *notch* morpholino-injected donor embryo cells also affect surrounding wild-type host cells (Matsuda and Chitnis, 2009), suggesting that the Notch1a and Notch3 receptors are cell-autonomous and non-cell autonomous, simultaneously. The authors of this research use a better definition of the differing activities of these cell surface proteins: interactions *in trans* (between opposing cell membranes) and *in cis* (within a single cell membrane).

The zebrafish model organism is well-suited to this technique because of the accessibility of embryos, their rapid growth and well-documented fate-map (Kimmel *et al*, 1990; reviewed in Woo *et al*, 1995). An abundant cell type, such as somitic fast muscle precursors, are easily targeted. Rare cells are less amenable, but still possible to study; for example, specific neural cell types such as primary motor neurons that arise within the neural tube (Eisen, 1991). With respect to myoblast fusion, the phenotype of transplanted cells is easily assayed by staining host embryos with a fluorescent nuclear dye. Fluorescently-labelled myofibres are determined to be mononucleate (unfused donor cell) or multinucleate (fused donor cell) by observation using confocal microscopy. Quantification of mononucleate and multinucleate fibres gives a reasonable estimate of the degree of fusion that occurs in each combination of donor:host genotype, except where wild-type donor-donor cell fusion events could confound this. Such events are unlikely in transplants with either *jamb*^{HU3319} or *jamc*^{sa0037} donor cells, as demonstrated by the lack of fusion in *jamb*^{HU3319} and *jamc*^{sa0037} mutant embryos (see Chapter 6).

I performed a series of transplant experiments using wild-type, *jamb*^{HU3319} and *jamc*^{sa0037} embryos to characterise the function and necessity of interaction between Jamb and Jamc *in trans* for fusion.

7.2 Characterising the function of the physical interaction between Jamb and Jamc in myoblast fusion *in vivo*

To characterise the function of Jamb and Jamb during myoblast fusion, I transplanted fluorescent dextran-labelled wild-type, *jamb*^{HU3319} and *jamc*^{sa0037} mesoderm cells into the margin of wild-type, *jamb*^{HU3319} and *jamc*^{sa0037} unlabelled host embryos between high and dome stages (figure 7.1). Transplanted embryos were allowed to develop until 48 h. p. f., to ensure the completion of primary myogenesis, before fixation. Fixed embryos were then stained with DAPI to stain nuclei and analysed by confocal microscopy (figure 7.2). Fluorescently-labelled fast muscle fibres, which must be derived from donor cells, were classified as multinucleate

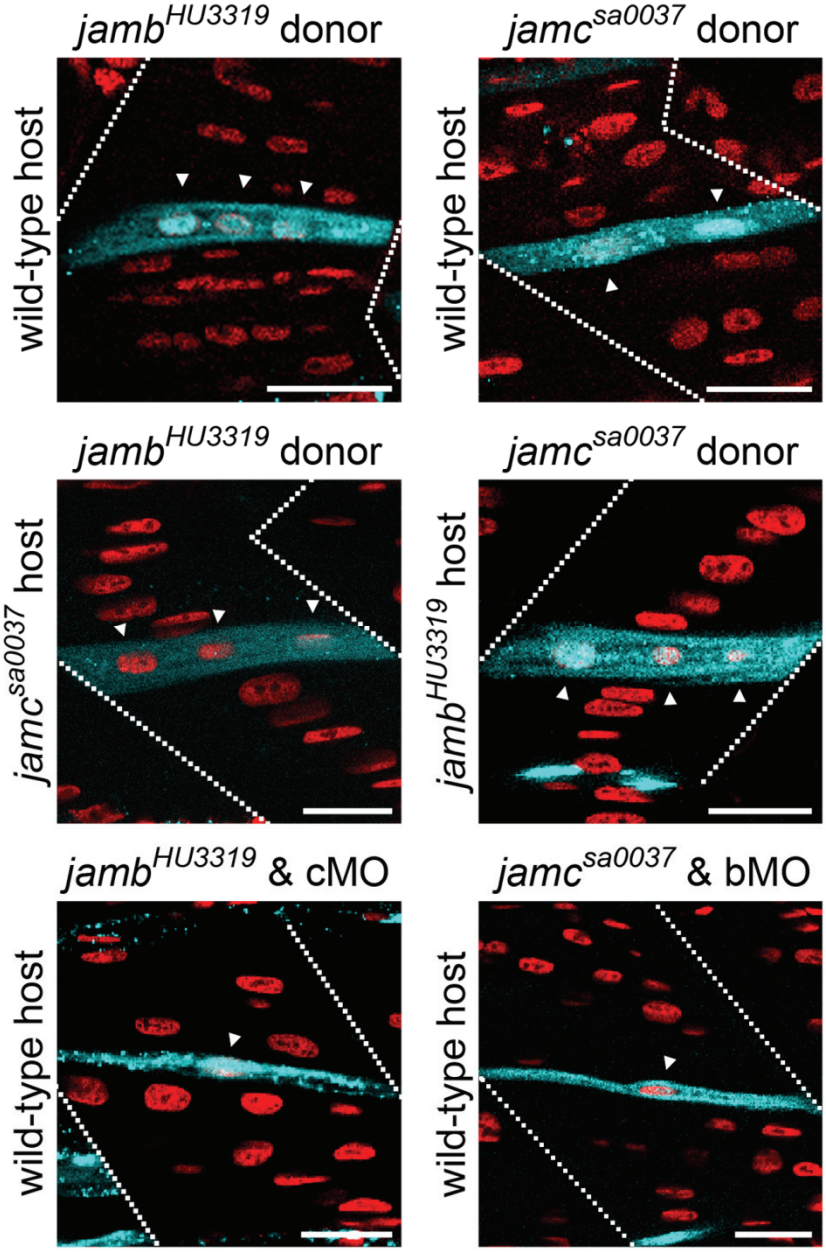

Figure 7.2 The interaction between Jamb and Jamc *in trans* is required for myoblast fusion.

Fluorescent dextran-labelled cells (blue) from *jamb*^{HU3319} (left) and *jamc*^{sa0037} (right) donors can form multinucleate fibres with wild-type (top), *jamc*^{sa0037} (middle left) and *jamb*^{HU3319} (middle right) host cells. Transplanted cells from doubly-deficient *jamb*^{HU3319}, *jamc* morpholino-injected (bottom left) or *jamc*^{sa0037}, *jamb* morpholino-injected (bottom right) donors do not fuse with wild-type host cells, suggesting both proteins are required and interact *in trans*. Confocal microscopy images from 48 h. p. f. embryos; anterior left. Dotted lines indicate myotome boundaries; arrowheads indicate nuclei within labelled fibres. Nuclei stained with DAPI (red). Scale bars represent 20 μm.

(fused) or mononucleate (unfused) and counted (table 7.1, summarised in figure 7.3).

7.3 Jamb and Jamc do not function as homophilic receptors

As expected, mutant donor cells could not form multinucleate fibres in same mutant host embryos e.g. *jamb*^{HU3319} donor cells transplanted into *jamb*^{HU3319} host embryos (table 7.1). Donor cells from *jamb*^{HU3319} embryos were able to fuse efficiently with wild-type hosts and *vice versa*, demonstrating that Jamb does not act as a homophilic receptor required for myoblast fusion (figure 7.2). Similarly, donor cells from *jamc*^{sa0037} embryos were able to fuse to wild-type hosts and *vice versa*, suggesting it also does not act as a homophilic receptor (figure 7.2).

There is a considerable decrease in efficiency of fusion when *jamc*^{sa0037} donor cells are transplanted into wild-type host embryos. The lack of efficiency was not seen in the reciprocal transplant, wild-type donor cells transplanted into *jamc*^{sa0037} host embryos, possibly because of donor-donor cell fusions (table 7.1).

7.4 Jamb and Jamc interact *in trans* during myoblast fusion

Taken together, these results suggest that expression of functional Jamb and Jamc protein *in trans* is essential for myoblast fusion. In support of this conclusion, *jamb*^{HU3319} donor cells were able to efficiently complement *jamc*^{sa0037} host cells and *vice versa* (figure 7.2), discounting the possibility of either protein acting in separate but redundant pathways. Interestingly, *jamc*^{sa0037} donor cells fuse much more efficiently to *jamb*^{HU3319} host cells than wild-type host cells. This suggests that Jamb has an additional function that is inhibitory to myoblast fusion.

To test the importance of an interaction between Jamb and Jamc *in trans*, I transplanted *jamb*^{HU3319} mesoderm cells from embryos injected with a *jamc* morpholino, or *jamc*^{sa0037} mesoderm cells from embryos injected with a *jamb* translation-blocking morpholino, into wild-type hosts. Doubly-deficient donor cells were unable to fuse to wild-type host cells (figure 7.2, table 7.1). The small amount of residual fusion events are likely a result of incomplete morpholino knockdown, as demonstrated by transplanting *jamc* morpholino-injected, *jamb*^{HU3319} donor cells into *jamc*^{sa0037} host cells and *jamb* morpholino-injected, *jamc*^{sa0037} donor cells into *jamb*^{sa0037} host cells (table 7.1). Morpholino-injected *jamb*^{HU3319} and *jamc*^{sa0037} embryos were able to undergo myogenesis (figure 7.4) suggesting no confounding effects from a synthetic phenotype.

Table 7.1 Quantification of fused (multi-nucleated) and unfused (mono-nucleated) fluorescently-labelled fast muscle fibres in transplanted hosts.

Donor genotype	Host genotype: wild-type			Host genotype: *jamb*^{HU3319}			Host genotype: *jamc*^{sa0037}		
	unfused	fused	n	unfused	fused	n	unfused	fused	n
wild-type	8 3.1%	246 96.9%	6	38 5.3%	674 94.7%	7	34 8.4%	369 91.6%	9
jamb^{HU3319}	23 6.7%	318 93.3%	8	499 94.9%	27 5.1%	6	23 4.4%	502 95.6%	9
jamc^{sa0037}	449 71.3%	181 28.7%	10	30 5.2%	552 94.8%	7	186 85.3%	32 14.7%	9
jamb^{HU3319} & *jamc* MO	648 87.8%	90 12.2%	16	n. d.			301 74.0%	106 26.0%	9
jamc^{sa0037} & *jamb* MO	190 76.0%	60 24.0%	11	128 83.7%	25 16.3%	6	n. d.		

n = number of host embryos analysed. n. d. not determined.

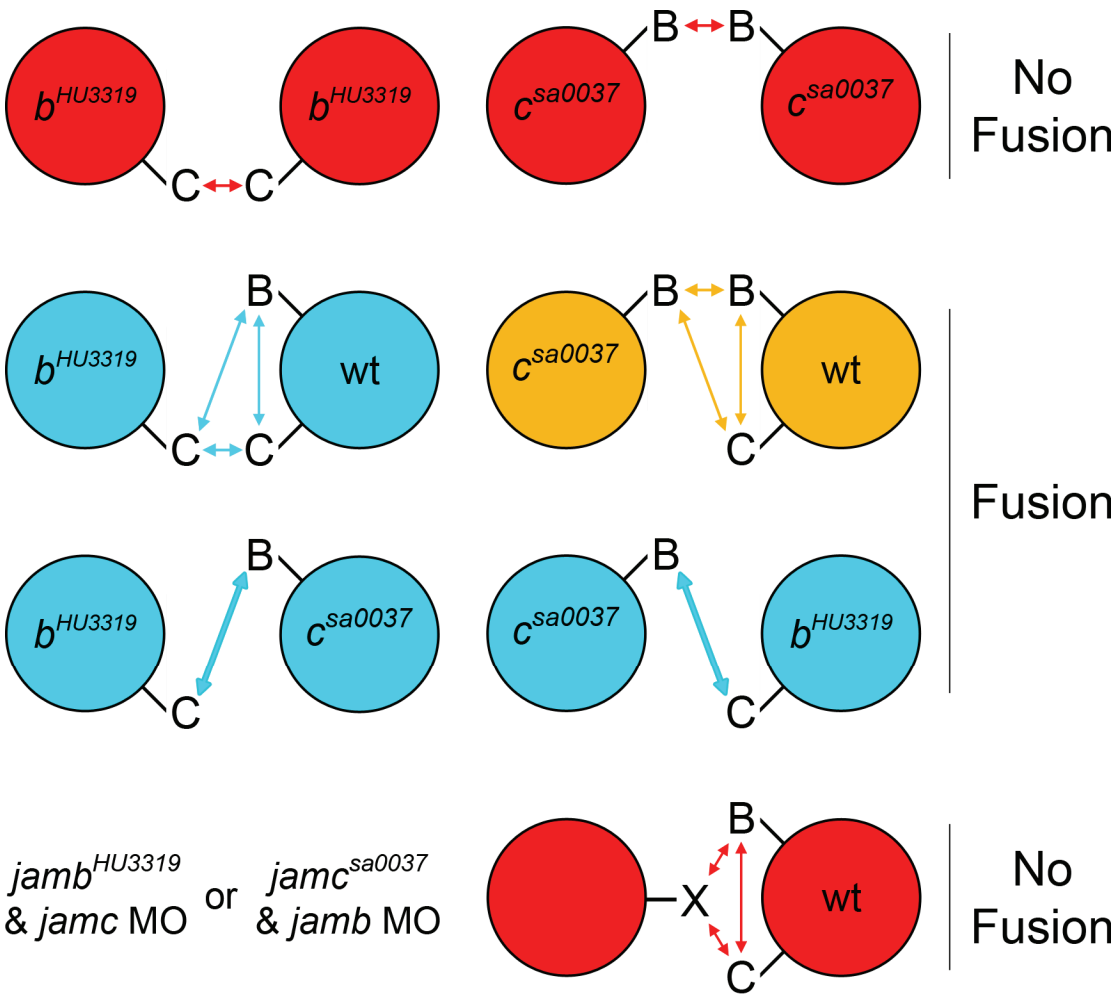

Figure 7.3 Reductive model of *jamb* and *jamc* -mediated myoblast fusion.

Diagram summarising results from transplant experiments. Each panel represents two myoblasts expressing either Jamb and/or Jamc depending upon genotype, arrows represent possible interactions. From top to bottom: myoblast fusion fails between two cells lacking the same protein (top, red), but the introduction of either protein on either cell restores fusion (cyan; second row, left), inefficiently in the case of Jamc (orange; second row, right). Loss of function of the complementary protein does not reduce the degree of fusion (third row), and restores it to wild-type levels in the case of Jamc (third row, right) suggesting interaction between Jamb *in trans* is inhibitory. Removing the function of both proteins on the same cell prevents fusion, demonstrating that the interaction between Jamb and Jamc *in trans* is necessary for myoblast fusion *in vivo* and there are no other interacting partners.

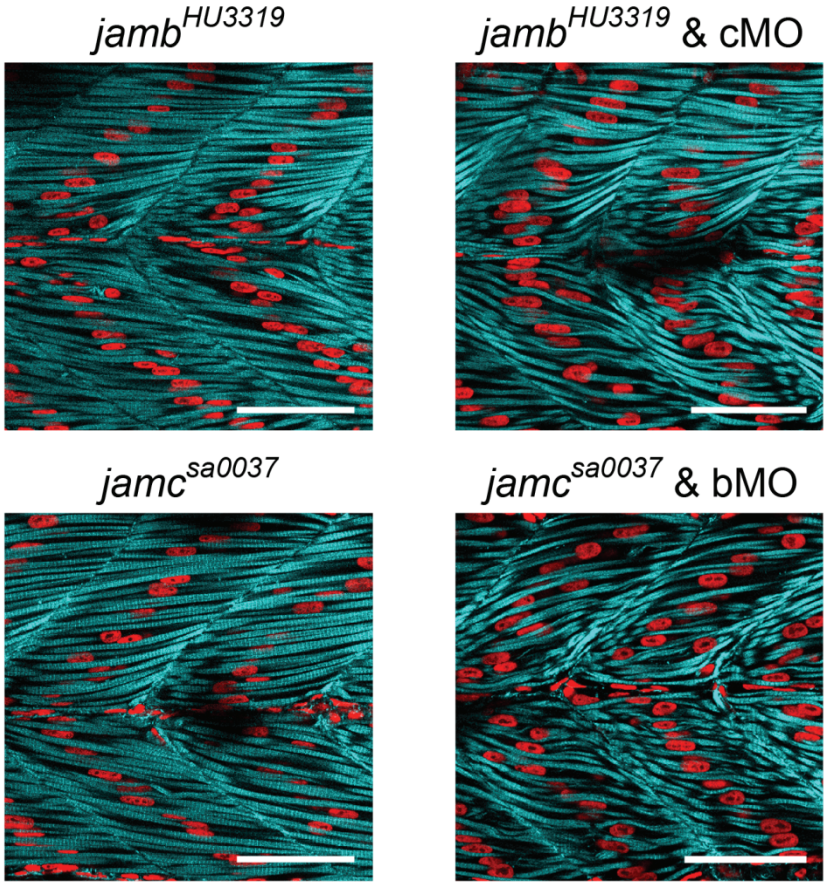

Figure 7.4 Combined knockdown of *jamb* and *jamc* does not result in a synthetic myogenesis phenotype.

Morpholino knockdown of *jamc* in *jamb*^{HU3319} embryos (top right) or *jamb* in *jamc*^{sa0037} embryos (bottom right) does not result in any further disruption of myogenesis than that observed in *jamb*^{HU3319} (top left) or *jamc*^{sa0037} (bottom left) at 48 h. p. f., suggesting no synthetic effect of combined knockdown of both genes. Confocal sections of myotomes 12-13 in 48 h. p. f. embryos, stained for F-actin (cyan) and nuclei (red). Anterior left; scale bars represent 50 μm.

7.5 Discussion

Previous experiments have demonstrated that both Jamb and Jamc are necessary for myoblast fusion to occur *in vivo*. I sought to gain further insight into the mechanism and importance of interactions between Jamb and Jamc during primary myogenesis through a systematic set of transplant experiments, making use of the mutant alleles I have characterised. The results described above indicate that the interaction between the two proteins *in trans* is a critical requirement for fusion to occur. Regulation of expression of Jamc by local signalling events (see Chapter 4) might thus contribute to controlling the process of myoblast fusion.

To draw conclusions from these experiments, I based the results on a reductive model of two myoblasts in contact, both expressing Jamb and Jamc (as established previously, see Chapter 4; see results summary in figure 7.3). Transplant experiments demonstrate that removing the function of Jamb and Jamc in the same cell prevents fusion, ruling out the possibility of other interacting partners.

The experiments show that removing the function of Jamb in either cell does not prevent fusion, but loss of Jamb in both cells does. Loss of Jamb in one cell and Jamc in the other does not prevent fusion. These results are consistent with the requirement for Jamb and Jamc to interact *in trans* in neighbouring myoblasts for efficient fusion. Removing the function of both genes in a donor cell renders it incompetent for myoblast fusion, demonstrating that Jamb and Jamc must interact *in trans*.

Loss of function of Jamc in both cells prevents fusion. Jamc activity in only one cell does not, although the efficiency of fusion is greatly reduced. Interestingly, removing the function of Jamb expression in the neighbouring Jamc deficient cell restores the efficiency of fusion, suggesting interactions between Jamb expressed by both cells inhibits fusion in these circumstances. This could suggest another level of regulation of the process; only cells that have responded to local signalling and have expressed Jamc are fully competent for fusion. However, wild-type donor cells transplanted into *jamc*^{sa0037} host embryos do not show such an effect. Refinement of the experiment to distinguish between donor-donor cell and donor-host cell fusions is necessary to test this hypothesis, before any further exploration of this putative function of Jamb is warranted. This might be acheived by labelling donor or host cell nuclei with a labelled nucleotide analogue such as bromodeoxyuridine (BrdU) or 5-ethynyl-2´ -deoxyuridine (EdU) in addition to fluorescently-labelled dextran. Another approach would be to use transgenic embryos containing a yeast upstream-

activating sequence (UAS) coupled to a fluorescent reporter as donors, and transgenic 'driver' embryos, homozygous for *jamc*^{sa0037}, in which the yeast transcription factor Gal4 is expressed in myoblasts, as host. For expression of the fluorescent reporter, the *jamc*^{sa0037}, Gal4 expressing mutant host myoblasts must fuse to the UAS-reporter transgenic donor myoblasts. Donor-donor or host-host cell fusions would not result in fluorescent fibres and would remain undetected.

The results of the transplant experiments described here do not provide any evidence to support a vertebrate equivalent of the founder cell paradigm, established through extensive studies of myoblast fusion in *Drosophila melanogaster* (reviewed in Rochlin *et al,* 2009; see Chapter 6 for further explanation). Briefly, myoblasts within the invertebrate hemi-segment are divided into a rare 'informed' population, termed founder cells, and a more numerous 'naïve' population, dubbed fusion-competent myoblasts. Fusion only occurs between the two populations – the founder cells determine the characteristics of each of the 30 muscles within the body wall, while the FCMs act as a substrate that provides bulk to each muscle by fusing to the founder cell. If vertebrate axial myotome myogenesis is based upon pre-configuration of the myotome by a small sub-population of myoblasts founder cells, then one might expect intermediate levels of fusion to be observed in wild-type donor, mutant host transplants. Only a small proportion of wild-type donor cells would differentiate into founder myoblasts and so form multinucleate muscles by fusing to the mutant host cells. The remaining donor cells would be unable to fuse to mutant myoblasts as none of the host cells could act as competent founders, and thus remain mononucleate. This was not observed in either transplant into *jamb*^{HU3319} *or jamc*^{sa0037} mutant host embryos, further supporting the hypothesis of equivalence between vertebrate myoblasts. However, as suggested above, it is possible that donor-donor cell fusions might obscure this effect. This might be resolved by differential labelling of donor and host cells, as described above.

In summary, further investigation of the function of Jamb and Jamc through transplant experiments have demonstrated that Jamb and Jamc interact *in trans* to allow fusion between myoblasts, potentially regulating the process through controlled expression of Jamc. This conclusion supports previous results demonstrating differential regulation of *jamc*, but not *jamb* or *kirrel*, by the transcription factor *prdm1* (see Chapter 4), but remains to be fully tested.

Chapter 8

Discussion

Summary

To determine the function of the interaction between Jamb and Jamc during embryonic development, I studied the expression and biochemistry of both proteins, characterized the phenotype of loss-of-function mutations of both genes and determined the mechanism and necessity of physical interaction between Jamb and Jamc *in trans* for myoblast fusion *in vivo*.

In this chapter I will discuss the importance and implications of these findings in the context of vertebrate myogenesis, unanswered and open questions and future directions.

8.1 Novel regulation of myoblast fusion in vertebrates

The central aim of this project was to discover a biological function for the interaction between Jamb and Jamc during embryonic development of zebrafish. I examined the orthology and evolutionary conservation of all the members of the zebrafish *jam* family, identifying two novel paralogues, *jama2* and *jamc2* (Chapter 3). Once aware of the extent of duplication of the gene family in teleosts, I sought to explore the possibility of redundancy between paralogues through a thorough analysis of their respective expression patterns and biochemical properties. I determined that the *JAM-B*-like and *JAM-C*-like paralogues were expressed in different tissues in different developmental stages, suggesting little conservation of regulatory elements between them (Chapter 4). In addition, the *JAM-B*-like and *JAM-C*-like paralogues had retained similar binding specificity but with varied relative strengths of interaction, suggesting that they are not equivalent biochemically (Chapter 5). I then characterised the phenotypes of embryos containing heritable mutations in *jamb* and *jamc* (Chapter 6). The mutant embryos displayed a near-complete block in myoblast fusion, resulting in a striking arrangement of nuclei positioned centrally with respect to myotome boundaries in each somite. Interestingly, there was a concomitant increase in the number of fast muscle fibres of approximately 1.8-fold in both mutants compared to wild-type embryos. This suggests that the majority, if not all, myoblasts within the somite are able to form a muscle fibre in the absence of fusion. Through transplant experiments, I determined that Jamb and Jamc do not interact *in cis* or with any other ligand, but instead interact between cells *in trans*, and this interaction is essential for myoblast fusion (Chapter 7).

These findings are not consistent with the currently held paradigm of muscle development, first identified in grasshopper (Ho *et al*, 1983) and thoroughly characterised in *Drosophila* (recently reviewed in Rochlin *et al*, 2010; Haralalka and Abmayr, 2010). The founder cell model posits that a muscle fibre is pre-figured by specification of a rare sub-population of myoblasts as founder cells. These cells contain all the information necessary to form any of the 30 possible body wall muscles in each hemisegment. In the absence of myoblast fusion, the founder cells still continue to develop, forming mononucleate and differentiated muscle fibres (Ruiz-Gomez *et al*, 2002). The remaining myoblast population, the fusion-competent myoblasts (FCMs), remain rounded, weakly express myosin and are cleared by macrophages (Rushton *et al*, 1995). Vertebrate myoblast fusion has largely been explored by comparison to this model. The conservation of activity of orthologues of

Drosophila proteins in vertebrate models, for example *kirrel*, has implied a conservation of mechanism. However, the phenotypes of disruption of these genes have suggested otherwise; a possibility that has not been acknowledged in the literature. For example, genetic disruption of the vertebrate homologues of *myoblast city*, *Dock1* and *Dock5*, does result in a block in myoblast fusion – the involvement of the orthologues in this process is clearly conserved. However, loss-of-function of these genes does not result in a small number of elongated muscle fibres and a numerous population of rounded myoblasts that undergo apoptosis. In contrast, each muscle contains elongated and aligned differentiated muscle fibres (Laurin *et al*, 2008). The loss-of-function of Jamb and Jamc illustrate this clearly and unequivocally. In addition, *jamb* and *jamc* represent a novel, vertebrate signalling pathway, suggesting innovation of the process during evolution, at least at the cell surface.

Identification and characterisation of the critical cell surface proteins involved in myoblast fusion in *Drosophila* has been of key importance to the understanding of the invertebrate mechanism of myoblast fusion, primarily because loss-of-function of these genes results in a complete block of the process. An important aspect of the founder cell model is the mutually exclusive expression of the key cell surface receptors, *dumbfounded* expressed by founder cells (Ruiz-Gomez *et al*, 2000; Artero *et al*, 2001) and *sticks and stones* expressed by fusion-competent myoblasts (Bour *et al*, 2000). Biochemical interaction between *sticks and stones* and either *dumbfounded* (or *roughest*, a paralogue expressed by all myoblasts) is necessary for fusion (Strunkelnberg *et al*, 2001; Bour *et al*, 2000; Galletta *et al*, 2004). Restricted expression of the receptors to the different cell types presumably prevents fusion within the two different populations. In contrast to this, *jamb* and *jamc* are co-expressed by myoblasts (Chapter 4). However, *jamc* is expressed very dynamically in comparison to its binding partner, *jamb*. It is first expressed in a small medial sub-population of *jamb* expressing myoblasts in rostral somites, after approximately 10-13 somites have formed. The *jamc* expression domain expands throughout the transitional myotome during segmentation and is then attenuated by the end of primary myogenesis. This expression pattern is reminiscent of *sox6* (von Hofsten *et al*, 2008), a transcription factor that reinforces the fast muscle fate of somitic myoblasts (Hagiwara *et al*, 2005; von Hofsten *et al*, 2008) and myogenin (Weinberg *et al*, 1996), a transcription factor linked with the terminal differentiation of myoblasts (reviewed in Pownall *et al*, 2002). Whether or not *jamc* is a direct target of either of these transcription factors remains to be determined. In addition, *jamc* is mis-

expressed in the adaxial cells of *prdm1* mutant embryos, but *jamb* and *kirrel* are not. The expression of this critical myoblast fusion cell surface receptor is carefully regulated during differentiation of the primary axial fast muscle fibres, whilst its binding partner is present throughout.

From these results I propose a new model for vertebrate myogenesis (figure 8.1). I hypothesise that differentiation of the fast muscle myoblasts is initiated by local dynamic signalling. Myoblasts nearest to this signal respond by elongating and expressing *sox6* and *jamc*, making them fully competent for fusion with nearby myoblasts that are primed for fusion by expression of *jamb*.

In the zebrafish axial musclulature, a subset of myoblasts must elongate and connect to myotome boundaries before they can fuse to other rounded cells (Snow *et al*, 2008b). This process is similar to that of avian primary myogenesis (Gros *et al*, 2004), suggesting it is a general characteristic of vertebrates. How does a myoblast decide between elongation or fusing to a nearby elongated fibre? In *Drosophila*, this decision is made by early specification into two distinct cell types. In chick, this process is regulated by temporal separation of elongation of myocytes into a primary myotome, followed by fusion (Gros *et al*, 2004). The phenotypic consequences of a complete block of fusion, outlined in this thesis, demonstrate that this decision is likely to be stochastic in zebrafish. I propose that local signalling directs a limited population of nearby myoblasts to elongate. The remaining myoblasts do not perceive this signal, but are primed for fusion through the expression of *jamb*.

8.2 Determining candidate signalling pathways

The model I have proposed defines some of the characteristics of the signalling necessary for the development of the primary axial fast muscle fibres, based upon observations of this process in the literature and those of the function of *jamb* and *jamc*.

Firstly, the signal should at least regulate transcription of *jamc,* and other genes that induce aspects of the differentiation programme, such as elongation. The transcription factor *sox6* is a possible target of this signal. Secondly, fast muscle myoblasts differentiate in a medio-lateral wave (Henry and Amacher, 2004) and elongation begins from the most posterior border of the somite (Stellabotte *et al*, 2007). Therefore, the differentiation signal should begin in the medio-posterior region of each somite, and propagate laterally. Thirdly, this process begins in early segmentation, seemingly simultaneously in the rostral somites of 10-13 somites stage embryos (see Chapter 4). The signal must be regulated in a timely fashion.

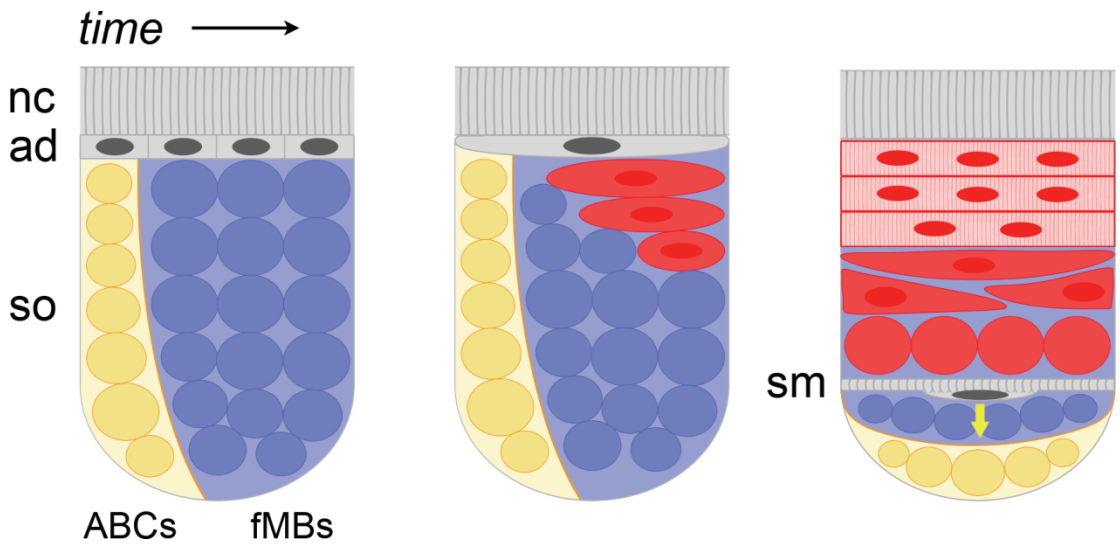

Figure 8.1 Proposed model of primary fast muscle development.

Diagram illustrating proposed regulatory model depicting key developmental changes in a single somite (so). Jamb^{+}, Kirrel^{+} fast muscle myoblasts (fMBs) are specified shortly after somite formation and are primed for fusion (left). Fast muscle myoblast differentiation starts in medio-posterior cells which begin to elongate and express *jamc* (red cells; middle). Fully elongated myocytes start to fuse with other myoblasts to form myofibres (right). This process progresses medio-laterally as slow muscle fibres (sm) migrate towards their superficial position (yellow arrow). nc: notochord; ad: adaxial cells; ABCs: anterior border cells (yellow cells).

Fourthly, myocytes elongate towards the anterior boundary of the somite, in parallel, and stop elongating upon reaching a defined myotome boundary (Henry *et al*, 2005). These elongated fibres do not undergo fusion until such contact is made (Snow *et al*, 2008b). There must therefore be a directional cue that also regulates competence of elongated myocytes for fusion.

I hypothesise that these features are regulated by combinatorial input of different signalling pathways. There are a wide range of secreted signals involved in the development of the musculature (discussed in Chapter 1) and any combination could be responsible for these behaviours. There may also be spatio-temporal redundancy amongst the signals. Disruption of individual pathways at different timepoints may not be sufficient enough to disrupt the process of differentiation, which may explain why no individual signal has previously been identified. I will outline several possible approaches to begin to characterise the molecular nature of these differentiation signals.

I believe that studying slow muscle development is of great importance to understanding the process of differentiation of fast muscle, as exemplified by studying the expression of critical receptors for myoblast fusion in *prdm1* mutants (Chapter 4). The mutant adaxial cells are able to fuse to nearby myoblasts, suggesting they are competent for fusion. This context provides an opportunity to test if *jamb*, *jamc* or *kirrel*, or the interaction between Jamb and Jamc, is sufficient for myoblast fusion. Movement of the slow muscle has also been demonstrated as important for differentiation for fast muscle fibres (Henry and Amacher, 2004). The signal(s) that trigger the migration of slow muscle through the myotome might also trigger fast muscle differentiation. Indeed, the migrating slow muscle cells may form an important part of the morphogenetic signal itself by virtue of its medio-lateral progression. A suitable test of this hypothesis would be to look at the position of slow muscle fibres during their migration and the expression domain of *jamc;* if slow muscle is part of the signalling process, then *jamc* expression must be limited by the extent of its migration. It would also be interesting to assess fast muscle differentiation in zebrafish embryos lacking *m-* or *n-cadherin*, as loss of either gene disrupts migration, but not specification of slow muscle (Cortés *et al*, 2003). Hedgehog signalling has been shown to play a role in the elongation of fast muscle myocytes. Inhibition of hedgehog signalling in *laminin γ1* mutants enhances the elongation defect observed in fast muscle (Peterson and Henry, 2010). Interestingly, this effect appears to be indirect and dependent on the correct development of slow muscle. Slow muscle cannot be the only source of signalling however, as loss of slow

muscle does not block fast muscle differentiation or myoblast fusion (Ingham and Kim, 2005).

Another means of elucidating the molecular signalling involved in this process is a thorough analysis of the regulatory elements that control *jamc*, in comparison to *jamb* and *sox6*. I propose a reporter gene assay performed *in vivo* in which different non-coding regions of the *jamc* loci be placed upstream of a reporter gene in a plasmid and injected in to wild-type embryos. This could be used to determine the regulatory regions responsible for spatial and temporal activation of *jamc*. These could then be compared to the *sox6* and *jamb* loci to identify informative similarities and differences. It would be also interesting to determine the effect of disruption of known signalling pathways, such as FGF or Hedgehog, on the reporter gene constructs containing regulatory elements of interest, *in vivo*, in addition to any effect on the expression patterns of *jamb* and *jamc*.

A whole transcriptome approach applied to dissociated myoblasts could also be informative. $Jamb^+$ single positive and $Jamb^+$, $Jamc^+$ double positive cells could be isolated by dissociation of early segmentation embryos followed by fluorescence-activated cell sorting (FACS). Purified mRNA from these cells could then be used in transcript-counting or microarray experiments to identify differentially regulated genes between undifferentiated $Jamb^+$ cells and differentiated $Jamb^+$, $Jamc^+$ cells. This process might help identify intracellular effectors of differentiation and help determine the function of signalling pathways in this context.

8.3 Relative roles of cell surface receptors in myoblast fusion

Whilst many cell surface receptors have been identified as important for myoblast fusion in vertebrates, very few cell surface proteins have been demonstrated to have a significant effect on myoblast fusion in mouse (Krauss, 2010), leading to the suggestion that there is significant functional redundancy between different proteins. This is in stark contrast to myoblast fusion in *Drosophila*, in which only four receptors (*dumbfounded/roughest* and *sticks and stones/hibris*) are critical for fusion (Haralalka and Abmayr, 2010). The strength of the phenotype of loss-of-function of *jamb* and *jamc* and the necessity of interaction between the two proteins in the zebrafish myotome demonstrate that I have identified a critical receptor:ligand pair for the initiation of myoblast fusion. Whether or not these proteins also play a critical role in mammals remains to be determined.

Both Jam-B and Jam-C are expressed in the developing skeletal muscle of mouse embryos (Visel *et al*, 2004). Several mutant mouse lines for *Jam-B* (Sakaguchi *et al*,

2006; Tang *et al*, 2010) and *Jam-C* (Gliki *et al*, 2004; Praetor *et al*, 2008) have been reported. No myogenesis phenotype has been described in reports of any of the *Jam* mutants, although no direct attempt to analyse muscle development has been made. *Jam-C* mutant mice die very shortly after birth, are cyanotic and unable to breathe (Praetor *et al*, 2008), a phenotype consistent with previously reported myoblast fusion defects, for example *Dock1* knockout mutants (Laurin *et al*, 2008). However, this may be confounded by defects in the immune system (Imhof *et al*, 2007). Surviving mutant *Jam-C* mice exhibit growth retardation (Imhof *et al*, 2007; Ye *et al*, 2009) which may suggest a general defect in myogenesis. Significant reduction in stride length and grip strength has also been described, although the authors attribute this to defective nerve conduction (Scheiermann *et al*, 2007). Jam-C knockout mice also present with megaoesophagus which the authors attribute to dysfunctional smooth muscle cells (Imhof *et al*, 2007). However, it is worth noting that the oesophageal muscle is unusual, because it contains a mixture of striated and smooth muscle (Shiina *et al*, 2010). Surprisingly, no phenotype has been identified for *Jam-B* mutant mice (Sakaguchi *et al*, 2006), even though spermatogenesis was expected to be as defective as in the *Jam-C* mutant (Gliki *et al*, 2004).

Previously, orthologues of *Drosophila* myoblast fusion cell surface proteins have been studied in order to understand the process of vertebrate myoblast version. For example, morpholino knockdown of *kirrel,* a zebrafish orthologue of the paralogues *dumbfounded* and *roughest*, has revealed a near-complete block in myoblast fusion, with an equivalent degree of mononucleate fibres to that of *jamc*^{sa0037} mutant embryos, approximately 80% (Srinivas *et al*, 2007). In contrast to the phenotype of both *jamb* and *jamc* mutants, a ‘large’ number of rounded, unfused myoblasts are observed in the embryo. It is unclear what proportion of these cells, if any, remain as rounded cells and are destroyed by phagocytosis, or elongate into mononucleate fibres at a later stage. What the relative roles of *kirrel*, *jamb* and *jamc* are in zebrafish myoblast fusion remains to be assessed.

Identification of any interacting partners of Kirrel at the cell surfaces would be of great interest. Srinivas *et al* (2007) used transplant experiments to establish if *kirrel* was required cell-autonomously. If so, Kirrel must therefore interact with an unknown ligand for myoblast fusion. The authors were unable to draw any sound conclusion from the results of these experiments. I believe that the reason for this is flaws in the experimental procedures. Firstly, any donor-donor fusion events they identified were categorised as ‘unfused’, biasing their results heavily in the wild-type donor, morpholino-injected host transplants. In addition, it is unclear how the authors could

reliably identify any such donor-donor fusion events. A transgenic strain expressing a nuclear-localised histone2A.F/Z-GFP fusion protein (H2A.F/Z-GFP) was used as the donor strain. Within the results, it appears that any binucleate fibres in which both nuclei are labelled with GFP are referred to as donor-donor cell fusions, with the presumption that only donor cell nuclei are labelled with GFP. This runs contrary to the syncytial nature of myofibres. The contents of the donor cell, including the mRNA encoding H2A.F/Z-GFP, must diffuse throughout the syncytia formed between the fused cells. This has been demonstrated quite elegantly through time-lapse studies of *MAZe* embryos (Collins *et al*, 2010). Myoblasts, containing the recombined transgene, expressing a nuclear-localised RFP (nlsRFP) and GFP and are observed fusing to other myoblasts, which do not express nlsRFP or GFP, to form a fibre. Subsequently, other nuclei within the syncytia are labelled with nlsRFP, and the cytoplasmic GFP spreads throughout the fibre. I would improve the *kirrel* transplant experiment in much the same manner as I have proposed for my own transplants: labelling of donor cell DNA through nucleotide analogues, or use of a bi-partite reporter gene expression system (Chapter 7). Kirrel has been used in a recent AVEXIS screen for potential ligands and found to interact homophilically, but no other binding partners were identified (Martin *et al*, 2010). One proposed binding partner for Kirrel is Nephrin, based upon its orthology to *sticks and stones* (Sohn *et al*, 2009). It has been previously associated with severe forms of nephritic syndrome (reviewed in Hauser *et al*, 2009), but no muscle phenotype has been described for *Nephrin* knockout mice mutants. The role of *nephrin* in myoblast fusion has been poorly characterised in zebrafish.

8.4 Intracellular effectors of Jamb and Jamc signalling

The precise functional role of the interaction between Jamb and Jamc in myoblast fusion remains to be characterised. For example, binding between Jamb and Jamc might be necessary for adhesion between myoblasts, cellular recognition between primed myoblasts and elongated myocytes, or to activate signalling pathways between myocytes for fusion. Both proteins are thought to play important roles in tight junctions and are known to interact with cytoplasmic proteins through a C-terminal PDZ domain-binding motif. For example, JAM-B and JAM-C have been shown to interact with the well-known cell polarity protein PAR-3 (Ebnet *et al*, 2003). Of particular interest is the possibility of interactions between Jamb and Jamc and Cdc42, through Par3, Par6 and aPKC (Gliki *et al*, 2004), as Cdc42 is known to play a vital role in myoblast fusion (Vasyutina *et al*, 2009). Interaction between Jamb and Jamc might lead to enrichment of Cdc42 activity to sites of fusion. Both JAM-B and

JAM-C interact with the tight junction protein ZO-1 (Ebnet *et al*, 2003), a membrane-associated guanylate kinase (MAGUK; Stevenson *et al*, 1986) that is known to bind F-actin (Fanning *et al*, 2002). This suggests a direct link between the JAM proteins and the actin cytoskeleton in epithelia, but this requires further investigation in the context of myoblast fusion. Jam-C has also previously been shown to regulate the expression of β1-integrins (Mandicourt *et al* 2007) which are known to be critical for muscle differentiation (Schwander *et al*, 2003; Conti *et al*, 2009).

To test the functions of both proteins it would be possible to use splice-blocking morpholinos to truncate the cytoplasmic domains. If the interaction between Jamb and Jamc is necessary for adhesion and recognition, but not signalling, then one might expect myoblast fusion to occur normally. It would be interesting to test the function of Kirrel in the same manner.

8.5 Future directions

The issues discussed above represent outstanding long-term questions relating to the deeper understanding of the process of myogenesis. Before submission, I began to prepare reagents for future experiments to explore the function of Jamb and Jamc further and a possible role of both genes in other muscle tissues and in later development. These avenues of investigation remain incomplete.

Gain-of-function and rescue experiments can provide new functional data and generate new hypotheses. To perform these experiments I designed plasmids to simultaneously express membrane-targetted RFP and a gene of interest, either enhanced green fluorescent protein (eGFP), full-length *jamb* or full-length *jamc*, from separate CMV promoters. I prepared these plasmids in collaboration with Dr Céçile Wright-Crosnier, and injected the control plasmid containing mRFP and eGFP into 1-2 cell stage embryos. I observed co-expression of mRFP and eGFP in injected embryos, suggesting that both CMV promoters are active in the same cells (figure 8.2). In the future I intend to attempt rescue of $jamb^{HU3319}$ and $jamc^{sa0037}$ myoblasts by injecting dual promoter plasmids containing full length wild-type *jamc* or *jamb*. This can be extended to a functional dissection of the proteins by replacing the full length wild-type genes with truncated or mutated versions.

At later stages of development, *jamb* and *jamc* were found to be co-expressed in the presumptive craniofacial mesoderm, hypaxial, epaxial and pectoral fin (see Chapter 4), suggesting that Jamb and Jamc may play a role in myoblast fusion in the development of craniofacial and limb musculature. To address this possibility, I intend to observe the morphology and number of nuclei in these muscles using

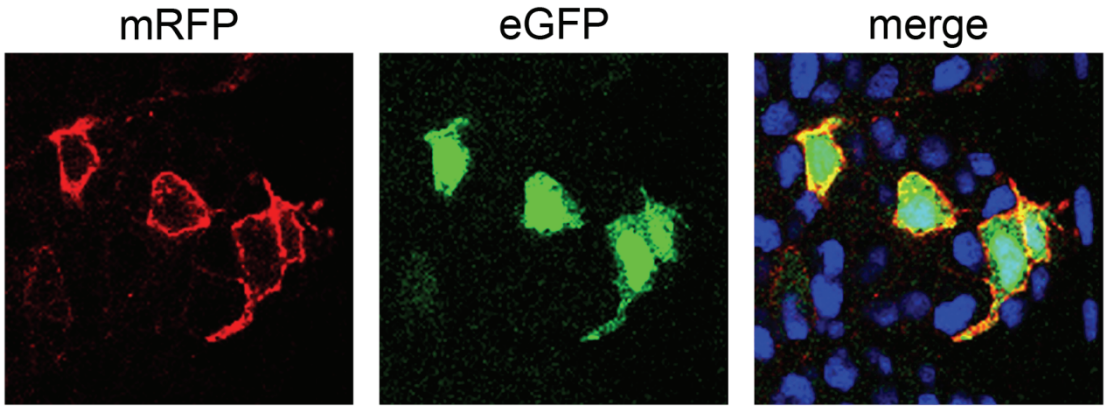

Figure 8.2 Co-expression of fluorescent reporter genes in transfected zebrafish embryos.

Confocal microscopy images of myoblast cells co-expressing membrane-targetted RFP (red) and eGFP (green) in a zebrafish embryo transfected with a dual reporter construct. Both promoters are active within the same cells (merge). Images from a fixed 14 somites stage embryo counterstained with DAPI to highlight nuclei (blue).

immunohistochemistry.

Given the near-complete absence of fusion in both *jamb*^{HU3319} and *jamc*^{sa0037} mutants and the persistence of this phenotype until at least 120 h. p. f., it was a surprise to find that homozygous mutant embryos are viable and fertile. In collaboration with Dr Céçile Wright-Crosnier, we attempted to isolate muscle fibres from dissected adult fish muscles to see if they remained mononuclear. This remains ongoing.

8.6 Concluding Remarks

With thorough application of many different techniques, I believe I have succeeded in characterising an important interaction between a vertebrate-specific receptor:ligand pair previously unknown to be necessary for myoblast fusion. I believe that my research has the potential to help other scientists elucidate the general principles and molecules that govern how muscle tissue forms in vertebrates.

There are many outstanding questions and many new avenues of research made possible by these discoveries. I hope that in the future my efforts contribute in some small way to improved treatment and even prevention of the painful, debilitating and often terminal muscular diseases that blight the lives of many, sufferers and carers alike.

Chapter 9

Bibliography

Arrate, M. P., Rodriguez, J. M., Tran, T. M., Brock, T. A. and Cunningham, S. A., 2001. Cloning of human junctional adhesion molecule 3 (JAM3) and its identification as the JAM2 counter-receptor. Journal of Biological Chemistry 276, 45826 – 45832.

Artero, R. D., Castanon, I. and Baylies, M. K., 2001. The immunoglobulin-like protein Hibris functions as a dose-dependent regulator of myoblast fusion and is differentially controlled by Ras and Notch signaling. Development 128, 4251 – 4264.

Aurrand-Lions, M., Duncan, L., Ballestrem, C. and Imhof, B. A., 2001. JAM-2, a novel immunoglobulin superfamily molecule, expressed by endothelial and lymphatic cells. Journal of Biological Chemistry 276, 2733 – 2741.

Aurrand-Lions, M., Lamagna, C., Dangerfield, J. P., Wang, S., Herrera, P., Nourshargh, S. and Imhof, B. A., 2005. Junctional adhesion molecule-C regulates the early influx of leukocytes into tissues during inflammation. Journal of Immunology 174, 6406 – 6415.

Bae, G. U., Yang, Y. J., Jiang, G., Hong, M., Lee, H. J., Tessier-Lavigne, M., Kang, J. S. and Krauss, R. S., 2009. Neogenin regulates skeletal myofiber size and focal adhesion kinase and extracellular signal-regulated kinase activities *in vivo* and *in vitro*. Molecular Biology of the Cell 20, 4920 – 4931.

Bassett, D. I., Bryson-Richardson, R. J., Daggett, D. F., Gautier, P., Keenan, D. G. and Currie, P. D., 2003. Dystrophin is required for the formation of stable muscle attachments in the zebrafish embryo. Development 130, 5851 – 5860.

Bate, M., 1990. The embryonic development of larval muscles in Drosophila. Development 110, 791 – 804.

Baylies, M. K., Bate, M. and Ruiz-Gomez, M., 1998. Myogenesis: a view from Drosophila. Cell 93, 921 – 927.

Beckett, K. and Baylies, M. K., 2007. 3D analysis of founder cell and fusion competent myoblast arrangements outlines a new model of myoblast fusion. Developmental Biology 309, 113 – 125.

Bendsten, J. D., Nielsen, H., von Heijne, G. and Brunak, S., 2004. Improved prediction of signal peptides: SignalP 3.0. Journal of Molecular Biology 340, 783 – 795.

Bibikova, M., Golic, M., Golic, K. G. and Carroll, D., 2002. Targeted chromosomal cleavage and mutagenesis in *Drosophila* using zinc-finger nucleases. Genetics 161, 1169 – 1175.

Bill, B. R., Petzold, A. M., Clark, K. J., Schimmenti, L. A. and Ekker, S. C., 2009. A primer for morpholino use in zebrafish. Zebrafish 6, 69 – 77.

Bonanomi, D. and Pfaff, S. L., 2010. Motor axon pathfinding. Cold Spring Harbor Perspectives in Biology 2, a001735.

Bour, B. A., Chakravarti, M., West, J. M. and Abmayr, S. M., 2000. Drosophila SNS, a member of the immunoglobulin superfamily that is essential for myoblast fusion. Genes and Development 14, 1498 – 1511.

Boussif, O., Lezoualc'h, F., Zanta, M. A., Mergny, M. D., Scherman, D., Demeneix, B. and Behr, J. P., 1995. A versatile vector for gene and oligonucleotide transfer into cells in culture and in vivo: polyethylenimine. Proceedings of the National Academy of Sciences of the U. S. A. 92, 7297 – 7301.

Broadie, K. and Bate, M., 1993. Muscle development is independent of innervation during Drosophila embryogenesis. Development 119, 533 – 543.

Brown, M. H. and Barclay, A. N., 1994. Expression of immunoglobulin and scavenger receptor superfamily domains as chimeric proteins with domains 3 and 4 of CD4 for ligand analysis. Protein Engineering 7, 515 – 521.

Buas, M. F., Kadesch, T., 2010. Regulation of skeletal myogenesis by Notch. Experimental Cell Research, *in press*.

Bushell, K. M., Söllner, C., Schuster-Boeckler, B, Bateman, A. and Wright, G. J., 2008. Large-scale screening for novel low-affinity extracellular protein interactions. Genome Research 18, 622 – 630.

Capers, C. R., 1960. Multinucleation of skeletal muscle *in vitro*. Journal of Biophysical and Biochemical Cytology 7, 559 – 566.

Carmena, A., Bate, M. and Jiménez, F., 1995. Lethal of scute, a proneural gene, participates in the specification of muscle progenitors during Drosophila embryogenesis. Genes and Development 9, 2372 – 2783.

Cera, M. R., Del Prete, A., Vecchi, A., Corada, M., Martin-Padura, I., Motoike, T., Tonetti, P., Bazzoni, G., Vermi, W., Gentili, F., Bernasconi, S., Sato, T. N., Mantovani, A. and Dejana, E., 2004. Increased DC trafficking to lymph nodes and contact hypersensitivity in junctional adhesion molecule-A-deficient mice. Journal of Clinical Investigation 114, 729 – 738.

Charlton, C. A., Mohler, W. A., Radice, G. L., Hynes, R. O. and Blau, H. M., 1997. Fusion competence of myoblasts rendered genetically null for N-cadherin in culture. Journal of Cell Biology 138, 331 – 336.

Charlton, C. A., Mohler, W. A. and Blau, H. M., 2000. Neural cell adhesion molecule (NCAM) and myoblast fusion. Developmental Biology 221, 112 – 119.

Charrasse, S., Comunale, F., Fortier, M., Portales-Casamer, E., Debant, A. and Gauthier-Rouvière, C., 2007. M-cadherin activates Rac1 GTPase through the Rho-GEF trio during myoblast fusion. Molecular Biology of the Cell 18, 1734 – 1743

Chavakis, T., Keiper, T., Matz-Westphal, R., Hersemeyer, K., Sachs, U. J., Nawroth, P. P., Preissner, K. T. and Santoso, S., 2004 The junctional adhesion molecule-C promotes neutrophil transendothelial migration in vitro and in vivo. Journal of Biological Chemistry 279, 55602 – 55608.

Cole, F., Zhang, W., Geyra, A., Kang, J. S. and Krauss, R. S., 2004. Positive regulation of myogenic bHLH factors and skeletal muscle development by the cell surface receptor CDO. Developmental Cell 7, 843 – 854.

Collins, R. T., Linker, C. and Lewis, J., 2010. MAZe: a toll for mosaic analysis of gene function in zebrafish. Nature Methods 7, 219 – 223.

Condon, K., Silberstein, L., Blau, H. M. and Thompson, W. J., 1990. Differentiation of fiber types in aneural musculature of the prenatal rat hindlimb. Developmental Biology 138, 275 – 295.

Conti, F. J., Monkley, S. J., Wood, M. R., Critchley, D. R., Müller U., 2009. Talin 1 and 2 are required for myoblast fusion, sarcomere assembly and the maintenance of myotendinous junctions. Development 136, 3597 – 3606.

Cooke, V. G., Naik, M. U. and Naik, U. P., 2006. Fibroblast growth factor-2 failed to induce angiogenesis in junctional adhesion molecule-A-deficient mice. Arteriosclerosis, Thrombosis and Vascular Biology 26, 2005 – 2011.

Cornelison, D. D., 2008. Context matters: *in vivo* and *in vitro* influences on muscle satellite cell activity. Journal of Cellular Biochemistry 105, 663 – 669.

Cortés, F., Daggest, D., Bryson-Richardson, R. J., Neyt, C., Maule, J., Gautier, P., Hollway, G. E., Keenan, D. and Currie, P. D., 2003. Cadherin-mediated differential cell adhesion controls slow muscle cell migration in the developing zebrafish myotome. Developmental Cell 5, 865 – 876.

Coutelle, O., Blagden, C. S., Hampson, R., Halai, C., Rigby, P. W. and Hughes, S. M., 2001. Hedgehog signalling is required for maintenance of myf5 and myoD expression and timely terminal differentiation in zebrafish adaxial myogenesis. Developmental Biology 236, 136 – 150.

Cunningham, S. A., Arrate, M. P., Rodriguez, J. M., Bjercke, R. J., Vanderslice, P., Morris, A. P. and Brock, T. A., 2000. A novel protein with homology to the junctional adhesion molecule. Characterization of leukocyte interactions. Journal of Biological Chemistry 275, 34750 – 34756.

Cunningham, S. A., Rodriguez, J. M., Arrate, M. P., Tran, T. M. and Brock, T. A., 2002. JAM2 interacts with alpha4beta1. Facilitation by JAM3. Journal of Biological Chemistry 277, 27589 – 27592.

Dietrich, S., Abou-Rebyeh, F., Brohmann, H., Bladt, F., Sonnenberg-Riethmacher, E., Yamaai, T., Lumsden, A., Brand-Saberi, B. and Birchmeier, C., 1999. The role of SF/HGF and c-Met in the development of skeletal muscle. Development 126, 1621 – 1629.

Devoto, S. H., Melançon, E., Eisen, J. S. and Westerfield, M., 1996. Identification of separate slow and fast muscle precursor cells in vivo, prior to somite formation. Development 122, 3371 – 3380.

Doberstein, S. K., Fetter, R. D., Mehta, A. Y. and Goodman, C. S., 1997. Genetic analysis of myoblast fusion: blown fuse is required for progression beyond the prefusion complex. Journal of Cell Biology 136, 1249 – 1261.

Donoviel, D. B., Freed, D. D., Vogel, H., Potter, D. G., Hawkins, E., Barrish, J. P., Mathur, B. N., Turner, C. A., Geske, R., Montgomery, C. A., Starbuck, M., Brandt, M., Gupta, A., Ramirez-Solis, R., Zambrowicz, B. P. and Powell, D. R., 2001. Proteinuria and perinatal lethality in mice lacking NEPH1, a novel protein with homology to NEPHRIN. Molecular and Cellular Biology 21, 4829 – 4836.

Driever, W., Solnica-Krezel, L., Schier, A. F., Neuhauss, S. C. F., Malicki, J., Stemple, D. L., Stainier, D. Y. R., Zwartkruis, F., Abdelilah, S., Rangini, Z., Belak, J. and Boggs, C., 1996. A genetic screen for mutations affecting embryogenesis in zebrafish. Development 123, 37 – 46.

Durocher, Y., Perret, S. and Kamen, A., 2002. High-level and high-throughput recombinant protein production by transient transfection of suspension-growing human 293-EBNA1 cells. Nucleic Acids Research 30, e9.

Ebnet, K., Aurrand-Lions, M., Kuhn, A., Kiefer, F., Butz, S., Zander, K., Meyer zu Brickwedde, M. K., Suzuki, A., Imhof, B. A. and Vestweber, D., 2003. The junctional adhesion molecule (JAM) family members JAM-2 and JAM-3 associate with the cell polarity protein PAR-3: a possible role for JAMs in endothelial cell polarity. Journal of Cell Science 116, 3879 – 3891.

Ebnet, K., Suzuki, A., Ohno, S. and Vestweber, D., 2004. Junctional adhesion molecules (JAMs): more molecules with dual functions? Journal of Cell Science 117, 19 – 29.

Eisen, J. S., 1991. Motoneuronal development in the embryonic zebrafish. Development Supplement 2, 141 – 147.

Eisen, J. S. and Smith, J. C., 2008. Controlling morpholino experiments: don't stop making antisense. Development 135, 1735 – 1743.

Estrada, B., Maeland, A. D., Gisselbrecht, S. S., Bloor, J. W., Brown, N. H. and Michelson, A. M., 2007. The MARVEL domain protein, Singles Bar, is required for progression past the pre-fusion complex stage of myoblast fusion. Developmental Biology 307, 328 – 339.

Fanning, A. S., Ma, T. Y. and Anderson, J. M., 2002. Isolation and functional characterization of the actin binding region in the tight junction protein ZO-1. FASEB Journal 16, 1835 – 1837.

Feng, X., Adiarte, E. G. and Devoto, S. H., 2006. Hedgehog acts directly on the zebrafish dermomyotome to promote myogenic differentiation. Developmental Biology 300, 736 – 746.

Galletta, B. J., Chakravarti, M., Banerjee, R. and Abmayr, S. M., 2004. SNS: Adhesive properties, localization requirements and ectodomain dependence in S2 cells and embryonic myoblasts. Mechanisms of Development 121, 1455 – 1468.

Gautam, M., Noakes, P. G., Mudd, J., Nichol, M., Chu, G. C., Sanes, J. R. and Merlie, J. P., 1995. Failure of postsynaptic specialization to develop at neuromuscular junctions of rapsyn-deficient mice. Nature 377, 232 – 236.

Geetha-Loganathan, P., Nimmagadda, S., Pröls, F., Patel, K., Scaal, M., Huang, R. and Christ, B., 2005. Ectodermal Wnt-6 promotes Myf5-dependent avian limb myogenesis. Developmental Biology 288, 221 – 233.

Gill, S. C. and von Hippel, P. H., 1989. Calculation of protein extinction coefficients from amino acid sequence data. Analytical Biochemistry 182, 319 – 326.

Gitton, Y., Dahmane, N., Baik, S., Ruiz i Altaba, A., Neidhardt, L., Scholze, M., Herrmann, B. G., Kahlem, P., Benkahla, A., Schrinner, S., Yildirimman, R., Herwig, R., Lehrach, H. and Yaspo, M. L.; HSA21 expression map initiative, 2002. A gene expression map of human chromosome 21 orthologues in the mouse. Nature 420, 586 – 590.

Gliki, G., Ebnet, K., Aurrand-Lions, M., Imhof, B. A. and Adams, R. H., 2004. Spermatid differentiation requires the assembly of a cell polarity complex downstream of junctional adhesion molecule-C. Nature 431, 320 – 324.

Granato, M., van Eeden, F. J., Schach, U., Trowe, T., Brand, M., Furutani-Seiki, M., Haffter, P., Hammerschmidt, M., Heisenberg, C. P., Jiang, Y. J., Kane, D. A., Kelsh, R. N., Mullins, M. C., Odenthal, J. and Nüsslein-Volhard, C., 1996. Genes controlling and mediating locomotion behavior of the zebrafish embryo and larva. Development 123, 399 – 413.

Gros, J., Scaal, M. and Marcelle, C., 2004. A two-step mechanism for myotome formation in chick. Developmental Cell 6, 875 – 882.

Gros, J., Serralbo, O. and Marcelle, C., 2009. WNT11 acts as a directional cue to organize the elongation of early muscle fibres. Nature 457, 589 – 593.

Groves, J. A., Hammond, C. L. and Hughes, S. M., 2005. Fgf8 drives myogenic progression of a novel lateral fast muscle fibre population in zebrafish. Development 132, 4211 – 4222.

Hagiwara, N., Ma, B. and Ly, A., 2005. Slow and fast fiber isoform gene expression is systematically altered in skeletal muscle of the Sox6 mutant, p100H. Developmental Dynamics 234, 301 – 311.

Hall, T. E., Bryson-Richardson, R. J., Berger, S., Jacoby, A. S., Cole, N. J., Hollway, G. E., Berger, J. and Currie, P. D., 2007. The zebrafish candyfloss mutant implicates extracellular matrix adhesion failure in *laminin α2*-deficient congenital muscular dystrophy. Proceedings of the National Academy of Sciences of the U. S. A. 104, 7092 – 7097.

Hämäläinen, N. and Pette, D., 1995. Patterns of myosin isoforms in mammalian skeletal muscle fibres. Microscopy Research and Technique 30, 381 – 389.

Hammond, C. L., Hinits, Y., Osborn, D. P. S., Minchin, J. E. N., Tettamenti, G. and Hughes, S. M., 2007. Signals and myogenic regulatory factors restrict *pax3* and *pax7*

expression to dermomyotome-like tissue in zebrafish. Developmental Biology 302, 504 – 521.

Haralalka, S. and Abmayr, S. M., 2010. Myoblast fusion in *Drosophila*. Experimental Cell Research, *in press*.

Hauser, P. V., Collino, F., Bussolati, B. and Camussi, G., 2009. Nephrin and endothelial injury. Current Opinion in Nephrology and Hypertension 18, 3 – 8.

Henry, C. A. and Amacher, S. L., 2004. Zebrafish slow muscle cell migration induces a wave of fast muscle morphogenesis. Developmental Cell 7, 917 – 923.

Henry, C. A., McNulty, I. M., Durst, W. A., Munchel, S. E. and Amacher, S. L., 2005. Interactions between muscle fibers and segment boundaries in zebrafish. Developmental Biology 287, 346 – 360.

Ho, R. K., Ball, E. E. and Goodman, C. S., 1983. Muscle pioneers: large mesodermal cells that erect a scaffold for developing muscles and motoneurones in grasshopper embryos. Nature 301, 66 – 69.

Ho, R. K. and Kane, D. A., 1990. Cell-autonomous action of zebrafish *spt-1* mutation in specific mesodermal precursors. Nature 348, 728 – 730.

Hoffman, B. G., Zavaglia, B., Witzsche, J., Ruiz de Algara, T., Beach, M., Hoodless, P. A., Jones, S. J., Marra, M. A. and Helgason, C. D., 2008. Identification of transcripts with enriched expression in the developing and adult pancreas. Genome Biology 9, R99.

Hollnagel, A., Grund, C., Franke, W. W. and Arnold, H. -H., 2002. The cell adhesion molecule M-cadherin is not essential for muscle development and regeneration. Molecular and Cellular Biology 22, 4760 – 4770.

Hollway, G. E., Bryson-Richardson, R. J., Berger, S., Cole, N. J., Hall, T. E. and Currie, P. D., 2007. Whole-somite rotation generates muscle progenitor cell compartments in the developing zebrafish embryo. Developmental Cell 12, 207 – 219.

Hubbard, T. J., Aken, B. L., Beal, K., Ballester, B., Caccamo, M., Chen, Y., Clarke, L., Coates, G., Cunningham, F., Cutts, T., Down, T., Dyer, S. C., Fitzgerald, S., Fernandez-Banet, J., Graf, S., Haider, S., Hammond, M., Herrero, J., Holland, R., Howe, K., Howe, K., Johnson, N., Kahari, A., Keefe, D., Kokocinski, F. *et al*, 2007. Ensembl 2007. Nucleic Acids Research 35, D610 – D617.

Hughes, D. S., Schade, R. R. and Ontell M., 1992. Ablation of the fetal mouse spinal cord: the effect on soleus muscle cytoarchitecture. Developmental Dynamics 193, 164 – 174.

Imhof, B. A., Zimmerli, C., Gliki, G., Ducrest-Gay, D., Juillard, P., Hammel, P., Adams, R. and Aurrand-Lions, M., 2007. Pulmonary dysfunction and impaired granulocyte homeostasis result in poor survival of *Jam-C*-deficient mice. Journal of Pathology 121, 198 – 208.

Ingham, P. W. and Kim, H. R., 2005. Hedgehog signalling and the specification of muscle cell identity in the zebrafish embryo. Experimental Cell Research 306, 336 – 342.

Jing, L., Lefebvre, J. L., Gordon, L. R. and Granato, M., 2009. Wnt signals organize synaptic prepattern and axon guidance through the zebrafish unplugged/MuSK receptor. Neuron 61, 721 – 733.

Johnson-Léger, C. A., Aurrand-Lions, M., Beltraminelli, N., Fasel, N. and Imhof, B. A., 2002. Junctional adhesion molecule-2 (JAM-2) promotes lymphocyte transendothelial migration. Blood 100, 2479 – 2486.

Kahane, N., Cinnamon, Y. and Kalcheim, C., 2002. The roles of cell migration and myofiber intercalation in patterning formation of the postmitotic myotome. Development 129, 2675 – 2687.

Kawakami, K., Takeda, H. Kawakami, N., Kobayashi, M., Matsuda, N. And Mishina, M., 2004. A transposon-mediated gene trap approach identifies developmentally regulated genes in zebrafish. Developmental Cell 7, 133 – 144.

Kesper, D. A., Stute, C., Buttgereit, D., Kreisköther, N., Vishnu, S., Fischbach, K. F. and Renkawitz-Pohl, R., 2007. Myoblast fusion in Drosophila melanogaster is mediated through a fusion-restricted myogenic-adhesive structure (FuRMAS). Developmental Dynamics 236, 404 – 415.

Kim, I. J., Zhang, Y., Yamagata, M., Meister, M. and Sanes, J. R., 2008. Molecular identification of a retinal cell type that responds to upward motion. Nature 452, 478 – 482.

Kim, N. and Burden, S. J., 2008. MuSK controls where motor axons grow and form synapses. Nature Neuroscience 11, 19 – 27.

Kim, S., Shilagardi, K., Zhang, S., Hong, S. N., Sens, K. L., Bo, J., Gonzalez, G. A. and Chen, E. H., 2007. A critical function for the actin cytoskeleton in targeted

exocytosis of prefusion vesicles during myoblast fusion. Developmental Cell 12, 571 – 586.

Kimmel, C. B., Warga, R. M. and Schilling, T. F., 1990. Origin and organization of the zebrafish fate map. Development 108, 581 – 594.

Kimmel, C. B., Ballard, W. W., Kimmel, S. R., Ullmann, B. and Schilling, T. F., 1995. Stages of embryonic development of the zebrafish. Developmental Dynamics 203, 253 – 310.

Kostrewa, D., Brockhaus, M., D'Arcy, A., Dale, G. E., Nelboeck, P., Schmid, G., Mueller, F., Bazzoni, G., Dejana, E., Bartfai, T., Winkler, F. K. and Hennig, M., 2001. X-ray structure of junctional adhesion molecule: structural basis for homophilic adhesion via a novel dimerization motif. EMBO Journal 20, 4391 – 4398.

Kramer, S. G., Kidd, T., Simpson, J. H. and Goodman, C. S., 2001. Switching repulsion to attraction: changing responses to slit during transition in mesoderm migration. Science 292, 737 – 740.

Krauss, R. S., 2010. Regulation of promyogenic signal transduction by cell-cell contact and adhesion. Experimental Cell Research, *in press*.

Krogh, A., Larsson, B., von Heijne, G. and Sonnhammer, E. L., 2001. Predicting transmembrane protein topology with a hidden Markov model: application to complete genomes. Journal of Molecular Biology 305, 567 – 580.

Kudo, H., Amizuka, N., Araki, K., Inohaya, K. and Kudo, A., 2004. Zebrafish periostin is required for the adhesion of muscle fiber bundles to the myoseptum and for the differentiation of muscle fibers. Developmental Biology 267, 473 – 487.

Kumar, S., Tamura, K. and Nei, M., 2004. MEGA3: integrated software for molecular evolutionary genetics analysis and sequence alignment. Briefings in Bioinformatics 5, 150 – 163.

Lamagna, C., Hodivala-Dilke, K. M., Imhof, B. A. and Aurrand-Lions, M., 2005a. Antibody against junctional adhesion molecule-C inhibits angiogenesis and tumor growth. Cancer Research 65, 5703 – 5710.

Lamagna, C., Meda, P., Mandicourt, G., Brown, J., Gilbert, R. J., Jones, E. Y., Kiefer, F., Ruga, P., Imhof, B. A. and Aurrand-Lions, M. 2005b. Dual interaction of JAM-C with JAM-B and alpha(M)beta2 integrin: function in junctional complexes and leukocyte adhesion. Molecular Biology of the Cell. 16, 4992 – 5003

Laurin, M., Fradet, N., Blangy, A., Hall, A., Vuori, K. and Côté, J. -F., 2008. The atypical Rac activator Dock180 (Dock1) regulates myoblast fusion *in vivo*. Proceedings of the National Academy of Sciences of the U. S. A. 105, 15446 – 15451.

Lennon, G., Auffray, C., Polymeropoulos, M. and Soares, M. B., 1996. The I.M.A.G.E. consortium: an integrated molecular analysis of genomes and their expression. Genomics 33, 151 – 152.

Liang, T. W., Chiu, H. H., Gurney, A., Sidle, A., Tumas, D. B., Schow, P., Foster, J., Klassen, T., Dennis, K., DeMarco, R. A., Pham, T., Frantz, G. and Fong, S., 2002. Vascular endothelial-junctional adhesion molecule (VE-JAM)/JAM 2 interacts with T, NK, and dendritic cells through JAM 3. Journal of Immunology 168, 1618 – 1626.

Ludwig, R. J., Zollner, T. M., Santoso, S., Hardt, K., Gille, J., Baatz, H., Johann, P. S., Pfeffer, J., Radeke, H. H., Schön, M. P., Kaufmann, R., Boehncke, W. H. and Podda, M., 2005. Junctional adhesion molecules (JAM)-B and -C contribute to leukocyte extravasation to the skin and mediate cutaneous inflammation. Journal of Investigative Dermatology 125, 969 – 976.

Mandell, K. J., McCall, I. C. and Parkos, C. A., 2004. Involvement of the junctional adhesion molecule-1 (JAM1) homodimer interface in regulation of epithelial barrier function. Journal of Biological Chemistry 279, 16254 – 16262.

Mandicourt, G., Iden, S., Ebnet, K., Aurrand-Lions, M. and Imhof, B. A., 2007. JAM-C regulates tight junctions and integrin-mediated cell adhesion and migration. Journal of Biological Chemistry 282, 1830 – 1837.

Martin, B. L. and Kimelman, D., 2008. Regulation of canonical wnt signaling by *brachyury* is essential for posterior mesoderm formation. Developmental Cell 15, 121 – 133.

Martin, S., Söllner, C., Charoensawan, V., Adryan, B., Thisse, B., Thisse, C., Teichmann, S. A. and Wright, G. J., 2010. Construction of a large extracellular protein interaction network and its resolution by spatiotemporal expression profiling. Molecular and Cellular Proteomics, *in press*.

Matsuda, M. and Chitnis, A., 2009. Interaction with Notch determines endocytosis of specific Delta ligands in zebrafish neural tissue. Development 135, 197 – 206.

McCallum, C. M., Comai, L., Greene, E. A. and Henikoff, S., 2000. Targeted screening for induced mutations. Nature Biotechnology 18, 455 – 457.

Mirza, M., Hreinsson, J., Strand, M. L., Hovatta, O., Söder, O., Philipson, L., Pettersson, R. F. and Sollerbrant, K., 2006. Coxsackievirus and adenovirus receptor (CAR) is expressed in male germ cells and forms a complex with the differentiation factor JAM-C in mouse testis. Experimental Cell Research 312, 817 – 830.

Moore, C. A., Parkin, C. A., Bidet, Y. and Ingham, P. W., 2007. A role for *myoblast city* homologues *dock1* and *dock5* and the adaptor proteins *crk* and *crk-like* in zebrafish myoblast fusion. Development 134, 3145 – 3153.

Muller, W. A., 2003. Leukocyte–endothelial-cell interactions in leukocyte transmigration and the inflammatory response. Trends in Immunology 24, 326 – 333.

Murakami, M., Francavilla, C., Torselli, I., Corada, M., Maddaluno, L., Sica, A., Matteoli, G., Iliev, I. D., Mantovani, A., Rescigno, M., Cavallaro, U. and Dejana, E., 2010. Inactivation of junctional adhesion molecule-A enhances antitumoral immune response by promoting dendritic cell and T lymphocyte infiltration. Cancer Research 70, 1759 – 1765.

Naik, U. P., Ehrlich, Y. H. and Kornecki, E., 1995. Mechanisms of platelet activation by a stimulatory antibody: cross-linking of a novel platelet receptor for monoclonal antibody F11 with the Fc gamma RII receptor. Biochemical Journal 310, 155 – 162.

Ovcharenko, I., Loots, G. G., Hardison, R. C., Miller, W. and Stubbs, L., 2004. zPicture: dynamic alignment and visualization tool for analyzing conservation profiles. Genome Research 14, 472 – 477.

Palmeri, D., van Zante, A., Huang, C. C., Hemmerich, S. and Rosen, S. D., 2000. Vascular endothelial junction-associated molecule, a novel member of the immunoglobulin superfamily, is localized to intercellular boundaries of endothelial cells. Journal of Biological Chemistry 275, 19139 – 19145.

Parris, J. J., Cooke, V. G., Skarnes, W. C., Duncan, M. K. and Naik, U. P., 2005. JAM-A expression during embryonic development. Developmental Dynamics 233, 1517 – 1524.

Peterson, M. T. and Henry, C. A., 2010. Hedgehog signalling and laminin play unique and synergistic roles in muscle development. Developmental Dynamics 239, 905 – 913.

Pickart, M. A., Klee, E. W., Nielsen, A. L., Sivasubbu, S., Mendenhall, E. M., Bill, B. R., Chen, E., Eckfeldt, C. E., Knowlton, M., Robu, M. E., Larson, J. D., Deng, Y., Schimmenti, L. A., Ellis, L. B. M., Verfaillie, C. M., Hammerschmidt, M., Farber, S. A.

and Ekker, S. C., 2006. Genome-wide reverse genetics framework to identify novel functions of the vertebrate secretome. PLoS One 1, e104.

Pownall, M. E., Gustafsson, M. K. and Emerson, C. P. Jr., 2002. Myogenic regulatory factors and the specification of muscle progenitors in vertebrate embryos. Annual Review of Cell and Developmental Biology 18, 747 – 783.

Praetor, A., McBride, J. M., Chiu, H., Rangell, L., Cabote, L., Lee, W. P., Cupp, J., Danilenko, D. M. and Fong, S., 2009. Genetic deletion of JAM-C reveals a role in myeloid progenitor generation. Blood 113, 1919 – 1928.

Prota, A. E., Campbell, J. A., Schelling, P., Forrest, J. C., Watson, M. J., Peters, T. R., Aurrand-Lions, M., Imhof, B. A., Dermody, T. S. and Stehle, T., 2003. Crystal structure of human junctional adhesion molecule 1: implications for reovirus binding. Proceedings of the National Academy of Sciences of the U. S. A. 100, 5366 – 5371.

Rabquer, B. J., Amin, M. A., Teegala, N., Shaheen, M. K., Tsou, P. S., Ruth, J. H., Lesch, C. A., Imhof, B. A. and Koch, A. E., 2010. Junctional adhesion molecule-C is a soluble mediator of angiogenesis. Journal of Immunology 185, 1777 – 1785.

Ravi, V. and Venkatesh, B., 2008. Rapidly evolving fish genomes and teleost diversity. Current Opinion in Genetics and Development 18, 544 – 550.

Rehder, D., Iden, S., Nasdala, I., Wegener, J., Brickwedde, M. K., Vestweber, D. and Ebnet, K., 2006. Junctional adhesion molecule-a participates in the formation of apico-basal polarity through different domains. Experimental Cell Research 312, 3389 – 3403.

Richardson, B. E., Beckett, K., Nowak, S. J. and Baylies, M. K., 2007. SCAR/WAVE and Arp2/3 are crucial for cytoskeletal remodeling at the site of myoblast fusion. Development 134, 4357 – 4367.

Rochlin, K., Shanon, Y., Roy, S. and Baylies, M. K., 2009. Myoblast fusion: when it takes more to make one. Developmental Biology 341, 66 – 83.

Ross, J. J., Duxson, M. J. and Harris, A. J., 1987. Neural determination of muscle fibre numbers in embryonic rat lumbrical muscles. Development 100, 395 – 409.

Roy, S., Wolff, C. and Ingham, P. W., 2001. The *u-boot* mutation identifies a hedgehog-related myogenic switch for fiber-type diversification in the zebrafish embryo. Genes and Development 15, 1563 – 1576.

Ruiz-Gomez, M., Coutts, N., Price, A., Taylor, M. V. and Bate, M., 2000. *Drosophila dumbfounded*: a myoblast attractant essential for fusion. Cell 102, 189 – 198.

Ruiz-Gomez, M., Coutts, N., Suster, M. L., Landgraf, M. and Bate, M., 2002. *myoblasts incompetent* encodes a zinc finger transcription factor required to specify fusion-competent myoblasts in *Drosophila*. Development 129, 133 – 141.

Rushton, E., Drysdale, R., Abmayr, S. M., Michelson, A. M. and Bate, M., 1995. Mutations in a novel gene, *myoblast city*, provide evidence in support of the founder cell hypothesis for Drosophila muscle development. Development 121, 1979 – 1988.

Sakaguchi, T., Nishimoto, M., Miyagi, S., Iwama, A., Morita, Y., Iwamori, N., Nakauchi, H., Kiyonari, H., Muramatsu, M. and Okuda, A., 2006. Putative "stemness" gene *jam-B* is not required for maintenance of stem cell state in embryonic, neural, or hematopoietic stem cells. Molecular Cell Biology 26, 6557 – 6570.

Santoso, S., Sachs, U. J., Kroll, H., Linder, M., Ruf, A., Preissner, K. T. and Chavakis, T., 2002. The junctional adhesion molecule 3 (JAM-3) on human platelets is a counterreceptor for the leukocyte integrin Mac-1. Journal of Experimental Medicine 196, 679 – 691.

Santoso, S., Orlova, V. V., Song, K., Sachs, U. J., Andrei-Selmer, C. L. and Chavakis, T. 2005. The homophilic binding of junctional adhesion molecule-C mediates tumor cell-endothelial cell interactions. Journal of Biological Chemistry, 280, 36326 – 36333.

Scheiermann, C., Meda, P., Aurrand-Lions, M., Madani, R., Yiangou, Y., Coffey, P., Salt, T. E., Ducrest-Gay, D., Caille, D., Howell, O., Reynolds, R., Lobrinus, A., Adams, R. H., Yu, A. S., Anand, P., Imhof, B. A. and Nourshargh, S., 2007. Expression and function of junctional adhesion molecule-C in myelinated peripheral nerves. Science 318, 1472 – 1475.

Schnorrer, F., and Dickson, B. J., 2004. Muscle building; mechanisms of myotube guidance and attachment site selection. Developmental Cell 7, 9 – 20.

Schnorrer, F., Kalchhauser, I. and Dickson, B. J., 2007. The transmembrane protein Kon-tiki couples to Dgrip to mediate myotube targeting in Drosophila. Developmental Cell 12, 751 – 766.

Schwander, M., Leu, M., Stumm, M., Dorchies, O. M., Ruegg, U. T., Schittny, J. and Müller, U., 2003. Beta1 integrins regulate myoblast fusion and sarcomere assembly. Developmental Cell 4, 673 – 685.

Scumpia, P. O., Kelly-Scumpia, K. M., Delano, M. J., Weinstein, J. S., Cuenca, A. G., Al-Quran, S., Bovio, I., Akira, S., Kumagai, Y. and Moldawer, L. L., 2010. Cutting edge: bacterial infection induces hematopoietic stem and progenitor cell expansion in the absence of TLR signaling. Journal of Immunology 184, 2247 – 2251.

Shao, M., Ghosh, A., Cooke, V. G., Naik, U. P. and Martin-DeLeon, P. A., 2008. JAM-A is present in mammalian spermatozoa where it is essential for normal motility. Developmental Biology 313, 246 – 255.

Shelton, C., Kocherlakota, K. S., Zhuang, S. and Abmayr, S. M., 2009. The immunoglobulin superfamily member Hbs functions redundantly with Sns in interactions between founder and fusion-competent myoblasts. Development 136, 1159 – 1168.

Shiina, T., Shima, T., Wörl, J., Neuhuber, W. L. and Shimizu, Y., 2010. The neural regulation of the mammalian esophageal motility and its implication for esophageal diseases. Pathophysiology 17, 129 – 133.

Shirasaki, R., Lewcock, J. W., Lettieri, K. and Pfaff, S. L., 2006. FGF as a target-derived chemoattractant for developing motor axons genetically programmed by the LIM code. Neuron 50, 841 – 853.

Snow, C. J., Peterson, M. T., Khalil, A. and Henry, C. A., 2008a. Muscle development is disrupted in zebrafish embryos deficient for fibronectin. Developmental Dynamics 237, 2542 – 2553.

Snow, C. J., Goody, M., Kelly, M. W., Oster, E. C., Jones, R., Khalil, A. and Henry, C. A., 2008b. Time-lapse analysis and mathematical characterization elucidate novel mechanisms underlying muscle morphogenesis. PLoS Genetics 4, e1000219.

Sobocka, M. B., Sobocki, T., Banerjee, P., Weiss, C., Rushbrook, J. I., Norin, A. J., Harting, J., Salifu, M. O., Markell, M. S., Babinska, A., Ehrlich, Y. H. and Kornecki, E., 2000. Cloning of the human platelet F11 receptor: a cell adhesion molecule member of the immunoglobulin superfamily involved in platelet aggregation. Blood 95, 2600 – 2609.

Sohn, R. L., Huang, P., Kawahara, G., Mitchell, M., Guyon, J., Kalluri, R., Kunkel, L. M. and Gussoni, E., 2009. A role for nephrin, a renal protein, in vertebrate skeletal muscle cell fusion. Proceedings of the National Academy of Sciences of the U. S. A. 106, 9274 – 9279.

Srinivas, B. P., Woo, J., Leong, W. Y. and Roy, S., 2007. A conserved molecular pathway mediates myoblast fusion in insects and vertebrates. Nature Genetics 39, 781 – 786.

Steigemann, P., Molitor, A., Fellert, S., Jäckle, H. and Vorbrüggen, G., 2004. Heparan sulfate proteoglycan syndecan promotes axonal and myotube guidance by slit/robo signaling. Current Biology 14, 225 – 230.

Stellabotte, F., Dobbs-McAuliffe, B., Fernández, D. A., Feng, X. and Devoto, S. H., 2007. Dynamic somite cell rearrangements lead to distinct waves of myotome growth. Development 134, 1253 – 1257.

Stevenson, B. R., Siliciano, J. D., Mooseker, M. S. and Goodenough, D. A., 1986. Identification of ZO-1: a high molecular weight polypeptide associated with the tight junction (zonula occludens) in a variety of epithelia. Journal of Cell Biology 103, 755 – 766.

Strünkelnberg, M., Bonengel, B., Moda, L. M., Hertenstein, A., de Couet, H. G., Ramos, R. G. and Fischbach, K. F., 2001. *rst* and its paralogue *kirre* act redundantly during embryonic muscle development in *Drosophila*. Development 128, 4229 – 4239.

Tang, T., Li, L., Tang, J., Li, Y., Lin, W. Y., Martin, F., Grant, D., Solloway, M., Parker, L., Ye, W., Forrest, W., Ghilardi, N., Oravecz, T., Platt, K. A., Rice, D. S., Hansen, G. M., Abuin, A., Eberhart, D. E., Godowski, P., Holt, K. H., Peterson, A., Zambrowicz, B. P. and de Sauvage, F. J., 2010. A mouse knockout library for secreted and transmembrane proteins. Nature Biotechnology, 28, 749 – 755.

Tenan, M., Aurrand-Lions, M., Widmer, V., Alimenti, A., Burkhardt, K., Lazeyras, F., Belkouch, M. C., Hammel, P., Walker, P. R., Duchosal, M. A., Imhof, B. A. and Dietrich, P. Y., 2010. Co-operative expression of junctional adhesion molecule-C and -B supports growth and invasion of glioma. Glia 58, 524 – 537.

Thisse, C. and Thisse, B., 2008. High-resolution *in situ* hybridization to whole-mount zebrafish embryos. Nature Protocols 3, 59 – 69.

Thomas, F. C., Sheth, B., Eckert. J. J., Bazzoni, G., Dejana, E. and Fleming, T. P., 2004. Contribution of JAM-1 to epithelial differentiation and tight-junction biogenesis in the mouse preimplantation embryo. Journal of Cell Science 117, 5599 – 5608.

Urnov, F. D., Rebar, E. J., Holmes, M. C., Zhang, H. S. and Gregory, P. D., 2010. Genome editing with engineered zinc finger nucleases. Nature Reviews Genetics 11, 636 – 646.

van der Merwe, P. A. and Barclay, A. N., 1996. Analysis of cell-adhesion molecule interactions using surface plasmon resonance. Current Opinion in Immunology 8, 257 – 261.

Vasyutina, E., Martarelli, B., Brakebusch, C., Wende, H. and Birchmeier, C., 2009. The small G-proteins Rac1 and Cdc42 are essential for myoblast fusion in the mouse. Proceedings of the National Academy of Sciences of the U. S. A 106, 8935 – 8940.

Visel, A., Thaller, C. and Eichele, G., 2004. GenePaint.org: an atlas of gene expression patterns in the mouse embryo. Nucleic Acids Research 32, D552 – 556.

Volff, J. –N., 2005. Genome evolution and biodiversity in teleost fish. Heredity 94, 280 – 294.

von Hofsten, J., Elworthy, S., Gilchrist, M. J., Smith, J. C., Wardle, F. C. and Ingham, P. W., 2008. Prdm1- and Sox6-mediated transcriptional repression specifies muscle fibre type in the zebrafish embryo. EMBO Reports 9, 683 – 689.

Vonlaufen, A., Aurrand-Lions, M., Pastor, C. M., Lamagna, C., Hadengue, A., Imhof, B. A. and Frossard, J. L., 2006. The role of junctional adhesion molecule C (JAM-C) in acute pancreatitis. Journal of Pathology 209, 540 – 548.

Wang, D., Jao, L. E., Zheng, N., Dolan, K., Ivey, J., Zonies, S., Wu, X., Wu, K., Yang, H., Meng, Q., Zhu, Z., Zhang, B., Lin, S. and Burgess, S. M., 2007. Efficient genome-wide mutagenesis of zebrafish genes by retroviral insertions. Proceedings of the National Academy of Sciences of the U. S. A. 104, 12428 – 12433.

Wang, Y. and Lui, W. Y., 2009. Opposite effects of interleukin-1alpha and transforming growth factor-beta2 induce stage-specific regulation of junctional adhesion molecule-B gene in Sertoli cells. Endocrinology 150, 2404 – 2412.

Weber, C., Fraemohs, L. and Dejana, E., 2007. The role of junctional adhesion molecules in vascular inflammation. Nature Reviews Immunology 7, 467 – 477.

Weinberg, E. S., Allende, M. L., Kelly, C. S., Abdelhamid, A., Murakami, T., Andermann, P., Doerre, O. G., Grunwald, D. J. and Riggleman, B., 1996. Developmental regulation of zebrafish MyoD in wild-type, no tail and spadetail embryos. Development 122, 271 – 280.

Woo, K., Shih, J. and Fraser, S. E., 1995. Fate maps of the zebrafish embryo. Current Opinion in Genetics and Development 5, 439 – 443.

Xu, Q., Stemple, D. and Joubin, K., 2008. Microinjection and cell transplantation in zebrafish embryos. Methods in Molecular Biology 461, 513 – 520.

Yang, X., Arber, S., William, C., Li, L., Tanabe, Y., Jessell, T. M., Birchmeier, C. and Burden, S. J., 2001. Patterning of muscle acetylcholine receptor gene expression in the absence of motor innervation. Neuron 30, 399 – 410.

Ye, M., Hamzeh, R., Geddis, A., Varki, N., Perryman, M. B. and Grossfeld, P., 2009. Deletion of JAM-C, a candidate gene for heart defects in Jacobsen syndrome, results in a normal cardiac phenotype in mice. American Journal of Medical Genetics, Part A 149A, 1438 – 1443.

Zhang, J., Lefebvre, J. L., Zhao, S. and Granato, M., 2004. Zebrafish *unplugged* reveals a role for muscle-specific kinase homologs in axonal pathway choice. Nature Neuroscience 7, 1303 – 1309.

Zimmerli, C., Lee, B. P., Palmer, G., Gabay, C., Adams, R., Aurrand-Lions, M. and Imhof, B. A., 2009. Adaptive immune response in JAM-C-deficient mice: normal initiation but reduced IgG memory. Journal of Immunology 182, 4728 – 4736.